

7-2-2014 12:00 AM

Effect of Nozzle Geometry on Jet Bed Interaction: Experiments with Commercial Scale Nozzles and Eroded Nozzles

Nicholas A. Prociw, *The University of Western Ontario*

Supervisor: Dr. Cedric Briens, *The University of Western Ontario*

Joint Supervisor: Dr. Franco Berutti, *The University of Western Ontario*

A thesis submitted in partial fulfillment of the requirements for the Master of Engineering Science degree in Chemical and Biochemical Engineering

© Nicholas A. Prociw 2014

Follow this and additional works at: <https://ir.lib.uwo.ca/etd>

 Part of the [Petroleum Engineering Commons](#), and the [Transport Phenomena Commons](#)

Recommended Citation

Prociw, Nicholas A., "Effect of Nozzle Geometry on Jet Bed Interaction: Experiments with Commercial Scale Nozzles and Eroded Nozzles" (2014). *Electronic Thesis and Dissertation Repository*. 2424.
<https://ir.lib.uwo.ca/etd/2424>

This Dissertation/Thesis is brought to you for free and open access by Scholarship@Western. It has been accepted for inclusion in Electronic Thesis and Dissertation Repository by an authorized administrator of Scholarship@Western. For more information, please contact wlsadmin@uwo.ca.

EFFECT OF NOZZLE GEOMETRY ON JET-BED INTERACTION.
EXPERIMENTS WITH COMMERCIAL SCALE NOZZLES AND ERODED NOZZLES

by

Nicholas Prociw

Graduate Program in Chemical and Biochemical Engineering

A thesis submitted in partial fulfillment
of the requirements for the degree of
Masters of Engineering Sciences

The School of Graduate and Postdoctoral Studies
The University of Western Ontario
London, Ontario, Canada

© Nicholas Prociw 2014

Abstract

Liquid injection into fluidized bed reactors has several industrial applications, such as Fluid Catalytic Cracking, Gas Phase Polyethylene production, and Fluid Coking. High quality liquid distribution is essential to maximize the yield of desirable products, and minimize agglomeration.

The objectives of this thesis are: to develop a method that measures the rate of liquid released from agglomerates formed as a result of liquid injection into a fluidized bed; to use this method to determine the effect of internal erosion on nozzle performance; and to compare the performance of current commercial spray nozzles to nozzles with altered geometries. To achieve these objectives, gas-atomized liquid sprays were produced inside a large scale fluidized bed using commercial scale nozzles. Liquid distribution was monitored by measuring the conductance of the fluidized bed. Results indicate that the altered geometry caused by erosion may enhance liquid distribution among the fluidized bed particles and increase the rate of moisture released from these agglomerates.

Key words: Fluidized bed, Fluid Coking, spray nozzle, spray nozzle erosion, agglomeration, jet expansion, conductance electrodes

Co-Authorship Statement

The journal articles written from the present work are listed below, and the individual contributions of all the members are indicated.

Chapter 2

Article Title: Method to Measure the Rate of Liquid Released from Agglomerates Produced by Gas-Atomized Liquid Injection into a Fluidized Bed
Authors: Nicholas Prociw, Cedric Briens, Franco Berruti, Tarek Jamaledine
Article Status: To be submitted for possible publication in Powder Technology
This work was supervised by C. Briens and F. Berruti. Various drafts of the paper were reviewed by C. Briens and F. Berruti. All the experiments and data analysis were conducted by N. Prociw. N. Prociw wrote the manuscript. Tarek Jamaledine helped with operation of the large scale fluidized bed.

Chapter 3

Article Title: Effect of Nozzle Erosion on Jet Interaction in a Fluidized Bed
Authors: Nicholas Prociw, Cedric Briens, Franco Berruti
Article Status: To be submitted for possible publication in Fuel
This work was supervised by C. Briens and F. Berruti. Various drafts of the paper were reviewed by C. Briens and F. Berruti. All the experiments and data analysis were conducted by N. Prociw. N. Prociw wrote the manuscript.

Chapter 4

Article Title: Effect of Spray Nozzle Attachment Geometry on Rate of Liquid Released from Agglomerates Produced by Gas-Atomized Liquid Injection into a Fluidized Bed
Authors: Nicholas Prociw, Cedric Briens, Franco Berruti
Article Status: To be submitted for possible publication in Powder Technology
This work was supervised by C. Briens and F. Berruti. Various drafts of the paper were reviewed by C. Briens and F. Berruti. All the experiments and data analysis were conducted by N. Prociw. N. Prociw wrote the manuscript. Tarek Jamaledine helped with operation of the large scale fluidized bed.

Acknowledgments

I would like to acknowledge Dr. Cedric Briens and Dr Franco Berruti for the excellent opportunity to work at ICFAR, and to present my results at Fluidization XIV. I would like to thank them for their help in completing this thesis as well.

Thank you to Tom Johnston, Quinn Rush, Rob Taylor, Clayton Cook, and the UMS crew for all the work they performed to maintain my lab equipment and help me solve many problems that I encountered.

Thank you to my parents, for inspiring me, and helping me through difficult times. It is through them I learned to never give up, and that any problem can be solved when you put your mind to it.

Table of Contents

Abstract	ii
Co-Authorship Statement.....	iii
Acknowledgments.....	iv
Table of Contents	v
List of Tables	ix
List of Figures	x
List of Symbols	xiv
List of Appendices	xvi
Chapter 1	1
1 Introduction	1
1.1 Applications Involving Liquid Injection into Fluidized Bed Reactors	1
1.1.1 Agitated Wet Granulation	1
1.1.2 LDPE Production	2
1.1.3 Fluid Catalytic Cracking	3
1.1.4 Fluid Coking TM	4
1.2 Agglomerate Formation in Fluidized Beds.....	10
1.3 Spray Nozzles	13
1.3.1 Standard Fluid Coker Spray Nozzle Description.....	13
1.3.2 Nozzle Additions and Alterations	14
1.3.3 Effervescent Nozzles and Atomization.....	18
1.4 Review of Liquid Distribution and Liquid/Solid Mixing Measurements Methods in a Fluidized Bed	20
1.5 Research Objectives.....	23
1.6 References:.....	24

Chapter 2.....	29
2 A METHOD TO MEASURE THE RATE OF LIQUID RELEASED FROM AGGLOMERATES PRODUCED BY GAS-ATOMIZED LIQUID INJECTION INTO A FLUIDIZED BED	29
2.1 Introduction.....	29
2.2 Apparatus	33
2.3 Procedure	38
2.3.1 Electrode Calibration	38
2.3.2 Agglomerate Moisture Release Experiments.....	43
2.4 Results and Discussion	46
2.4.1 Effect of GLR on Rate of Moisture Released from Agglomerates.....	46
2.4.2 Effect of Liquid Mass Flow Rate on the Rate of Moisture Released from Agglomerates	49
2.4.3 Evolution of Free Moisture throughout the Fluidized Bed.....	52
2.5 Conclusions.....	55
2.6 References	56
Chapter 3.....	58
3 Effect of Nozzle Erosion on Jet Interaction in a Fluidized Bed.....	58
3.1 Introduction:.....	58
3.2 Apparatus	61
3.2.1 Fluidized Bed	61
3.2.2 Spray Nozzle Apparatus	63
3.2.3 Conductance Measurement Apparatus	65
3.2.4 Spray Nozzles	66
3.3 Procedure	69
3.3.1 Nozzle Characteristics	71
3.3.2 Measuring the Rate of Liquid Released from Agglomerates to Assess Nozzle Performance in a Fluidized Bed	74

3.4 Results.....	77
3.4.1 Eroded Nozzle Characteristics	77
3.4.2 Effect of GLR on Standard TEB Nozzle and Eroded TEB Nozzle	81
3.4.3 The Effect of Nozzle Erosion on Jet-Bed Interaction at High Liquid Flow Rate	85
3.5 Conclusions.....	88
3.6 References.....	89
Chapter 4.....	92
4 Effect of Spray Nozzle Attachment Geometry on Rate of Liquid Released from Agglomerates Produced by Gas-Atomized Liquid Injection into a Fluidized Bed	92
4.1 Introduction.....	92
4.2 Apparatus	97
4.2.1 Fluidized Bed	97
4.2.2 Spray Nozzles	100
4.2.3 Conductivity Measurement Apparatus	103
4.3 Procedure	103
4.4 Results and Discussion	106
4.4.1 Open Air sprays	106
4.4.2 Cloverleaf Nozzle Attachment Performance in the Fluidized Bed.....	110
4.4.3 Conical Nozzle Attachment Performance in the Fluidized Bed	112
4.4.4 Comparison of Eroded Nozzles, Cloverleaf, and Conical Nozzle Attachments	113
4.5 Conclusions.....	114
4.6 References:.....	115
Chapter 5.....	118
5.1 Conclusions.....	118
5.2 Recommendations.....	120

5.3 References	122
Appendix A.....	123
Parts Required for Custom Eroded Nozzle Investigation.	123
Curriculum Vitae	133

List of Tables

Table 1.1: Typical dimensions of a Fluid Coker vessel (US Patent 2881130)	9
Table 2.1: Operating conditions tested	46
Table 3.1: Calculated nozzle throat areas based on upstream pressure drop measurement. *	
The angle produced by both jets were added together for Nozzle 3.....	79

List of Figures

Figure 1.1: Simplified process flow diagram of a Fluid Coker reactor	6
Figure 1.2: TEB nozzle developed by Base et al. (1999)	13
Figure 1.3: Formation of shockwaves inside a TEB nozzle (Base et al. 1999)	14
Figure 1.4: TEB nozzle attachment with conical nozzle attachment used in simulation by Poutgach et al. (2012)	15
Figure 1.5: Cloverleaf nozzle attachment (view of tip) (Chan et al. 2012)	16
Figure 1.6: Impact cone investigated by House et al. (2009)	17
Figure 1.7: Left - annular gas shroud. Right: Sonic gas shroud. Both shrouds were investigated by House et al. (2009).....	17
Figure 2.1: Simplified Process Flow Diagram of Experimental Apparatus	33
Figure 2.2: Top view of fluidized bed with dimensions (inches)	34
Figure 2.3: Standard TEB nozzle (Base et al. 1999).....	35
Figure 2.4: Premix chamber and nozzle assembly.....	36
Figure 2.5: Schematic diagram of conductance electrodes.....	37
Figure 2.6: Fluidized bed electrical conductance versus time after liquid injection for electrode calibration experiment (GLR = 30%).....	41
Figure 2.7: Calibration data points for electrode 1. A similar plot is produced for each electrode	42
Figure 2.8: Equations 2.7 a-c fitted to calibration data for electrode 1	43
Figure 2.9: Cumulative fraction of moisture freed from agglomerates (G(t)) versus time for four different GLR's (0.5%, 2%, 3.5%, 4.8%) (Liquid mass flow rate = 1.35 kg/s).....	47

Figure 2.10: Agglomerate moisture release rate time constant versus GLR	48
Figure 2.11: Cumulative fraction of moisture freed from agglomerates ($G(t)$) versus time for four different liquid flow rates (0.6, 1.2, 1.9, 2.5 kg/s) (GLR = 2%)	50
Figure 2.12: Effect of liquid mass flow rate on moisture release rate time constant (2% GLR)	51
Figure 2.13: Evolution of free moisture in fluidized bed after liquid injection is complete. Liquid flow rate = 1.35 kg/s. GLR = 2%. First 9 minutes	53
Figure 2.14: Evolution of free moisture in fluidized bed after liquid injection is complete. Liquid flow rate = 1.35 kg/s. GLR = 2%. Time step = 1 min.....	54
Figure 3.1: Simplified Process Flow Diagram of Experimental Apparatus	62
Figure 3.2: Top view of fluidized bed vessel (dimensions in inches)	62
Figure 3.3: Standard TEB nozzle (Base et al. 1999).....	64
Figure 3.4: Premix chamber and nozzle assembly.....	64
Figure 3.5: Schematic Diagram of Conductive Electrodes.....	66
Figure 3.6: Top: Eroded nozzle and standard nozzle (middle) tips. Bottom left: Erosion located at the first throat of the TEB nozzle. Bottom right: hole formed through the wall of nozzle 3.	67
Figure 3.7: Possible trajectory of entrained solid particle within two phase flow through a Fluid Coker spray nozzle (based on visual inspection of nozzle interior).....	68
Figure 3.8: Side view of each nozzle showing curved profile. The non-eroded TEB nozzle is shown in the middle for comparison.....	69
Figure 3.9: Images of free jets produced by each nozzle.....	78
Figure 3.10: Normalized throat area as a function of nozzle volume.....	80

Figure 3.11: Open air spray angle as a function of normalized nozzle throat area.....	80
Figure 3.12: Open air spray angle as a function of normalized volume	81
Figure 3.13: Fraction of injected liquid released from agglomerates vs. time after spray completion.....	82
Figure 3.14: Atomization power as a function of GLR for each nozzle.....	83
Figure 3.15: Agglomerate moisture release rate time constant vs. GLR for non-eroded TEB nozzle, and Eroded Nozzle 3 (1.5 kg/s).	84
Figure 3.16: Agglomerate moisture release rate time constant versus normalized nozzle exit orifice area. Constant upstream liquid pressure (2600 kPa (gauge)). Replicates for each nozzle are shown.....	86
Figure 3.17: Agglomerate moisture release rate time constant versus normalized nozzle exit orifice area. Constant liquid flow rate (3 kg/s, GLR = 2%). Replicates for each nozzle are shown.	86
Figure 3.18: Comparison of the effect of nozzle erosion on the agglomerate moisture release rate time constant for constant upstream liquid pressure case and constant liquid flow rate case.....	87
Figure 4.1: Turbulent eddy formation inside draft tube (Zhou et al. 2004).....	93
Figure 4.2 Annular shroud (left) and sonic shroud (right) investigated by House et al. (2008)	94
Figure 4.3: TEB nozzle with diverging nozzle tip investigated by Portoghese et al. (2010) .	95
Figure 4.4: Simplified Process Flow Diagram of Experimental Apparatus	98
Figure 4.5: Top view of fluidized bed vessel (dimensions in inches)	98
Figure 4.6: Standard TEB nozzle used to distribute liquid in the Fluid Coking process.....	100

Figure 4.7: Geometry of cloverleaf nozzle attachments. Left: Standard cloverleaf. Middle: Eroded Cloverleaf. Right: Square cloverleaf.	101
Figure 4.8: Side view of diverging conical nozzle attachment ($\beta = 5^\circ, 10^\circ, 20^\circ, 30^\circ, 40^\circ$).	101
Figure 4.9: Premix chamber and nozzle assembly.....	102
Figure 4.10: Schematic Diagram of Conductive Electrodes.....	103
Figure 4.11: Open air sprays produced with conical nozzle attachment (left). Open air sprays produced with cloverleaf nozzle attachment (Right)	107
Figure 4.12: Open air spray angles produced by conical nozzle tip attachments	108
Figure 4.13: Open air spray angles produced by each cloverleaf nozzle tested.	109
Figure 4.14: Agglomerate moisture released rate time constant for each cloverleaf nozzle tested. Results are compared to standard TEB nozzle. Liquid flow rate = 3 kg/s. GLR = 2% for each case.....	111
Figure 4.15: Effect of diverging nozzle tip angle on agglomerate moisture release rate time constant τ (Liquid flow rate = 3 kg/s, GLR = 2 wt%)	112
Figure 4.16: Effect of Spray Angle on Rate of Moisture Released from Agglomerates	114

List of Symbols

A_{throat}	Nozzle throat area (m ²)
C	Conductance of fluidized bed (micro Siemens)
f_e	Flow rate of water evaporated from the fluidized bed (kg/s)
F_g	Flow rate of atomization gas through spray nozzle (kg/s)
F_L	Mass flow rate of liquid through spray nozzle (kg/s)
$G(t)$	Fraction of liquid released from agglomerates after the end of injection (-)
\mathcal{H}^*	Humidity of incoming fluidization air (kg water/kg air)
\mathcal{H}_{in}	Humidity of fluidization air exiting fluidized bed (kg water/kg air)
k	Ratio of upstream nozzle pressure to nozzle throat pressure (-)
M_{agg}	Mass of water trapped in agglomerates (kg)
M_g	Molecular weight of atomization gas (kg/kmol)
M_{inj}	Mass of water injected water (kg)
M_L	Mass of liquid inside the fluidized bed (kg)
M_s	Mass of solids in fluidized bed (kg)
P_{throat}	Pressure at the throat of the nozzle (Pa)
P_{up}	Pressure upstream of the throat of the nozzle (Pa)
R	Universal gas constant (J/kg/K)

R_m	Measurement resistance (Ω)
T	Temperature of atomization gas (K)
t	Time after the end of liquid injection (s)
t_c	Time after injection at which the rate of change of conductance equals rate of change of water within fluidized bed (s)
u_{gas}	Velocity of atomization gas through spray nozzle (m/s)
u_{sound}	Speed of sound through gas (m/s)
V_1	Applied voltage (V)
V_2	Voltage drop across measurement resistor (V)
\dot{v}_a	Superficial velocity of fluidization gas (m/s)
\bar{x}	Average free moisture throughout fluidized bed as measured by conductance electrodes (-)
y	Average density of gas/liquid mixture (kg/m ³)
γ	Ratio of heat capacities (-)
ε_g	Void fraction of atomization gas at the tip of a spray nozzle (-)
ρ	Solid particle density (kg/m ³)
ρ_g	Density of atomization gas (kg/m ³)
ρ_L	Density of injected liquid (kg/m ³)
τ	Agglomerate moisture release time constant (s)

List of Appendices

Parts Required for Custom Eroded Nozzle Investigation	123
---	-----

Chapter 1

1 Introduction

The present work describes experiments that were performed to measure the rate of moisture released from agglomerates in a large scale fluidized bed. The developed method was used to compare the performance of various commercial scale spray nozzles applied to liquid distribution inside a fluidized bed. This is of particular importance for the Fluid Coking process which uses spray nozzles to inject liquid bitumen into a bed of fluidized coke particles.

The following chapter discusses the various applications for liquid injection into fluidized beds. The Fluid Coking process is reviewed in greater detail, as the experiments presented in this thesis are directly related to this process. The stability of agglomerates, which play an important role in influencing the performance of a Fluid Coker reactor, is discussed next. Spray nozzles are used to distribute liquid into Fluid Cokers, and are specially designed to minimize agglomerate formation and stability. There have been several proposed additions or modifications to the spray nozzles used in the Fluid Coker, some of which are reviewed here. A review of the various methods to measure liquid distribution inside a Fluid Coking unit is discussed next. The objectives of the thesis are described last.

1.1 Applications Involving Liquid Injection into Fluidized Bed Reactors

1.1.1 Agitated Wet Granulation

Granulation is a process through which small solid particles are stuck together to form larger agglomerates consisting of the same material. Granulation is an important process used in the mineral processing, agricultural, detergent, pharmaceutical, food and specialty chemicals industries. Reasons for producing granules include minimization of dust formation, improved flow characteristics of powders, control of dissolution rates of solids in a liquid, and the prevention of segregation of mixtures of powders (Iveson et al. 1996).

Wet agitated granulation involves the injection of a liquid binder into a fluidized bed of solid powder. The liquid binder is distributed into the fluidized bed by the spray nozzles and through the mixing action of the fluidized bed. As the liquid and solids mix, the solids become coated with the liquid binder solution. When coated particles come into contact, the liquid binder produces a liquid bridge, creating a cohesive force that binds the particles together. The liquid binder often contains a soluble material that is left deposited on the fluidized solid particles after the solvent evaporates, which holds the solid particles together. Granules of many different sizes may initially form; however, due to the shear forces present inside the fluidized bed, only small, stable granules survive. The size of the granules may be controlled using attrition nozzles that inject high velocity gas into the fluidized bed (Pacek et al. 1991).

1.1.2 LDPE Production

One process used to produce low density polyethylene (LDPE) incorporates a fluidized bed reactor using reacting monomer (ethylene) as the fluidization gas and catalyst particles as the fluidized solids. The reaction is exothermic; therefore heat must be removed from the reactor to ensure favorable equilibrium conditions are met. One way to cool the reactor is to condense monomer molecules using a compressor, a heat exchanger, and the addition of an inert condensable component to the feed stream. The condensable components raise the dew point of the monomer stream, thereby making it possible to produce liquid condensate. The condensate is injected back into the reactor through a series of spray nozzles located close to the fluidized bed distributor, where it evaporates, and cools the reactor contents (Jenkins III et al. 1986)

The higher the flow rate of liquid injected into the reactor, the larger the decrease in reactor temperature. However, if the liquid flow rate is too high, it will not evaporate fast enough, and the fluidized bed will begin to flood. Flooding leads to poor gas distribution and results in gas channeling through the fluidized bed. Liquid accumulation on the distributor grid can also lead to undesirable agglomerate formation on top of the distributor plate, leading to fouling and subsequent reactor malfunction.

The quality of liquid distribution inside a fluidized polyethylene reactor must be high to maximize the liquid flow rate into the reactor without leading to liquid

accumulation above the distributor grid. Smaller droplet sizes and uniform liquid distribution are necessary to ensure the rate of evaporation of liquid is fast enough to operate the reactor at the optimal reaction temperature without flooding. Spray nozzle geometry and location play an important role in setting these parameters and therefore optimizing the yield of desired products.

1.1.3 Fluid Catalytic Cracking

Fluidized Catalytic Cracking (FCC) is a process developed to convert heavy oil fractions into lighter, more valuable products such as olefins, gasoline and distillates (Patel et al. 2012). The FCC unit is a riser reactor comprising of three zones: feed injection, dense phase, and dilute phase region. The liquid reactants are sprayed into a rising stream of fluidization gas and catalyst pellets in the feed injection region. The liquid products quickly vaporize and contact the catalyst in the dense phase region. Cracked vapors are produced in the dense phase region and flow upwards into the dilute phase region. The product vapors and catalyst travel to the top of the reactor and are separated by means of centrifugal force. Product vapors are distilled, with heavy components recycled back to the FCC reactor. Spent catalyst is sent to a regenerator, which uses air to burn residual coke that has formed on the catalyst surface. The heat of combustion raises the temperature of the catalysts, and provides the heat necessary to drive the endothermic cracking reaction. The regenerated catalysts are recycled back to the feed injection zone, where they again react with the heavy oil reactants.

The quality of liquid feed distribution into the rising gas-catalyst stream can play an important role in affecting product selectivity. The distribution of liquid reactants across the cross section of the feed section must be as uniform as possible to optimize the contact area between the reactant and catalyst (Niccum, 1985), and to ensure fast vaporization of the feed droplets. Fast vaporization of liquid feed droplets is essential in order to maintain high velocities in the riser reactor (which increases the drag force on the rising catalyst particles) and to reduce the mass of catalyst required to vaporize all the feed (Gupta et al. 2010). Droplets that are too small lack enough momentum to travel into the center of the riser, thereby increasing the reactant concentration along the outer region of the riser, and wasting catalyst located in the central region (Patel et al. 2012). It is

often assumed that the rate at which liquid evaporates and is transported to the catalyst particle is much faster than the reaction time. However, this assumption is not necessarily valid if liquid droplets produced by the spray nozzles are too large. Large spray droplets take longer to vaporize and lead to excessive coke formation on the catalyst surface. Large droplets also lead to formation of wet liquid solid agglomerates, which may stick to the reactor wall and produce excessive fouling in regions throughout the reactor. Wilson (1997) outlines some of the previously developed FCC feed injection systems.

1.1.4 Fluid CokingTM

1.1.4.1 Process Description

In 2004, the Alberta Energy and Utilities Board estimated a total proven oil content of approximately 170.2 billion barrels in Northern Alberta, 99% of which is found in oil sands (Canada National Energy Board, 2004). Oil sands (also known as tar sands or bituminous sands) consist of bitumen impregnated into porous sandstone or carbonate rock (Speight et al. 2001). Bitumen is very high viscosity oil, consisting predominately of large aromatic rings of carbon compounds. Due to its high viscosity, bitumen does not flow easily, making it difficult to recover at reservoir conditions. For deposits located close to the surface, open pit mining is used as a method to recover bitumen from oil sands. For bitumen deposits located at a depth greater than 75 m below ground, an in-situ process is used (Williams et al. 2005). An in-situ process usually involves the injection of steam or a solvent underground in order to reduce the viscosity of the bitumen, allowing it to flow to the surface in a similar fashion to conventional oil recovery.

Bitumen consists of high molecular weight hydrocarbon compounds, and contains many impurities such as sulfur, nitrogen, oxygen, and heavy metals, thereby making it unsuitable to refine in most conventional refineries. After bitumen is recovered from the reservoir, it is sent to an upgrading facility. Upgraders contain the necessary unit operations required to reduce the molecular weight and impurity content of the bitumen before it is sent to a refinery. Some of the unit operations found at an upgrading facility includes atmospheric and vacuum distillation, thermal cracking, hydrocracking,

hydrotreating, and diluent blending. The product of upgrading bitumen is synthetic crude oil; an oil that may be sent to conventional refineries for further processing.

Fluid CokingTM is a process developed to thermally crack heavy, non-vaporizable hydrocarbon liquids into lighter distillable products, suitable for atmospheric and vacuum distillation units found at conventional refineries. The process begins by preheating bitumen to about 350°C to reduce its viscosity to that of water at room temperature (Pfeiffer et al. 1959). This provides some of the heat required to induce thermal cracking reactions, and also reduces the resistance of flow through the spray nozzles that inject the bitumen into the reactor. The bitumen is mixed with atomizing steam in a mixing chamber and the two-phase bubbly flow travels through a series of injection nozzles. These nozzles are located at various locations around the height and circumference of the reactor in order to improve liquid distribution and reduce the over-wetting of coke particles. The atomizing steam helps aid in the breakup of bitumen liquid into small droplets. As the droplets travel to the interior of the reactor, they coat hot coke particles, which transfer heat to the bitumen required to induce an endothermic cracking reaction. Volatile hydrocarbon molecules and coke are produced at the coke-bitumen interface. The volatile compounds diffuse through the layer of bitumen coating the coke particle into the bulk gas phase, where they are transported with the fluidization gas to the top of the reactor. The resulting coke forms a layer around the initial coke particle, causing the initial coke particle to grow in size.

The Fluid Coking vessel consists of various sections: the reaction zone, the stripping zone, the scrubbing zone, the fractionators and the burner. In the reaction zone, bitumen is introduced into the vessel via spray nozzles and is distributed among the individual coke particles. The temperature in this section is typically 480°C – 600°C and it operates at a pressure between 0-345 kPag (Pfeiffer et al. 1959). Hot product vapors and fluidization gas rise to the top of the reaction zone and flow through a series of cyclones. The cyclones separate solid particles that were entrained in the gas phase back to the reaction zone, and direct the flow of vapors to the scrubbing section. The scrubber cools the vapor products in order to condense and recycle high boiling point components, which are returned to the reaction zone. The scrubbed vapors pass through a fractionating section, which further separates the products based on vapor pressure. Heavier

components formed in the fractionating section condense, and are used to cool incoming vapors in the scrubbing section. Light components that do not condense in the fractionating section exit through the top of the Fluid Coking vessel, flow through a condenser, and are sent to another location within the upgrading facility. Heavier components are mixed with the incoming feed stream and are recycled back to the reactor for further cracking (Devuluri et al. 2012).

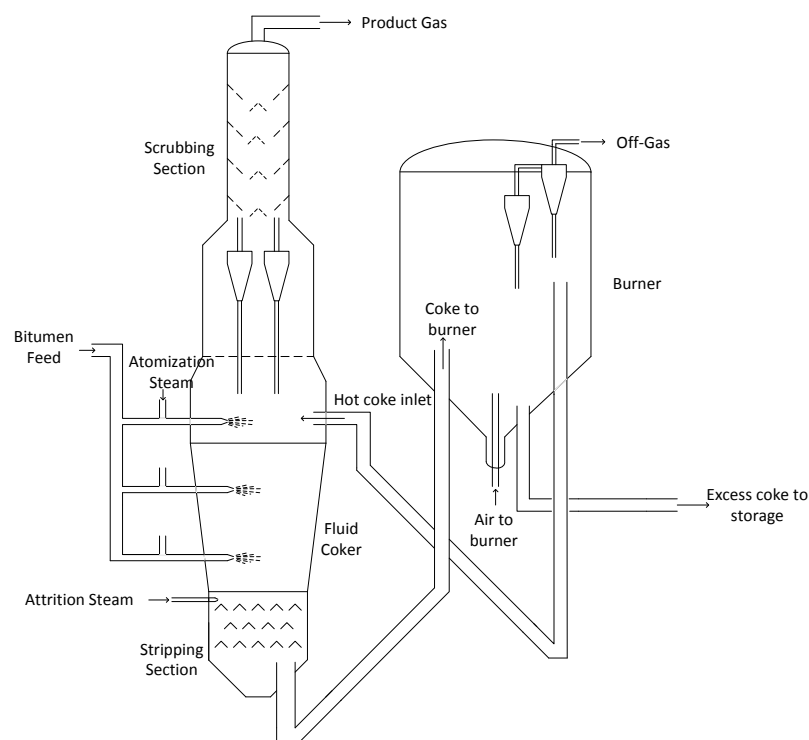


Figure 1.1: Simplified process flow diagram of a Fluid Coker reactor

Particles that fall to the bottom of the reactor pass through a stripping section to remove hydrocarbons trapped on the surface of the coke. The stripped coke particles are pneumatically transported to a burner, where air is introduced, partially combusting the coke to generate heat and combustion exhaust. The heat of combustion increases the temperature of the remaining, unburned coke particles, which are recycled back to the reaction section of the Fluid Coker or sent to storage.

1.1.4.2 Stripping Section

The stripping section of a Fluid Coker removes trapped hydrocarbon products from the surface of coke particles falling to the bottom of the reactor. This is necessary as it maximizes the conversion of reactants to desirable products and reduces the formation of undesirable vapors in the burner (that may lead to fouling and run length limitations in the burner overhead) (Devuluri et al. 2012). The stripper section consists of sheds (conduits) that span cord lengths along the cross section of the vessel at various heights. A gas sparger is located under the sheds at the bottom of the Fluid Coker, sending fluidization steam upwards through the stripping section, counter current to the direction of falling coke particles. The sheds redistribute the fluidization gas evenly across the cross section of the stripping zone, thereby enhancing the contact between the gases and descending coke particles.

An issue that is commonly encountered in the stripping section is the fouling of the stripper sheds. Wet agglomerates of coke particles may stick to the surface of the sheds, and reduce the area through which the fluidization gas can pass through. This can lead to poor coke circulation and reduced fluidization velocity throughout the reaction zone. Bi et al. (2004) discuss a V-shape stripper shed geometry that can be used to reduced stripper fouling and improve contact between the fluidization gas and descending coke particles. Sanchez et al. (2013) investigated the configuration of V-shape stripper sheds as well as the fraction of cross sectional area covered by the sheds in the stripper zone of a pilot scale cold model Fluid Coker. A grid-like mesh configuration was found to be advantageous for the prevention of liquid flow through the sheds, as well as the prevention of vapors reaching the stripper level inside the reactor. As well, it was found that using the current stripper shed configuration, the fraction of open area within the stripper section should be around 60-70% to reduce loss of valuable liquids to the burner.

1.1.4.3 Scrubber Section

Product vapors and steam rise to the top of the reaction zone and pass through one or more cyclones. The cyclones remove the majority of entrained solids by centrifugal

force, recycling these solids back into the reaction zone. The vapors pass through the top of the cyclones into the scrubbing section, where they ascend through a series of internal sheds. Cooling oil descends around the internal sheds, and contacts the rising vapors, cooling and removing heavy fractions from the vapors in the process (McKnight et al. 2011). The product vapors are cooled to a temperature of approximately 370°C - 400°C (Pfeiffer et al. 1959). Some of the liquids formed are cooled and recycled back to the top of the scrubbing zone, while the rest is recycled back to the reaction zone for further reaction.

The scrubbing section resides above the cyclones and consists of inverted V-shaped sheds to enhance the contact between the rising hot vapors and the descending cooling oil. A de-entrainment grid is located above the sheds to further remove solids and oil droplets from the vapor product stream.

Vapor products exiting the cyclones can enter the scrubbing section with a high rotational velocity, causing the majority of the vapor to migrate towards the walls of the vessel. The uneven distribution of product vapors in the scrubbing zone creates a high velocity region near the walls, where the hot gases carry oil droplets above the scrubber sheds and deposits these droplets on the de-entrainment grid. The deposited oil can react and form coke on the de-entrainment grid due to the heat provided by the rising product vapors, causing the grid to plug. This reduces the area through which the product vapors rise through the scrubbing section, increases the velocity, and decreases the contact time with the cooling oil. As fouling intensifies, the removal of solids, metals, and heavy components decrease, leading to poor product gas quality. This may have detrimental effects on downstream operations, such as catalyst poisoning in the Hydrotreating unit. One way to improve product gas/cooling oil contact is suggested by Bulbuc et al. (2010). Adding baffles above the cyclone exit can slow down the product vapor velocity near the walls and enhance the uniformity of the gas flow throughout the cross section of the scrubber section, thereby reducing the entrainment of liquid into the rising vapor product stream and reducing the formation of coke deposits on the de-entrainment grid located at the top of the scrubber section (McKnight et al. 2011).

1.1.4.4 Reaction Section

The reaction section of a Fluid Coker comprises of the following subsections:

Table 1.1: Typical dimensions of a Fluid Coker vessel (Pfeiffer et al. 1959)

Section	Diameter (m)	Height (m)
Top straight side	2.75	6
Wide Diameter	3.35	5
Middle section cone	1.2 x 3.35	10.3
Stripper section	1.2	3

The dimensions of Fluid Cokers currently in use may be different from that reported by Pfeiffer et al. (1959); however a similar geometry is still in use today for reasons explained below. The vessel expands in diameter from the bottom to the disengaging region at the top of the reaction zone in order to handle the increased mass flow rate of vapors that are formed when bitumen reacts on the surface of the coke particles, and to therefore keep the fluidization velocity constant along the height of the fluidized bed. The disengagement section at the top of the reactor is reduced in diameter in order to accelerate the velocity of the gas exiting the reactor and entering the cyclones. This reduction in diameter reduces the residence time of the product vapors in the reactor to prevent excessive thermal cracking reactions.

The reaction section operates at a temperature of approximately 480 °C. The high temperature is needed to supply the energy required to break apart the bonds holding the long hydrocarbon chains and aromatic rings together. The pressure of the reaction zone is generally kept quite low, and is set to approximately 75 kPag to promote the production of vapor products. The solids in the fluidized bed may reach a height of up to 18 m and they are constantly fluidized by steam and product vapors. A study by Song et al. (2004)

on Fluid Coker hydrodynamics revealed that the void fraction of the fluidized bed inside the reaction zone tends to be higher near the walls and lower in the center region, creating a core-annulus flow structure. The solids tend to fall to a lower elevation along the walls of the reactor, and are carried upward by fluidization gas in the center region. Since more solid coke particles tend to accumulate near the walls of the reactor, the solids are entrained in the feed jets formed by the spray nozzles. The interaction between the solid coke particles and the bitumen plays an important role in determining the overall conversion of bitumen to distillable liquids.

1.1.4.5 Burner

The burner is responsible for generating the heat of reaction necessary to carry out the endothermic cracking reactions in the reaction zone of the Fluid Coker. Solids that descend to the bottom of the reactor are pneumatically transported to a burner vessel. The burner is another fluidized bed consisting of coke particles fluidized by air. The temperature of the burner is operated higher than the reaction section (540°C - 820°C) and is controlled by adjusting the flow rate of air entering the vessel. Oxygen reacts with some of the coke particles residing inside the burner to produce exhaust and heat. The heat is transferred to the remaining coke particles, some of which are fed back to the reaction section of the Fluid Coker vessel (Worley et al. 1982). If excess coke is present in the burner, it is transferred pneumatically to storage. The feed rate of hot coke particles back to the reaction section is dependent on the temperature difference between the burner and reaction section (Pfeiffer et al. 1959). The higher the temperature difference, the lower the flow rate of coke particles recycled back to the reaction section.

1.2 Agglomerate Formation in Fluidized Beds

Agglomerate formation occurs when solids stick together due to short range chemical or physical processes among themselves, or by binders, which form cohesive bridges between the solid particles, holding them together (Pietsh, 2003). Bruhns et al. (2005) showed that agglomerates tend to form when a liquid is injected into a fluidized bed. Agglomerate formation is desirable in many chemical processes; however, it is detrimental to Fluid Coker performance. Agglomerates tend to decrease the yield of distillable liquids, increase the coke yield, and foul stripper sheds (Sanchez et al. 2013).

Gray (2002) describes the mechanism through which bitumen droplets coat coke particles in a Fluid Coker. Relatively large liquid droplets are injected into a fluidized bed and engulf several smaller solids, filling the pores between these solids. Cohesive forces between the solid particles and the liquid binder keep the granules intact. Shear forces generated by surrounding fluidized particles and granules act on the newly formed granules to break them apart. If the originally formed agglomerates are unstable, they will break apart into individually coated solid particles, which are desired for the Fluid Coking process. However, if the quality of the liquid distribution among the fluidized particles is poor, the agglomerates formed by the jet-bed interaction may not break apart easily. In this case, the agglomerates remain intact, and due to the weight of the agglomerate, the bed of solids will not remain properly fluidized.

Liquid injection applied to the Fluid Coking process tends to lead to the formation of agglomerates that are stabilized by unreacted bitumen, which acts as a liquid binder. The level of saturation within an agglomerate is a measure of the fraction of the pore space between the solid particles that is filled with liquid. An agglomerate in the pendular state of liquid saturation consists of solids that are held together by liquid bridges. Voids exist between the solid particles where no liquid or solids are present. An agglomerate in the capillary state consists of solids whereby each void is completely filled with a liquid binder. Agglomerates that have a portion of the void spaces between solids filled with liquid binder are termed *funicular*, and the forces that hold these agglomerates together are a combination of the forces that hold the pendular and capillary state agglomerate together.

The stability of agglomerates formed inside a fluidized bed is a complex phenomenon since there are many factors that can influence the outcome. The liquid content of an agglomerate does not necessarily predict its fate within a fluidized bed. It is the various forces that act on and within an agglomerate that are responsible for the overall stability of the agglomerate. The different forces that hold agglomerates together include surface tension and capillary forces, viscous forces, and inter-particle friction forces (Iveson, 2001). These forces may be altered by changing properties of the solids or liquid binders holding the agglomerates together. Surface tension tends to pull particles close together and is a function of liquid binder composition, temperature, particle

composition and geometry. The viscosity of the binder plays a large role in controlling how easily solid particles move within the agglomerate. The higher the viscosity, the higher the energy input required to move the solids through the liquid binder. In the Fluid Coking process, viscosity plays an important role, since the viscosity of the liquid film covering the bitumen particles tends to increase as the extent of reaction proceeds towards completion (Aminu et al. 2004).

Weber et al. (2008) studied the stability of agglomerates produced from sand/water and glass bead/water mixtures in a small scale fluidized bed. It was reported that the fluidization velocity plays a significant role in determining the type of breakage mechanism, erosion or fragmentation, which will cause agglomerate destruction. Erosion occurs at lower fluidization velocities, while fragmentation of agglomerates occurs at high fluidization velocities.

The properties of agglomerates that can affect their stability include initial agglomerate size, agglomerate density, and liquid binder composition (Weber et al. 2008). Large and dense agglomerates tend to be more stable at lower fluidization velocities, where erosion is the dominant mechanism of destruction. Weber et al. (2008) demonstrated how the effect of binder viscosity can have a significant impact on agglomerate stability, but the marginal increase in agglomerate stability is reduced as viscosity is increased.

In Fluid Cokers, high quality distribution of liquid among the coke particles is vital because it minimizes the formation of stable liquid-solid agglomerates, which reduce the conversion of bitumen to distillable products. These liquid solid agglomerates also stick to the Fluid Coker internals, which can hinder the quality of fluidization of solids. In order to reduce the impact of agglomeration, the reactor temperature must be raised to increase the rate of reaction. This helps to raise the temperature of bitumen trapped in agglomerates, allowing the liquid to react and form vapor products. Raising the reactor temperature above optimal conditions leads to higher energy input, increased pollutant generation, and a reduction in desirable product selectivity (House et al. 2004).

One of the main objectives of Fluid Coker spray nozzle design is to maximize the contact area between bitumen and hot coke particles. Maximum contact will occur when

agglomerate formation is minimized, and the stability of the agglomerates produced is low. Various spray nozzle designs have been proposed in academia and industry, and are discussed next.

1.3 Spray Nozzles

1.3.1 Standard Fluid Coker Spray Nozzle Description

Liquid feed is injected into the Fluidized Coker in the form of atomized droplets. The nozzle used to atomize the droplets and distribute them into the fluidized bed (Figure 1.2) is described by Base et al. (1999).

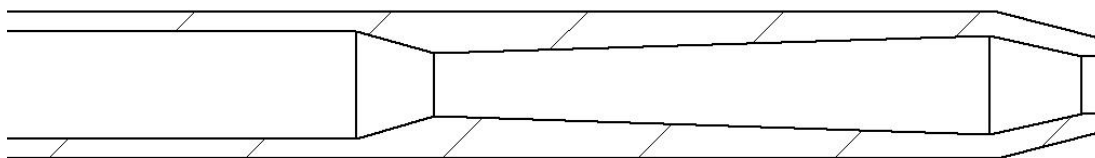


Figure 1.2: TEB nozzle developed by Base et al. (1999)

Atomization steam is injected along with liquid bitumen through the spray nozzles, producing a two phase bubbly flow. This type of atomization is known as effervescent atomization, and is reviewed in detail by Sovani et al. (1999). The two phase flow enters the nozzle at 8 (shown in Figure 1.3) as a continuous liquid phase with dispersed gas bubbles. Restriction 10 accelerates the fluid, creating a velocity gradient between the continuous liquid phase and gas bubbles. The difference in velocity between the two phases helps to enhance gas distribution inside the liquid, creating finer bubbles. Expansion section 11 and converging section 12 produce further shear between the two phases by changing the velocity of the fluid, further enhancing the mixture of gas and liquid. At the nozzle tip, (13 in Figure 1.3), the pressure of the two phase fluid rapidly decreases as it enters the reactor. The decrease in pressure causes the gas bubbles to expand, and a phase inversion occurs (Poutgatch et al. (2012)). The sudden expansion of the gas shatters the liquid into small droplets, and propels them both outwards away from the longitudinal axis of the nozzle, and towards the interior of the reactor.

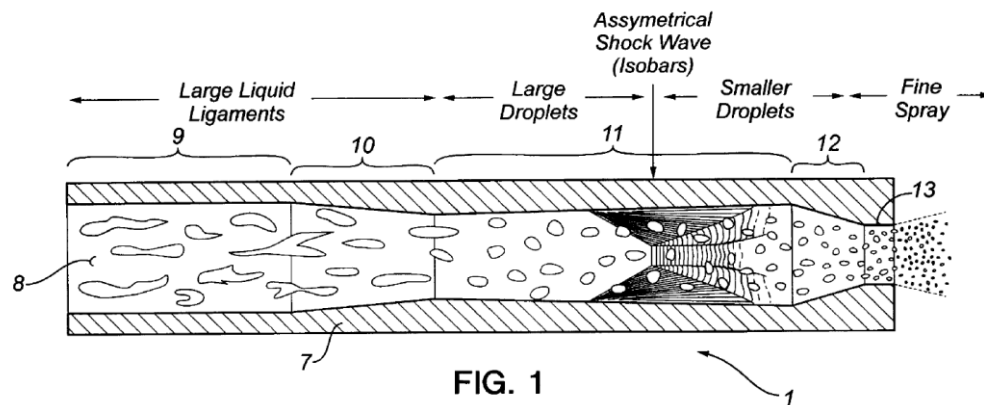


Figure 1.3: Formation of shockwaves inside a TEB nozzle (Base et al. 1999)

Adding more gas for a given liquid mass flow rate (increasing the gas-to-liquid mass ratio, or GLR) increases the pressure gradient at the tip of the nozzle, and enhances atomization and distribution of the droplets formed at the nozzle exit.

1.3.2 Nozzle Additions and Alterations

Various alterations and additions to the TEB spray nozzle have been proposed. These include changes to the internal geometry of the spray nozzle, attachments at the end such as a cloverleaf, impact plate, and draft tube.

Poutgatch et al. (2012) investigated the effect of a conical shaped diverging attachment to the end of the spray nozzle on droplet size and spray dispersion angle using

a numerical model. The addition of an attachment with an expansion angle smaller than the natural expansion angle of the spray decreased the spray angle and increased the droplet size. When the expansion angle of the conical attachment was increased to the natural expansion angle of the spray, it had a negligible impact on the resulting spray angle and droplet size. The authors concluded that conical attachments with small expansion angles may be useful for producing a spray of higher penetration and lower dispersion capability. However, it is apparent that a conical attachment reduced the radial momentum transfer between the gas and liquid, making it unsuitable for dispersion at low expansion angles, but possibly beneficial at large expansion angles.

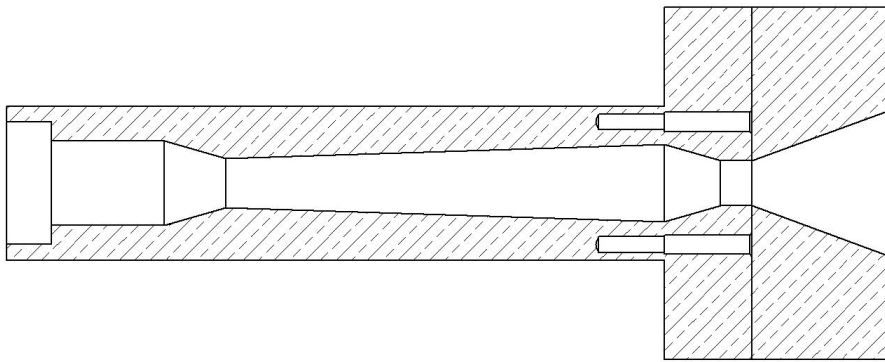


Figure 1.4: TEB nozzle attachment with conical nozzle attachment used in simulation by Poutgach et al. (2012)

One of the disadvantages of the spray nozzles currently used is that the spray produced by these nozzles is circular in cross section. A circular spray pattern minimizes the surface area to perimeter ratio of the spray. As a result, much of the coke surrounding the jet may not penetrate into the core of the jet, which reduces the contact area between the bitumen and coke particles (Chan et al. 2012). The cloverleaf nozzle attachment is added to the end of the spray nozzle presented by Base et al. (1999). It consists of four divergent, quasi-conical flow passages (lobes) that meet at the second convergent section of the regular nozzle. The purpose of these lobes is to increase the surface area to perimeter ratio of the spray injected into the fluidized bed, thereby increasing the contact area between the spray and fluid coke particles (Chan et al. 2012).

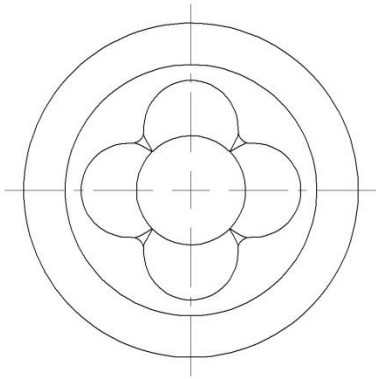


Figure 1.5: Cloverleaf nozzle attachment (view of tip) (Chan et al. 2012)

Sprays produced by Fluid Coker nozzles tend to have a liquid dense region at the center of the jet. McMillan et al. (2005) investigated the effect of adding an enhanced solids entrainment device (ESE) downstream of the nozzle exit in an effort to improve the distribution of liquid onto fluidized solids. The ESE is a curricular conduit installed coaxially downstream of the nozzle exit (Chan et al. 2006). The jet enters the fluidized bed at a high velocity, and produces a low pressure region adjacent to the jet boundary. Solids are entrained in the jet in this low pressure region. The jet then enters the ESE, where turbulence is enhanced due to the interaction of the spray and conduit walls. The turbulence aids in transferring solids from the jet periphery (where they are entrained), into the center of the jet, which is rich in liquid. This produces better contact between the liquid and solid particles.

House et al. (2009) investigated the effect of an impact cone on liquid dispersion in a fluidized bed. An impact cone is a conical attachment added at a distance downstream of the nozzle exit, with the point of the cone directed toward the nozzle exit orifice. The tip of the cone disperses the spray in a radial direction upon impact, thereby dispersing the dense liquid region which forms at the center of the jet. The authors showed that the impact plate distributes liquid most effectively when it is located in the immediate vicinity of the nozzle tip. A limitation of the impact cone is that a portion of the momentum carried by the jet is transferred to the impact cone, thereby reducing the penetration length of the jet.

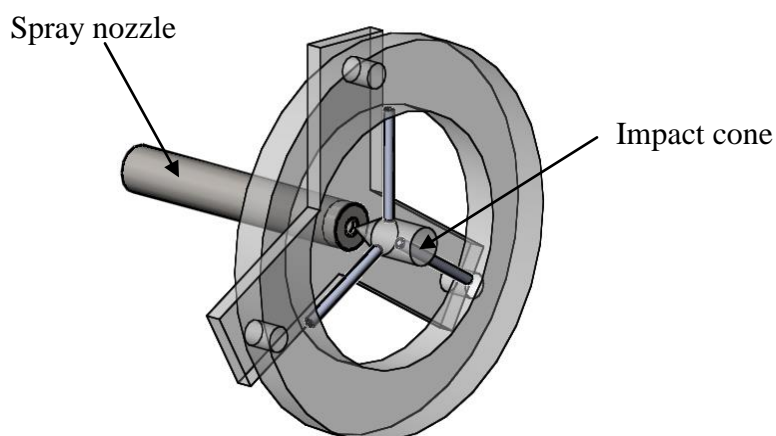


Figure 1.6: Impact cone investigated by House et al. (2009)

House et al. (2009) also investigated the effect of gas shrouds installed around the nozzle exit orifice. Gas shrouds were believed to aid in solids entrainment into the jet, and expand the size of the jet, thus increasing the contact area between the liquid and solid fluidized solids. The authors showed that the implementation of gas shrouds decreased the amount of liquid trapped in large agglomerates and therefore distributed the liquid better than the stand alone Fluid Coker nozzle.

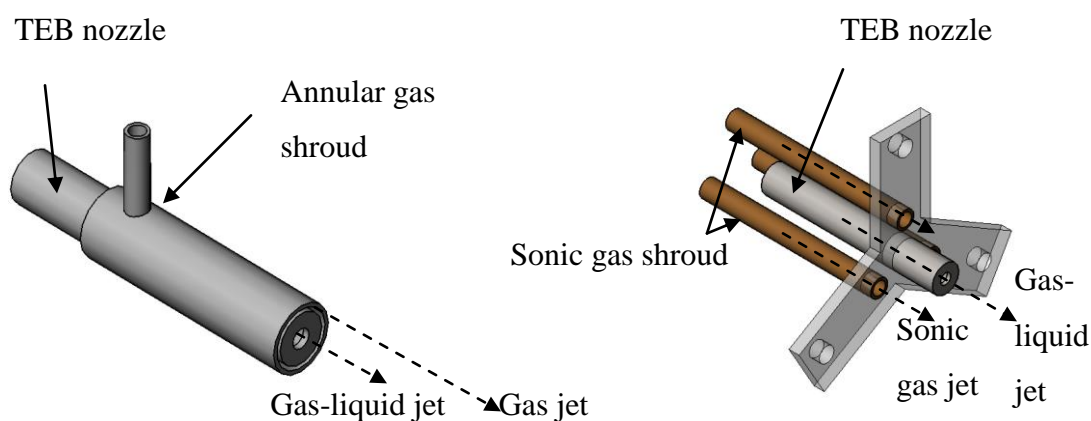


Figure 1.7: Left: annular gas shroud. Right: Sonic gas shroud. Both shrouds were investigated by House et al. (2009)

Portoghese et al. (2010) investigated the effect of the Fluid Coker geometry on the interaction between the gas-liquid spray and fluidized bed particles. A scaled down Fluid Coker nozzle was compared to a nozzle with an additional expansion zone downstream the second convergent section, and a nozzle with only one convergent and one divergent section. Using a conductance measurement technique to measure the quality of liquid distribution among the fluidized solid particles, the authors found that the best performing nozzle geometry is the current Fluid Coker nozzle with the additional expansion region. The addition of a final diverging section increases the stability of the spray, which the authors found to be a significant variable in determining liquid/solid contact efficiency.

1.3.3 Effervescent Nozzles and Atomization

Effervescent atomization nozzles involve internal mixing between an atomizing gas and a liquid. A two phase flow is produced within the nozzle body, and is ejected through an exit orifice. As the gas mixes with the liquid, it expands, producing bubbles, reducing the characteristic liquid dimensions within the discharge orifice (Sovani, et al. 2001). At the nozzle exit, the pressure is reduced, causing further gas expansion. The expanding gas bubbles at the nozzle exit break the liquid ligaments into small droplets. The TEB nozzle used for the Fluid Coking process may be classified as a type of effervescent nozzle, thus studies completed on effervescent atomization may be relevant to understanding the spray characteristics observed using Fluid Coking spray nozzles.

Effervescent nozzles consist of four main components: the gas and liquid supply ports, a mixing chamber, and an exit orifice. Since a two phase flow is formed, the flow through the exit orifice becomes choked at a much lower velocity than would occur if the fluid is a pure liquid or pure gas. For example, the speed of sound through an air/water mixture is about 20 m/s. The speed of sound through air alone is 340 m/s, and the speed of sound through pure water is 1440-1480 m/s (Kieffer et al. 1977). Thus the presence of both phases dramatically reduces the speed of sound through the fluid, allowing choked flow to be reached at much lower velocities compared to either fluid alone. Choked flow at the orifice exit is desirable, since it produces a steep pressure gradient. The expansion

of gas at the exit orifice from a high pressure to a low pressure helps to break the liquid ligaments into small droplets.

Two main characteristics of effervescent nozzles that distinguish them from other types of atomization are:

Gas takes up a portion of the exit orifice area, reducing the area for liquid to flow through. This helps to elongate the liquid into thin ligaments that can be easily broken apart.

A large pressure drop occurs at the orifice exit where gas bubbles or gas slugs expand. The expansion of the gas shatters the ligaments of liquid into small droplets. The higher the pressure of the atomization gas inside the nozzle, the greater the expansion of the gas upon exiting the orifice, and the smaller the resulting liquid droplet size.

Huang et al. (2008) investigated the flow pattern inside an effervescent nozzle using a high speed camera. The authors identified three different flow regimes that exist inside the nozzle: bubbly flow, intermittent, and annular flow. Bubbly flow is characterized by the presence of gas bubbles inside the nozzle, which remain separated as the gas-liquid mixture travels towards the orifice exit. Bubbly flow is stable, in that the flow pattern does not change with time. Bubbly flow tends to occur at very low gas-to-liquid ratios ($GLR < 3\%$). The authors note that at low GLR, the Sauter mean diameter (SMD) of the droplets tends to be much larger when compared to higher GLRs.

An intermittent flow regime occurs as the GLR is increased past 3%. Intermittent flow regimes are characterized by the formation of bubbles inside the mixing chamber, followed by the formation of an annular flow regime at a later time. The two regimes switch back and forth with time and form pressure instabilities within the mixing chamber.

Further decrease in the liquid flow rate (or rise in GLR) leads to the formation of an annular flow regime. This regime is characterized by the formation of a central gas rich flow surrounded by an annulus of liquid inside the nozzle mixing chamber. A gas slug is formed, and grows in length back towards the gas entrance into the nozzle. Liquid

forms an interface with the gas around the gas slug. As the gas slug grows in size, pressure instability develops causing the interface to break and liquid to penetrate into the center of the mixing chamber. This occurs in a periodic fashion, causing intermittent pulses of gas and liquid to flow through the exit orifice. The transition from the intermittent flow to annular flow regime is dependent upon the operating pressure of the nozzle.

For Fluid Cokers, an important characteristic of the spray produced by the spray nozzle is the Sauter-mean diameter of the droplets. Base et al. (1999) indicates that the probability of a collision between a bitumen droplet and coke particle is maximized when the diameter of the liquid droplet and coke particle is approximately equal. Smaller droplets will form when the operating pressure of the two phase flow is increased or the liquid flow rate is decreased. A compromise must be met between the droplet size, the spray penetration length, and the mass flow rate of atomization gas used.

1.4 Review of Liquid Distribution and Liquid/Solid Mixing Measurements Methods in a Fluidized Bed

The distribution of injected liquid inside a fluidized bed is essential for efficient reactor performance, as a better distribution of liquids leads to a larger reaction surface and reduces the tendency of solids to agglomerate together. Several researchers have developed methods to measure the quality of liquid/solid interaction inside a fluidized bed in order to quickly assess the performance of spray nozzle geometries and operating conditions.

Knapper et al. (2003) developed a method to investigate the liquid distribution produced by spray nozzles inside a hot model Fluid Coker. A pulse of copper naphthenate tracer was added to a stream of gas-atomized bitumen, which was ejected through a spray nozzle into a hot fluidized bed of coke particles. Upon entrance into the reactor, the bitumen reacted on the coke particle surface, leaving traces of copper. Samples of coke were retrieved from the vessel and were tested for bulk copper concentration (using Inductively Coupled Plasma) and individual particle copper concentration (using energy dispersive X-ray analysis). Analysis of copper concentration on individual coke particles indicated that many coke particles were not coated with

copper, and therefore had not been in contact with bitumen. This led the authors to believe that the current Fluid Coker nozzles were ineffective at evenly distributing liquid among the fluidized coke particles. The results identified a need for further research to improve the spray nozzle performance.

The technique developed by Knapper et al. (2003) was effective at evaluating spray nozzle performance; however, it is costly (due to the parts required for a pilot scale hot model Fluid Coker), and time consuming (due to the need to remove all coke particles after each test). As a result, researchers looked for alternative ways to investigate spray nozzle performance using a cold model (usually using sand to represent coke, water to represent bitumen, and air to represent steam).

Leach et al. (2008) developed a new method to quickly evaluate the performance of aerated spray nozzles in a cold model fluidized bed using a triboelectric charge technique. Fluidized silica sand particles were charged due to random collisions with the wall of the vessel. Water was injected through a converging-diverging spray nozzle, and shortly after, the bed was defluidized. The charges that had accumulated on the sand particles flowed through conductive paths in the sand created by moisture. The current travelled to an electrode installed inside the vessel, where it was converted to a voltage signal, amplified, and sent to a data acquisition system. A higher current measurement corresponded to more pathways for the charges to travel, and hence indicated better liquid distribution. The authors used this technique to measure the performance of two different variations of a Fluid Coker spray nozzle, and results agreed with past experimental data. The advantage of this technique was that spray nozzle liquid distribution data could be quickly obtained at a relatively low cost. The drawbacks were that the technique was only applicable to scaled down spray nozzles, and that only one electrode was used, meaning only local liquid distribution could be measured. As well, the accumulation of charges on the solid particles is dependent on the local hydrodynamics of the bed, which may vary significantly due to the variation in liquid distribution produced by different spray nozzles.

Portoghese et al. (2008) expanded upon the triboelectric charge technique by measuring the conductance of electricity through the fluidized bed after liquid had been

sprayed inside. A rod electrode was placed inside the fluidized bed, in series with a measurement resistor and a power supply. The walls of the bed were grounded to complete the circuit. After liquid was injected, and the bed was defluidized, current passed from the power supply through the measurement resistor, electrode, and wetted sand particles, to ground. A voltage reading across the measurement resistor was amplified and recorded. Using Ohm's Law, the conductance of the bed could be determined. The intensity of the conductance inside the fluidized bed related to the moisture distribution inside the bed. A higher conductance corresponded to better liquid distribution. Portoghese et al. developed this method using only one electrode, limiting its capability of measuring the average moisture distribution throughout the fluidized bed.

Farkhondehkavaki et al. (2012) also used the conductance technique to investigate the jet bed interaction and liquid distribution in a fluidized bed. The authors compared the results obtained using a metallic rod electrode (which protruded through the length of the fluidized bed), and the results obtained using non-intrusive metallic plates (which were installed with insulation on one side of the fluidized bed). After adjusting the gas-to-liquid ratio of the liquid injection in the fluidized bed, the authors found a similar conductance trend was observed using both types of electrodes. It was also found that the conductance measurements observed using the rod electrode was systematically higher than the conductance measurements observed using the plate electrodes. The authors attributed the difference in conductance readings to the fact that the rod electrode may influence the quality of fluidization near the center of the vessel, causing agglomerates to break around the electrode. As well, it was suggested (and verified) that the distribution of liquid throughout the fluidized bed was not even.

Zirgachian et al. (2013) expanded upon the conductance technique investigated by Farkhondehkavaki et al. (2012) by adding multiple rows of square plate electrodes to the wall of a fluidized bed, while keeping the opposite wall grounded. The plate electrodes were advantageous over previously used rod electrodes in that they were non-intrusive (they did not affect fluidization hydrodynamics). As well, using multiple electrodes, the authors were able to create contours of the uneven liquid distribution throughout the vessel, as well as obtain average bed moisture readings. The method was carried out on a large scale fluidized bed using a commercial scale Fluid Coker nozzle, so scale-up effects

were eliminated. The method proved useful in determining the effect of gas-to-liquid ratio on liquid distribution throughout a fluidized bed.

As an alternative to measuring the bed conductance, Mohagheghi et al. (2013) used capacitance electrodes in a similar fashion to the conductance electrodes used by ZirGachian et al. (2013). Due to the large difference in dielectric constants between water, sand, and air, the authors were able to measure the free moisture content (the liquid content inside a fluidized bed not trapped in agglomerates) throughout the fluidized bed based on the capacitance measurement of the bed at various locations. This method is advantageous as the capacitance electrodes are non-invasive, and therefore do not alter the fluidized bed hydrodynamics. Since the capacitance of the bed does not vary if liquid is trapped inside agglomerates, this technique was valuable in determining the rate of moisture released from agglomerates, as only free moisture could be measured. By monitoring the evaporation rate of water from the fluidized bed, and the capacitance of the bed with time, the authors were able to track the amount of moisture trapped in agglomerates as a function of time, and to identify the effect of bed hydrodynamics on the rate of liquid released from agglomerates.

1.5 Research Objectives

The preceding review has covered various aspects of the Fluid Coking process, including agglomerate formation and stability, spray nozzle performance, and measurement of liquid distribution inside fluidized beds. The major objective of this thesis is to further understand and improve the performance of a Fluid Coker nozzle applied to gas-liquid injection inside a fluidized bed. The performance of the nozzle will be evaluated by measuring the rate of liquid released from the agglomerates formed by the spray. The following steps will be taken to achieve the objective:

1. Develop a method to measure the rate of liquid released from agglomerates inside a fluidized bed. The method will expand upon the technique developed by ZirGachian et al. (2013) which used bed conductivity to measure the distribution of liquid inside a fluidized bed.
2. Use the method developed in step 1 to test the performance of a standard Fluid Coker nozzle at different operating conditions.

3. Use the method developed in step 1 to compare the performance of spray nozzles with altered internal geometry due to erosion.
4. Use the method developed in step 1 to compare the performance of new spray nozzle designs based on previous experimental research.
5. Identify the features of the sprays produced by each nozzle tested to provide a recommendation as to how to improve Fluid Coker nozzle performance based on experimental evidence.

1.6 References:

- Aminu, M.O., Elliott, J.A.W., McCaffrey, W.C., Gray, M.R. (2004) “Fluid Properties at Coking Process Conditions”, *Industrial & Chemistry Engineering Research*, vol. 43, no. 12, pp. 2929-2935.
- Base, T.E., Chan, E.W., Kennett, R.D., Emberley, D.A. (1999) *U.S. Patent 6,003,789*. Washington, D.C.: U.S. Patent and Trademark Office.
- Bruhns, S., Werther, J. (2005) “An Investigation of the Mechanism of Liquid Injection into Fluidized Beds”, *Particle Technology and Fluidization*, vol. 51, no. 3, pp. 766-775.
- Canada National Energy Board. (2004) “Canada oil sands: opportunities and challenges to 2015. An energy market assessment”. Calgary: Publications Office.
- Chan, E., Knapper, B., Mueller, E., McMillan, J., Tyler, J., Kiel, D., Rathna, P.D. (2012) *United States Patent Application Publication No. US 2012/0063961 A1*. Washington, D.C.: U.S. Patent and Trademark Office.
- Chan, E.W., McDougall, S., Knapper, B. (2006) *U.S. Patent 7,025,874 B2*, Washington, D.C.: U.S. Patent and Trademark Office.

- Davuluri, R.P., Bielenberg, J.R., Sutton, C.R., Raich, B.A. (2012) *U.S. 2011/0114468*. Washington, D.C.: U.S. Patent and Trademark Office.
- Farkhondehkavaki, M. (2012) “Developing Novel Methods to Characterize Liquid Dispersion in a Fluidized Bed”, *PhD Thesis*, University of Western Ontario, London.
- Gray, M.R. (2002) “Fundamentals of bitumen coking process: a critical review”, *Canadian Journal of Chemical Engineering*, vol. 80, no. 3, pp. 393-401.
- Gray M., Le, T., McCaffrey, W. Berruti, F., Soundarajan, S., Chan, E., Huq, I. Thorne, C. (2001) “Coupling of mass transfer and reaction in coking of thin films of an Athabasca Vacuum Residue”, *Industrial & Engineering Chemistry Research*, vol. 40, no. 15, pp. 3317-3324.
- Gupta, R.K., Kumar, V., Srivastava, V.K. (2010) “Modeling of Fluid Catalytic Cracker Riser Reactor: A Review”, *International Journal of Chemical Reactor Engineering*, vol 8.
- House, P.K., Briens, C.L., Berruti, F., Chan, E. (2009) “Effect of spray nozzle design on liquid–solid contact in fluidized beds”, *Powder Technology*, vol. 186, no. 1, pp. 89-98.
- House, P.K., Saberian, M., Briens, C., Berruti, F., Chan, E. (2004) “Injection of a Liquid Spray into a Fluidized Bed: Particle-Liquid Mixing and Impact on Fluid Coker Yields”, *Industrial Engineering Chemistry Research*, vol. 43, pp. 5663-5669.
- Huang, X., Wang, X., Liao, G. (2008) “Visualization of Two Phase Flow inside an Effervescent Atomizer”, *The Visualization Society of Japan Journal of Visualization*, vol. 11, no. 4, pp. 299-308.
- Iveson, S.M., Lister, J.D., Hapgood, K., Ennis, B.J. (2001) “Nucleation, growth, and breakage phenomena in agitated wet granulation processes – a review”, *Powder Technology*, vol. 117, pp. 3-39.

- Iveson, S.M., Page, N.W. (2001) "Tensile bond strength development between liquid-bound pellets during compression", *Powder Technology*, vol 117, no. 1-2, pp. 113-122.
- Jenkins III, J.M., Jones, R.L., Jones, T.M., Beret, S. (1986) *U.S. Patent 4,588,790*. Washington, D.C.: U.S. Patent and Trademark Office.
- Jiang, Y., McAuley, K.B., Hsu, J.C.C. (1997) "Heat removal from gas-phase polyethylene reactors in the supercondensed mode", *Industrial & Engineering Chemistry Research*, vol. 36, pp. 1176-1180.
- Kieffer, S. (1977) "Sound Speed in Liquid-Gas Mixtures' Water-Air and Water-Steam", *Journal of Geophysical Research*, vol. 82, no. 20, pp.2895-2904.
- Knapper, B.A., Gray, M.R., Chan, W., Mikula, R. (2003) "Measurement of Efficiency of Distribution of Liquid Feed in a Gas-Solid Fluidized Bed Reactor", *International Journal of Chemical Reactor Engineering*, vol. 1, Article A35.
- Leach, A., Portoghese, F., Briens, C., Berruti, F. (2008) "A new and rapid method for the evaluation of the liquid-solid contact resulting from liquid injection into a fluidized bed", *Powder Technology*, vol. 184, no. 1, pp. 44-51.
- McKnight, C.A., Hackman, L.P., Knapper, B.A., Bulbuc, D., Jones, G.B., Tyler, J., Kiel, D.K. (2011) *U.S. Patent 8,006,949*. Washington, D.C.: U.S. Patent and Trademark Office.
- McMillan, J., Zhou, D., Ariyapadi, S., Briens, C., Berruti, F. (2005) "Characterization of the Contact between Liquid Spray Droplets and Particles in a Fluidized Bed", *Industrial & Engineering Chemistry Research*, vol. 44, no. 14, pp. 4931-4939.
- Mohagheghi M., Hamidi, M., Berruti, F., Briens, C., McMillan, J. (2013) "Study of the effect of local hydrodynamics on liquid distribution in a gas-solid fluidized bed using a capacitance method", *Fuel*, vol. 107, pp. 236-245.
- Niccum, P.K. (1985) *European Patent 0 220 349 A1*, European Patent Office, Germany.

- Pacek, A.W., Nienow, A.W. (1991) "An application of jet grinding to fluidised bed granulation", *Powder Technology*, vol. 65, pp 305-310.
- Patel, R., Wang, D., Zhu, C., Ho, T.C. (2012) "Effect of Injection Zone Cracking on Fluid Catalytic Cracking", *AIChE Journal*, vol. 59, no. 4, pp. 1226-1235.
- Pfeiffer, R.W., Borey, D.S., Jahnig, C.E. (1959) *U.S. Patent No. 2,881,130*. Washington, D.C.: U.S. Patent and Trademark Office.
- Pietsch, W. (2003) "An interdisciplinary approach to size enlargement by agglomeration", *Powder Technology*, vol. 130, no. 1-3, pp. 8-13.
- Portoghese, F., Ferrante, L., Berruti, F., Briens, C., Chan, E. (2010) "Effect of the injection-nozzle geometry on the interaction between a gas-liquid jet and a gas-solid fluidized bed", *Chemical Engineering and Processing Process Intensification*, Vol. 49, no. 6, pp. 605-615.
- Portoghese, F., House, P.K., Berruti, F., Briens, C. (2008) "Electric conductance method to study the contact of injected liquid with fluidized particles", *AIChE Journal*, vol. 54, no. 7, pp. 1770-181.
- Pougatch, K., Salcudean, J., McMillan, J. (2012) "Influence of conical nozzle attachments on horizontal spray dispersion in a fluidized bed", *Chemical Engineering Research and Design*, vol. 90, no. 10, pp. 1506-1516.
- Sanchez, F.J., Granovskiy, M. (2013) "Application of radioactive particle tracking to indicate shed fouling in the stripper section of a Fluid Coker", *The Canadian Journal of Chemical Engineering*, vol. 91, no. 6, pp 1175-1182.
- Song, X., Bi, H., Lim, C.J., Grace, J.R., Chan, E., Knapper, B., McKnight, C. (2004) "Hydrodynamics of the reactor section in Fluid Cokers", *Powder Technology*, vol. 147, pp.126-136.
- Sovani, S., Sojka, P., Lefebvre A. H. (2001) "Effervescent atomization", *Progress In Energy and Combustion Science*, vol. 27, no. 4, pp. 483-521.

- Speight, J., Baki O. (2001) "Petroleum Refining Processes", Marcel Dekker Inc. New York.
- Weber, S., Briens, C., Berruti, F., Chan, E., Bray, M. (2006) "Agglomerate stability in fluidized beds of glass beads and silica sand", *Powder Technology*, vol. 165, no. 3, pp. 115-127.
- Weber, S., Briens, C., Berruti, F., Chan, E., Gray, M. (2008) "Effect of agglomerate properties on agglomerate stability in fluidized beds", *Chemical Engineering Science*, vol. 63, no. 17, pp. 4245-4256.
- Wilson, J.W. (1997) "Fluid Catalytic Cracking Technology and Operations", PennWell Books.
- Williams, P. (2005) "Oil Sands Mining", *Oil & Gas Investor*, vol 25, no. 9, pp.85.
- Worley, A.C. (1982) *U.S. Patent No. 4,317,798*, Washington D.C.: U.S. Patent and Trademark Office.
- ZirGachian, M.A., Soleimani, M., Briens, C., Berruti, F. (2013) "Electric conductance method for the assessment of liquid–gas injection into a large gas–solid fluidized bed", *Measurement*, vol. 46, no. 2, 893-903.

Chapter 2

2 A METHOD TO MEASURE THE RATE OF LIQUID RELEASED FROM AGGLOMERATES PRODUCED BY GAS-ATOMIZED LIQUID INJECTION INTO A FLUIDIZED BED

Nicholas Prociw¹, Cedric Briens¹, Franco Berruti¹, Tarek Jamaledidine¹

¹Institute for Chemicals and Fuels from Alternative Resources (ICFAR)
Engineering, University of Western Ontario
London, On, Canada N6A 5B9

2.1 Introduction

Gas-atomized liquid injection is commonly used in the chemical and petroleum processing industry to maximize the distribution of liquid reactants into a bed of fluidized solids. When liquid reactants contact the solid particles, a reaction occurs and vapors are produced. Common examples of these types of processes include fluid catalytic cracking (Niccum, 1985), gas-phase polymerization (Jenkins III et al. 1986), and Fluid CokingTM (Pfeiffer et al. 1959). The research presented here will focus on the Fluid Coking process but may be applied to similar processes involving the gas-atomized injection of a liquid reactant into a bed of fluidized solid particles.

The Fluid Coking process was developed to produce light distillable hydrocarbon compounds using non-volatile heavy oil residue or bitumen feedstock. The process involves contacting droplets of bitumen with large quantities of hot coke particles in order to transfer heat to liquid bitumen droplets, and induce a thermal cracking reaction. Bitumen is preheated to a temperature in the range of 350 °C and mixed with atomizing steam in a premixing chamber (Base et al. 1999). The two phase mixture flows through a spray nozzle that consists of a converging-diverging-converging section in-between, as outlined by Base et al. A series of these nozzles are located at various heights and radial locations around the circumference of the Fluid Coking vessel. The dimensions of a typical Fluid Coker are provided in more detail by Pfeiffer et al. (1959). The atomization gas and the internal geometry of the spray nozzle act to break the liquid bitumen feed into

small droplets, which are distributed among the fluidized coke particles. Once the liquid reactant contacts the solid coke particles, a reaction occurs at the surface, producing smaller molecular weight products. These volatile products diffuse through the liquid film covering the coke particle and evaporate into the bulk gas flow, where they are collected and further processed to produce synthetic crude oil.

A common phenomenon associated with injection of liquid into a fluidized bed is liquid-solid agglomeration. Agglomerates are comprised of a mixture of solid particles bound together by liquid. Bruhns et al. (2005) investigated the injection of liquid into a fluidized bed operating at a temperature well above the boiling temperature of the liquid. The authors reported that the instantaneous evaporation of the liquid did not occur as expected; indicating that some liquid was trapped inside agglomerates and was not heated by the surrounding environment. These agglomerates were transported away from the spray jet towards the interior of the bed, where they eventually broke apart and released the trapped moisture. In many instances, the liquid-solid mixture does not always break apart, and stable agglomerates are produced as a result. Weber et al. (2008) investigated how some of the agglomerate properties such as initial size, binder viscosity, and density affect the stability of prefabricated agglomerates in a fluidized bed after they are formed.

For industries such as fertilizer and pharmaceutical production, the formation and control of agglomerate size is important in order to produce proper dosage sizing or reduce dustiness. In Fluid Coking, agglomerate formation is not desired as it impairs heat and mass transfer affecting product yield, as well as stripper fouling (Gray 2002).

Several methods have been developed to study the distribution of liquid feed into a fluidized bed. Knapper et al. (2003) added a copper naphthenate tracer to liquid feed in order to quantify the dispersion of bitumen inside a bed of fluidized coke particles. Energy dispersive X-rays were implemented to measure the concentration of copper deposit on the surface of the coke particles after the liquid reacted and the products had vaporized. Using a scaled down nozzle similar to those used in commercial Fluid Cokers (Base et al. 1999) the authors determined that the spray nozzles used were not very effective at dispersing the liquid among the coke particles.

Leach et al. (2008) charged fluidized sand particles using a triboelectric approach. After liquid was injected into the bed of charged solids, the bed was defluidized, and a current passed from the charged solids, through the wetted sand particles to a grounded electrode. The intensity of the current measured at the electrode gave a measurement of the initial dispersion of liquid among the fluidized solids.

Portoghese et al. (2008) injected liquid into a fluidized bed using scaled down spray nozzles and measured the contact efficiency of the spray onto the fluidized solids using conductance measurements. After liquid was sprayed into the bed, fluidization was stopped, a voltage was applied to a rod electrode embedded into the bed, and the conductance of the bed between the electrode and the grounded bed wall was measured. A higher conductance corresponded to better liquid distribution.

Farkhondehkavaki et al. (2012) investigated the effect of electrode geometry on conductance measurements in a fluidized bed. A rod electrode similar to that used by Portoghese et al. (2008), as well as plate electrodes (installed on one wall of the fluidized bed) was investigated. It was concluded that the one disadvantage of using a rod electrode was that it interfered with the fluidized bed hydrodynamics. Bubbles were constantly bursting as they moved past the electrode, dispersing wetted solids on the surface of the electrode. This led to a higher conductance reading compared to the plate electrodes. The plate electrodes were non-intrusive, and therefore did not interfere with bed hydrodynamics. As well, the plate electrodes could be installed at multiple locations along the wall of the fluidized bed, allowing local bed moisture content measurements. This is advantageous, as the authors showed that the distribution of liquid throughout the fluidized bed is not even.

ZirGachian et al. (2013) used the conductance measurement technique developed by Farkhondehkavaki et al. (2012) on a large scale pilot plant fluidized bed to measure moisture distribution using commercial scale nozzles. A voltage was applied across the bed using twenty-four non-invasive electrode plate electrodes. After liquid injection and defluidization of the bed, a conductance measurement for each electrode was recorded. The authors were able to map the distribution of moisture produced by a commercial scale nozzle, and compare the performance of the nozzle at different gas-to-liquid ratios.

Previous experiments have focused on the distribution of liquid inside a fluidized bed through small scale experiments, or defluidized techniques. The defluidized bed techniques employed in previous research only provided a measure of the distribution of liquid inside a fluidized bed at one particular time, and have not been used to measure the dynamic behavior of liquid distribution throughout the bed at all times after liquid injection is complete. Although the properties and stability of various types of agglomerates have been studied extensively, the rate of moisture released from agglomerates produced in a large scale fluidized bed by commercial Fluid Coking nozzles has yet to be investigated. The objectives of this study were as follows:

1. Develop a method to measure the rate of moisture released from agglomerates produced by a gas-atomized liquid in an active fluidized bed
2. Utilize this method by measuring the rate of moisture released from agglomerates produced by a commercial scale Fluid Coker nozzle at commercial spray conditions.

Unlike the previous conductance measurement techniques discussed, the following proposed method does not involve defluidization of the fluidized bed. Conductance measurements are continuously made with 24 non-invasive electrodes throughout the duration of the experiment in order to measure agglomerate moisture release rate. The rate of moisture released from agglomerates produced by a gas-atomized liquid injection into a fluidized bed is an important variable that affects fluidized bed reactor performance. Slower moisture release rates correspond to a longer time that liquid remains trapped within agglomerates, and therefore does not react.

The 24 electrodes installed along the wall of the fluidized bed can be used to measure both the average free moisture content of the fluidized bed at any time, as well as the local free moisture content at different regions within the fluidized bed. Contours of conductance measurements can be used to visualize the evolution of free moisture throughout the bed after liquid is injected.

This technique may be applied to investigate the rate of free moisture released from agglomerates produced by full scale Fluid Coker spray nozzles at different operating conditions such as variable gas-to-liquid mass ratio (GLR) or liquid flow rates. These

operating conditions are presented in the present investigation. The technique may also be applied to future studies to compare the effectiveness of different nozzle geometries when applied to gas-atomized liquid flow inside a fluidized bed.

2.2 Apparatus

A schematic of the fluidized bed used for these experiments is shown in Figure 2.1.

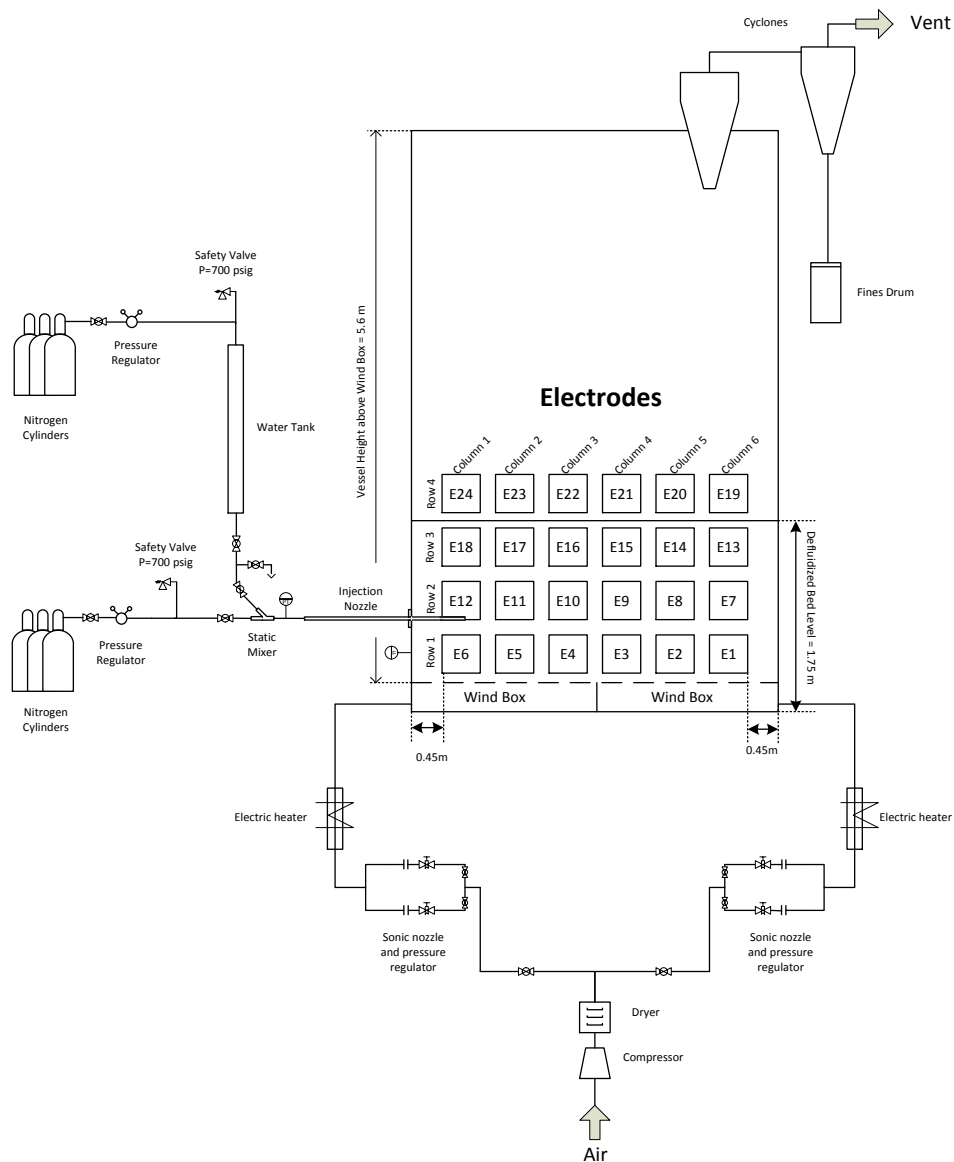


Figure 2.1: Simplified Process Flow Diagram of Experimental Apparatus

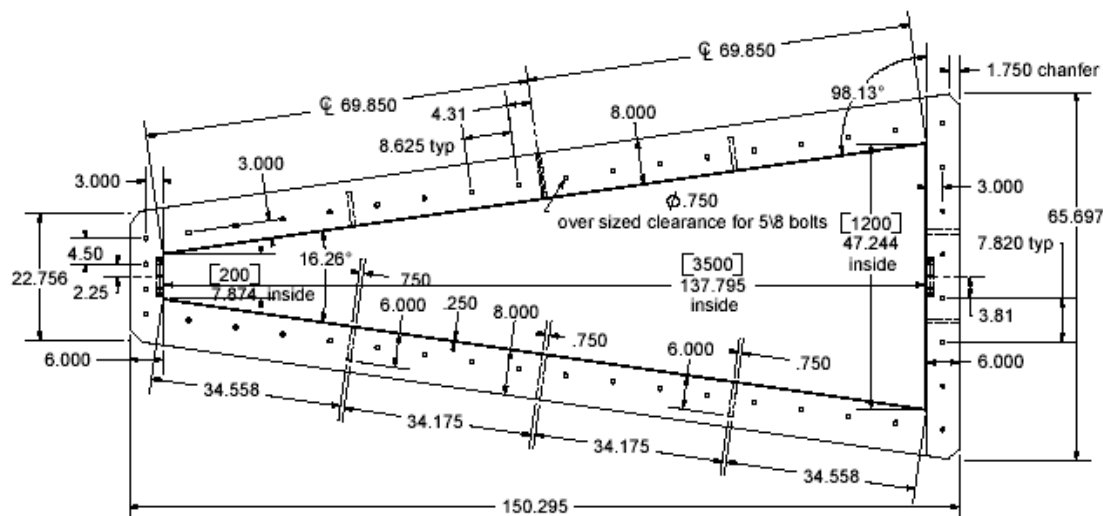


Figure 2.2: Top view of fluidized bed with dimensions (inches)

The cross sectional dimensions of the vessel (Figure 2.2) were 0.2 m x 1.2 m x 3.5 m, and the height was 6.1 m. The cross sectional area of the bed was chosen to represent the jet penetration zone of one Fluid Coker nozzle. The expansion angle of the bed was chosen based on a previous jet expansion study (Ariyapadi et al. 2003), and the length of the bed was chosen based on a previous jet penetration study (Ariyapadi et al. 2004).

Silica sand ($\rho = 2650 \text{ kg/m}^3$, Sauter mean diameter = $150 \text{ }\mu\text{m}$, Type B powder according to Geldart (1973)) was chosen to model coke in a cold model Fluid Coker. The injected liquid was deionized water ($20 \text{ }^\circ\text{C}$, $\rho = 998.5 \text{ kg/m}^3$) and the atomization gas was compressed nitrogen. Water at room temperature was used as it has a similar viscosity to bitumen at upstream nozzle conditions (about 350°C). Silica sand and water also have similar wettability characteristics to that of bitumen and coke, and this has been used in previous experiments (ZirGachian et al. 2013). Steam flow through the nozzle was simulated using nitrogen, as a past experiment has shown that the molecular weight of the atomization gas has a negligible impact on spray droplet size (Rahman et al. 2012).

The static height of solids inside the bed was 1.6 m, giving a total mass of approximately 6200 kg. The height of the bed was monitored using a manometer with pressure taps located at heights of 0.1, 0.89, 1.5, 2.11, and 3.93 m above the gas distributor.

The bed was fluidized at 0.15 m/s and air was supplied from a compressor capable of a maximum output pressure of about 100 psig. A bank of sonic nozzles controlled the mass flow rate of fluidization air, and air pressure was regulated using Wilkerson R40-OC-000 regulators with a pressure transducer (model # PT-1PTG0100D5F5) rated for 100 psig.

The nozzle used to spray the gas-atomized liquid was a full scale Fluid Coker nozzle of approximately 25 mm O.D., and has a similar geometry to the nozzle patented by Base et al. (1999) (Figure 2.3). The nozzle was installed on the narrow side of the bed, approximately 0.9 m above the distributor plate, and penetrated a distance of about 0.7 m into the bed. The nozzle penetration distance was chosen based on an estimation of the spray penetration using a correlation developed by Ariyapadi et al. (2004), and was chosen such that the jet would not reach the opposite side or walls of the vessel.

A premix chamber was installed upstream of the spray nozzle to mix atomization gas and water. The premixer used (Figure 2.4) contains two branch pipes that connect to the nozzle entrance at an angle of 30° below the horizontal axis of the nozzle.

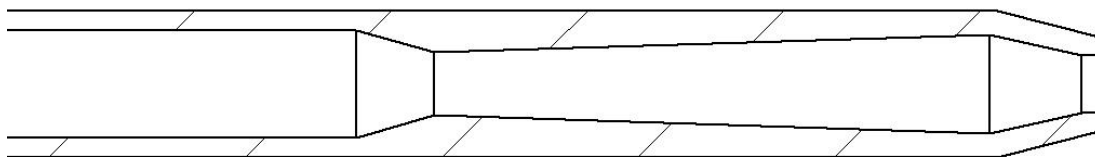


Figure 2.3: Standard TEB nozzle (Base et al. 1999)

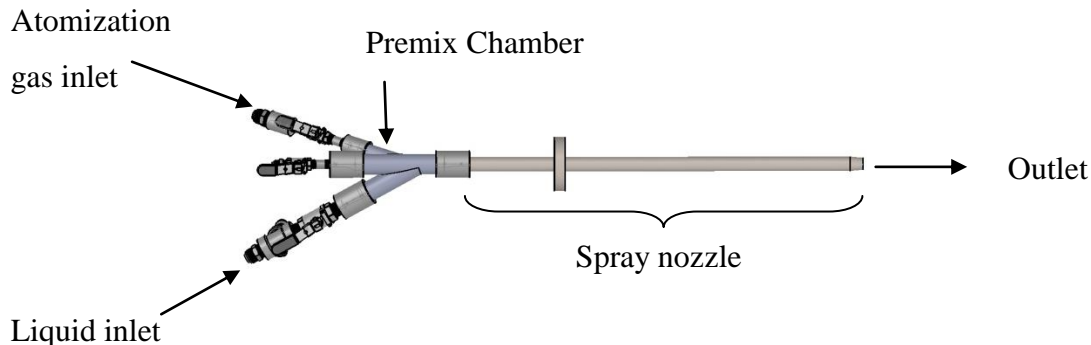


Figure 2.4: Premix chamber and nozzle assembly

In order to achieve flow rates similar to those used in industrial Fluid Coker reactors, a bank of high pressure cylinders (4500 psig) were connected to a blow tank filled with 15.3 L of water. When the liquid inlet valve was opened on the premix assembly, pressure exerted by nitrogen in the blow tank was used to push a float, forcing water through the ensuing piping and premix chamber to the spray nozzle. The flow rate of nitrogen to the blow tank was controlled using a Pro Star PRS 4095331 gas pressure regulator, and the pressure was monitored using a pressure transducer (Omega PX181B-500 psig).

Atomization gas was supplied using an identical nitrogen cylinder bank and pressure regulator. In order to achieve the desired mass flow rate of atomization gas, a sonic nozzle was installed inside the gas port of the premix chamber. The size of the sonic nozzle was chosen to ensure the upstream pressure was at least double the downstream pressure during water injection. This ensured the mass flow rate of atomization gas did not fluctuate during liquid injection.

A pressure transducer (Omega PX181B-500 psig) was installed at the mixing point of the fluids in order to measure the pressure drop upstream of the nozzle.

In order to ensure the temperature of the bed was kept constant for the start of each liquid injection, 3 J-type thermocouples were inserted into the bed, and another was

located in the secondary cyclone inlet. The temperature of the bed was controlled using an electric air heater connected to the fluidization gas inlet line.

Fluidized bed conductivity was measured using twenty-four metallic electrodes (25.4 x 25.4 cm), which were installed on one wall of the bed. Sheets of 19 mm thick high density polyethylene were placed between the wall of the bed and the electrodes in order to provide isolation from the metal wall of the vessel, which was electrically grounded. A power supply and signal generator were used to send a 6.5 V sinusoidal signal through a measurement resistor to the measurement electrodes (Figure 2.5). Current flowed from the 24 electrodes, through the fluidized bed, to the opposite grounded vessel wall. The voltage drop across the measurement resistor was recorded at a rate of 1000 Hz after spray completion, and was used to determine the instantaneous electrical conductance through the bed using the following voltage divider relationship:

$$C = \left\{ R_m \left(\frac{V_1}{V_2} - 1 \right) \right\}^{-1} \quad (2.1)$$

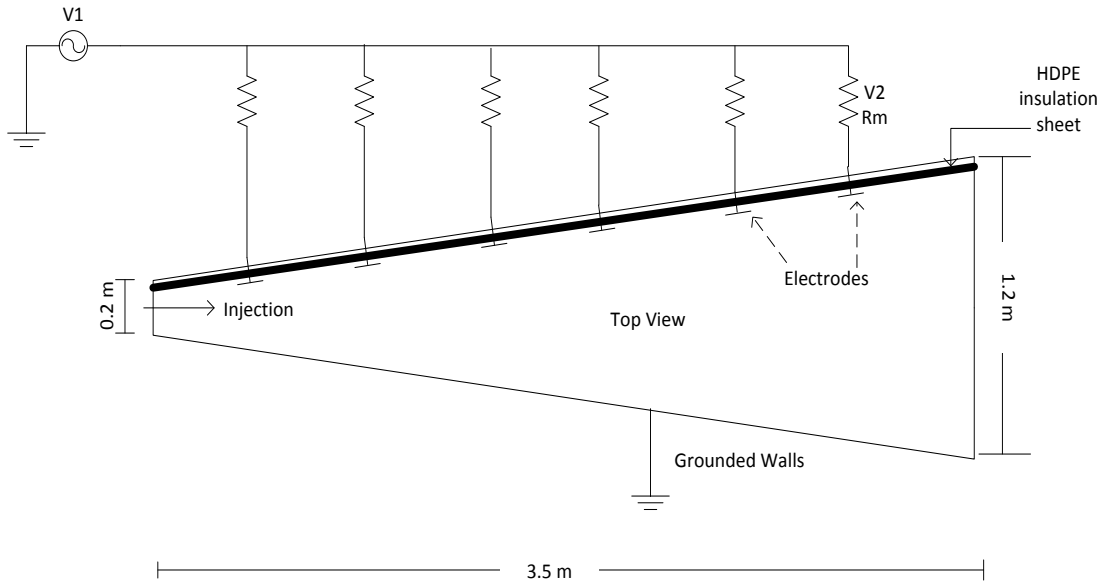


Figure 2.5: Schematic diagram of conductance electrodes

2.3 Procedure

2.3.1 Electrode Calibration

In order to relate the bed conductance reading to a bed moisture value, the electrodes must be calibrated by injecting a known quantity of free moisture into the fluidized bed. This was accomplished by spraying a pre-determined quantity of water into the fluidized bed at a very high gas-to-liquid (GLR) (approx. 30%) to create very fine liquid droplets and a wide spray angle. This helped to minimize the formation of agglomerates.

Free moisture can be defined as the mass of liquid injected into a fluidized bed that does not become trapped in agglomerates (as measured by electrical conductance) (eq. 2.2).

$$\%free\ moisture = \frac{\text{mass of water measured by conductance electrodes}}{\text{mass of water remaining in the fluidized bed}} \cdot 100\% \quad (2.2)$$

It has been previously shown (ZirGachian et al. 2013) that the electrical conductance through a bed of fluidized solids varies linearly in relation to the free moisture content of the bed.

$$\bar{x}(t) = aC + b \quad (2.3)$$

where $\bar{x}(t)$ represents the average free moisture-to-solid ratio as measured by the conductance electrodes, a and b are constants determined through calibration experiments, and C is the fluidized bed conductance as determined using eq. 2.1.

After the high GLR spray completed, water spread throughout the fluidized bed and the conductance was measured and recorded. The ratio of the total water to the mass of solids in the bed at any given time (t) was determined by subtracting the total mass of

moisture evaporated and the total water trapped in agglomerates at time t from the total amount of water injected at $t = 0$ s:

$$x(t) = \frac{M_{inj} - \int_0^t f_e dt - M_{agg}(t)}{M_s} \quad (2.4)$$

where M_{inj} is the mass of water injected into the fluidized bed, M_s is the mass of dry fluidized solids, $M_{agg}(t)$ is the mass of water trapped in agglomerates, t is the elapsed time since the start of the spray. f_e is the mass flow rate of evaporated water exiting the fluidized bed, as given by eq (2.5):

$$f_e = \left[\frac{d(M_s \bar{x})}{dt} \right]_e = \dot{v}_a \cdot A_{bed} \cdot (\mathcal{H}^* - \mathcal{H}_{in}) \quad (2.5)$$

In equation (2.5), f_e is the evaporated flow rate of water, \dot{v}_a is the superficial gas velocity, A_{bed} is the cross sectional area of the fluidized bed, \mathcal{H}^* is the saturated humidity of the air leaving the fluidized bed as determined by the outlet air temperature measurement, and \mathcal{H}_{in} is the humidity of the incoming fluidization air. It was assumed (and verified by ZirGachian et al. 2013) that the air exiting the fluidized bed was saturated with water, and that the relative humidity of the air leaving the fluidized bed was 100%. To further verify this assumption, the conductance and total bed moisture were plotted as a function of time (Figure 2.6). It was observed that the total bed moisture (as calculated using eq. (2.5)) reduced to 0 kg when the conductance of the fluidized bed returned to pre-injection values.

A plot of electrical conductance versus time is shown in Figure 2.6. After liquid injection began, the conductance started to rise due to the spreading of liquid throughout

the fluidized bed; mainly due to the breakage of some of the agglomerates that formed as a result of the jet-bed interaction.

At some time after the start of injection, the conductance started to drop at a constant rate. From Figure 2.6, it is evident that this occurs about 350 sec after the injection completed. At this time, the conductance of the fluidized bed measured by electrode 1 (see Figure 2.1 for location) is about 3.5 μS . The time at which the conductance began to change at a constant rate is referred to as t_c .

Beyond t_c , the mass of liquid released from any remaining agglomerates became negligible, so that change in the conductance of the bed was due to the evaporation of free moisture alone. Thus at time t_c , all water remaining in the fluidized bed was in the form of free moisture (eq. 2.6).

$$\left| \frac{dx(t)}{dt} \right|_{t > t_c} - |f_e| = 0 \quad (2.6)$$

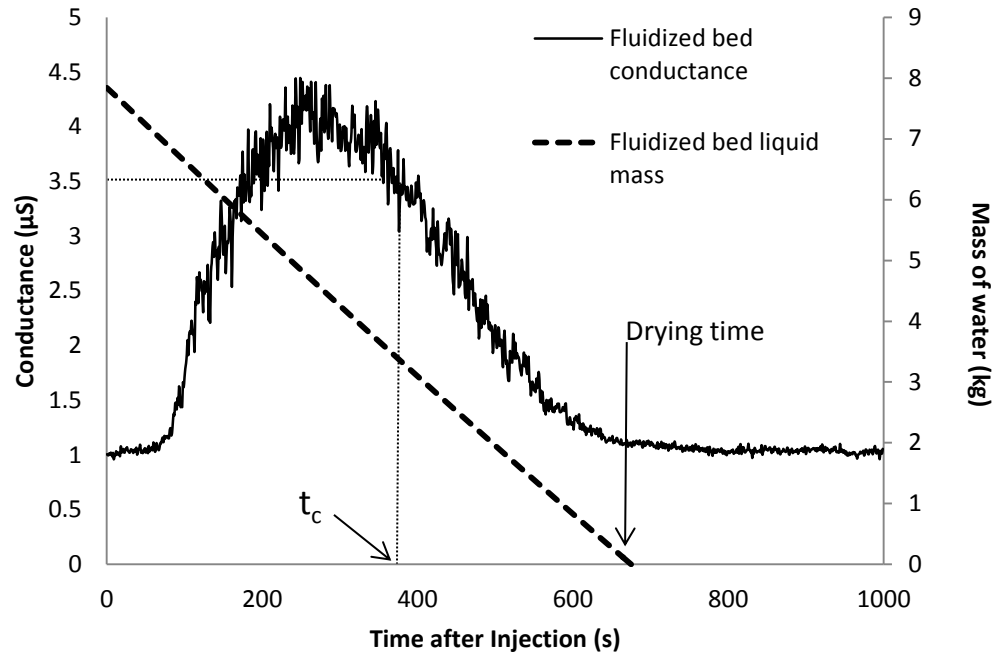


Figure 2.6: Fluidized bed electrical conductance versus time after liquid injection for electrode calibration experiment (GLR = 30%)

After time t_c , the calculated bed free moisture (in grams) per kg of bed solids was plotted as a function of conductance to produce a calibration curve that related the conductance measurement to the free moisture content of the bed (Figure 2.7).

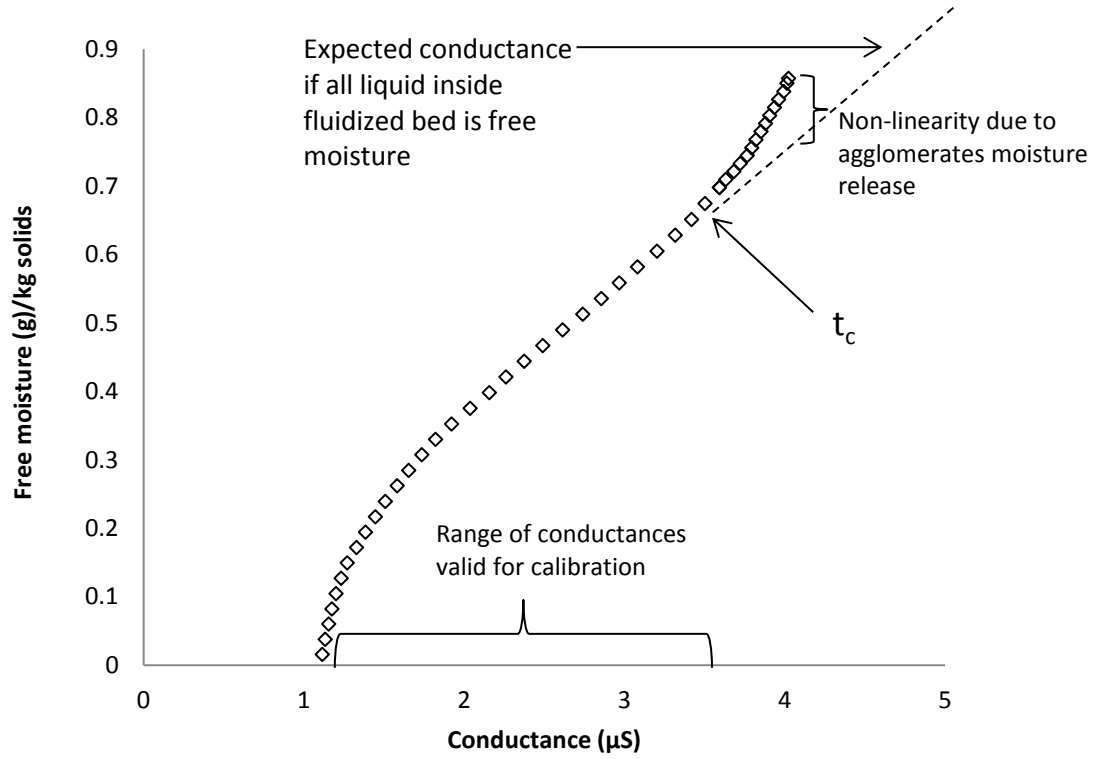


Figure 2.7: Calibration data points for electrode 1. A similar plot is produced for each electrode

The relationship between the conductance and free moisture content of the bed (Figure 2.7) becomes non-linear as the bed approached its drying point. Three piece-wise linear functions were fitted to the electrode calibration curve to account for this non-linear relationship (Figure 2.8). Therefore after time t_c ,

$$\bar{x}(t) = a_1 C + b_1 \quad \text{for } C_2 < C < C_1 \quad (2.7a)$$

$$\bar{x}(t) = a_2 C + b_2 \quad \text{for } C_3 < C < C_2 \quad (2.7b)$$

$$\bar{x}(t) = a_3 C + b_3 \quad \text{for } C_3 < C < C_4 \quad (2.7c)$$

C_1 - C_4 represents the free moisture bounds through which equations (2.8a-c) remains a valid approximation.

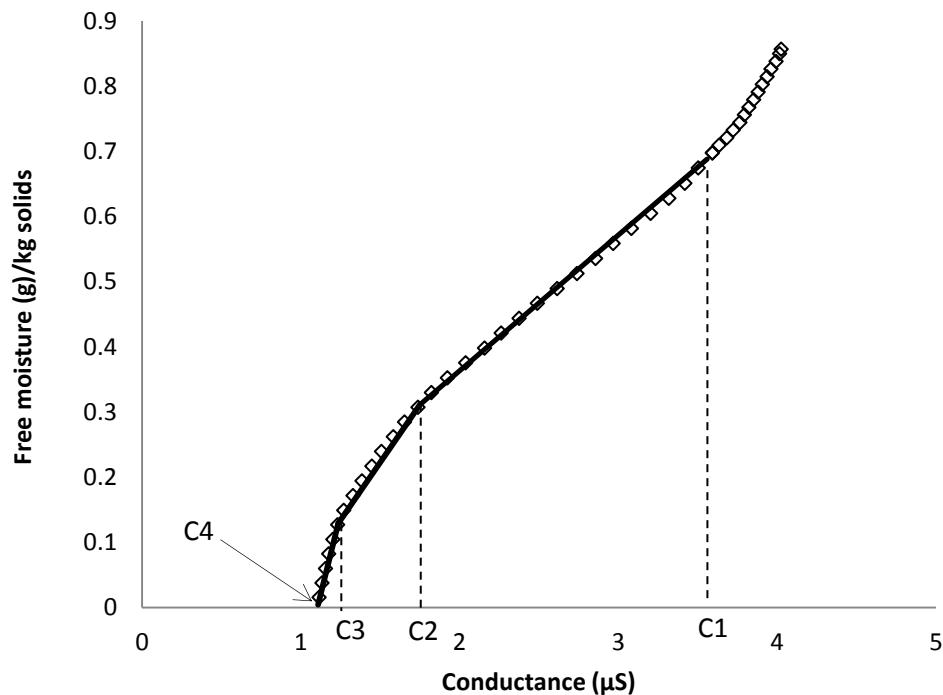


Figure 2.8: Equations 2.7 a-c fitted to calibration data for electrode 1

A curve similar to that shown in Figure 2.7 was produced for each electrode. The conductance from each electrode was used to determine the average fluidized bed free moisture content at any time after liquid injection.

2.3.2 Agglomerate Moisture Release Experiments

After the electrodes were calibrated, the following procedure was used to calculate the fraction of injected water released from agglomerates using a commercial scale Fluid Coker nozzle:

1. Pressure regulators located at the atomization gas cylinders and liquid pressure cylinders were used to set the desired flow rate and GLR.
2. Pressure regulators on the fluidization gas line were used to set the fluidization velocity at 0.15 m/s.

3. The bed freeboard was heated to a temperature of 24.5°C before each spray injection.
4. Liquid was injected into the bed at a specified flow rate, and the conductance of the bed was measured at a rate of 1000 Hz.
5. The temperature of the bed at three different locations, and the temperature of the freeboard were measured at a rate of 2.4 Hz. The temperature of the outlet air was used to calculate the humidity of the air, which in turn was used to calculate the mass flow rate of water from the bed (eq. 2.5)
6. The bed remained fluidized throughout the duration of the experiment. When the electrode conductance measurements reached the pre-injection values, data acquisition was ceased.

After injection into the bed, some of the liquid was distributed throughout the fluidized solids in the form of free moisture. The free moisture content was accounted for using the conductance measurements and electrode calibration curves. A portion of the liquid formed liquid-solid agglomerates, which were heavier than individual solid particles, and likely sank to the bottom of the fluidized bed. Agglomerates did not register conductance readings, as they do not provide a path for current to travel from the electrodes to the grounded wall of the bed (ZirGachian et al. 2013).

The total mass of water in the bed at any time was determined by subtracting the amount evaporated from the total mass of water injected. The free moisture of the bed was determined by matching the measured conductance reading to a free moisture value using the calibration curves for each electrode. The following mass balance was then used to calculate the mass of water trapped in agglomerates.

Free moisture can be produced through the destruction of agglomerates, and is consumed through the evaporation of water from the fluidized bed (Mohagheghi et al. 2013). Thus the rate of change of free moisture in the fluidized bed is:

$$\frac{d(M_s \bar{x})}{dt} = \left[\frac{d(M_s \bar{x})}{dt} \right]_{agg} - \left[\frac{d(M_s \bar{x})}{dt} \right]_e \quad (2.8)$$

The term on the left hand side of eq. (2.8) can be measured using the conductance measurements and the calibration curves for each electrode (eq. 2.7a-c). The second term on the right hand side of equation (2.8) represents the rate of water exiting the fluidized bed due to evaporation, and can be determined using eq. (2.5). Rearranging eq. (2.8) for the unknown term and substituting equation (2.5) gives:

$$\left[\frac{d(M_s \bar{x})}{dt} \right]_{agg} = \frac{d(M_s \bar{x})}{dt} + f_e \quad (2.9)$$

The cumulative mass of water released from agglomerates since the end of liquid injection can be calculated by integrating eq. (2.9):

$$(M_s \bar{x})_{agg} = \int_0^t \left[\frac{d(M_s \bar{x})}{dt} + f_e \right] dt \quad (2.10)$$

The fraction of water released from agglomerates (i.e. the fraction of injected liquid in the form of free moisture, $G(t)$), may be calculated using the following expression:

$$G(t) = \frac{(M_s \bar{x})_{agg}}{M_L} = \frac{M_s}{M_L} \left[\int_0^t \left[\frac{d\bar{x}}{dt} + \frac{f_e}{M_s} \right] dt \right] \quad (2.11)$$

where M_L is the mass of injected liquid, M_s is the mass of solids present in the fluidized bed, respectively, \bar{x} is the average free moisture content of the bed as determined using the conductance electrode measurements, and f_e is the flow rate of evaporated water leaving the bed. The function $G(t)$ ranges from 0 at the start of the experiment (where all moisture injected is initially trapped in agglomerates) to 1 at the end of the experiments

(where the fraction of water not trapped in agglomerates equals 1 or 100%). The faster $G(t)$ approached 1, the faster the agglomerates released their moisture into the surrounding fluidized solids. Values of $G(t)$ were determined and compared for various nozzle operating conditions (Table 2.1).

Table 2.1: Operating conditions tested

Case	Liquid Flow rate (kg/s)	GLR
Constant Flow rate	1.35	0.5%
Constant Flow rate	1.35	2%
Constant Flow rate	1.35	3.5%
Constant Flow rate	1.35	4.8%
Constant GLR	0.6	2%
Constant GLR	1.2	2%
Constant GLR	1.9	2%
Constant GLR	2.5	2%

2.4 Results and Discussion

2.4.1 Effect of GLR on Rate of Moisture Released from Agglomerates

Liquid was injected into the fluidized bed using a Fluid Coker nozzle at multiple GLRs. The cumulative fraction of liquid that has been freed from agglomerates is shown in Figure 2.9 for 4 different GLR's.

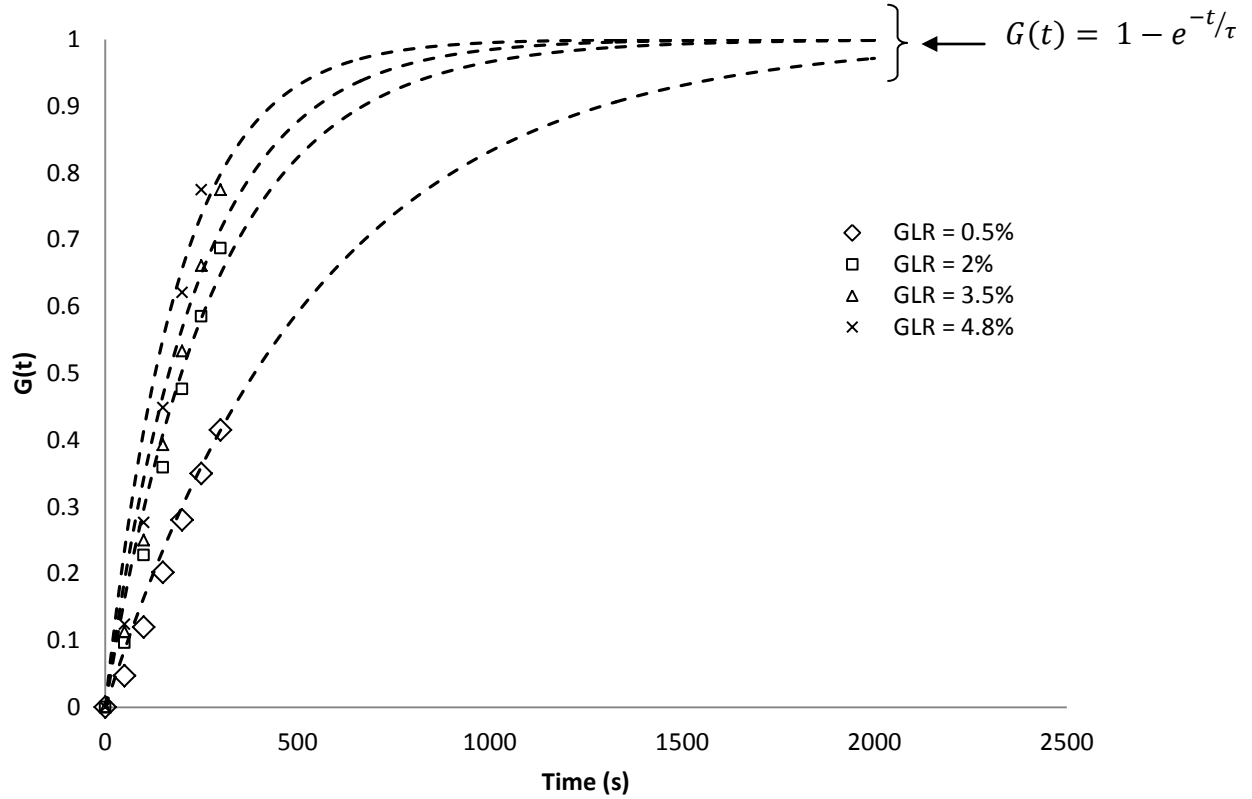


Figure 2.9: Cumulative fraction of moisture freed from agglomerates ($G(t)$) versus time for four different GLR's (0.5%, 2%, 3.5%, 4.8%) (Liquid mass flow rate = 1.35 kg/s)

Figure 2.9 indicates that the rate of moisture released from agglomerates increased as the GLR is increased. However, there appeared to be a diminishing effect as the GLR was raised past 2%.

Mohagheghi et al. (2014) used capacitance to measure the cumulative fraction of moisture released from agglomerates as a function of time. The authors found that for a short liquid injection into a fluidized bed (less than 10 s), the normalized cumulative mass of water released from trapped agglomerates could be approximated with the following first order exponential rate function (eq. 2.12):

$$G(t) = 1 - e^{-t/\tau} \quad (2.12)$$

In eq. 2.12, τ was used to compare the rate of moisture released from agglomerates produced at different nozzle operating conditions. τ represents the amount of time necessary for 62.5% of the moisture initially trapped in agglomerates to be released in the fluidized bed as free moisture. A plot of τ versus GLR% is shown in Figure 2.10.

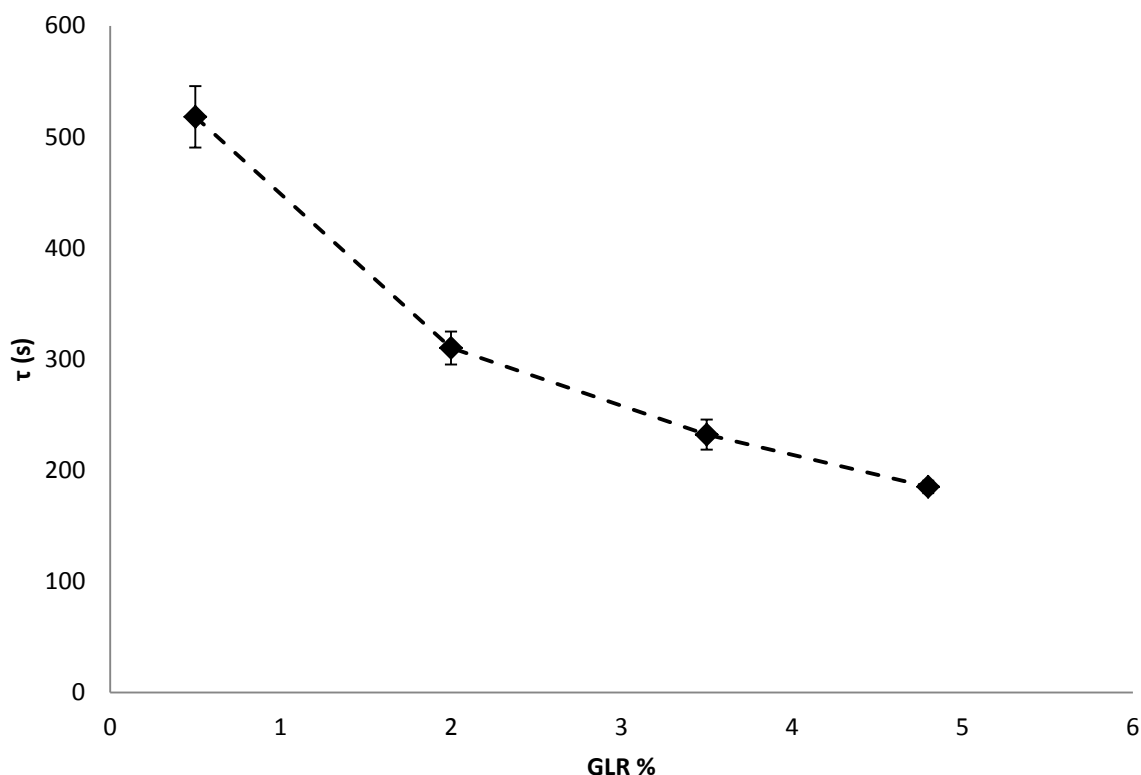


Figure 2.10: Agglomerate moisture release rate time constant versus GLR

The lower τ is, the faster moisture is released from agglomerates. Thus, low τ values are desirable.

Various experiments have investigated the effect of GLR on liquid distribution inside a fluidized bed (ZirGachian et al. (2013), Portoghese et al. (2007)). It was found that increasing the GLR enhances the distribution of the liquid inside the fluidized bed. It

has also been suggested that this is due to the decrease in droplet size, increase in jet spray angle and penetration depth, as well as an increase in solids entrainment into the spray jet cavity. Better liquid distribution in the fluidized bed results in a smaller liquid concentration in agglomerates. Since the trapped liquid holds agglomerates together, a smaller concentration of liquid within the jet should lead to less liquid trapped in the agglomerates and should reduce the forces holding the agglomerates together. Increasing the GLR not only leads to better spray distribution, but also increases the rate at which moisture is released from agglomerates.

2.4.2 Effect of Liquid Mass Flow Rate on the Rate of Moisture Released from Agglomerates

The same procedure was also used to investigate the effect of liquid mass flow rate on the rate of moisture released from agglomerates when liquid is sprayed into a fluidized bed. In this case, the GLR was kept constant at 2% while the liquid flow rate was increased from 0.6 kg/s to 2.5 kg/s. A plot of the cumulative fraction of moisture released from agglomerates at each flow rate is shown in Figure 2.11.

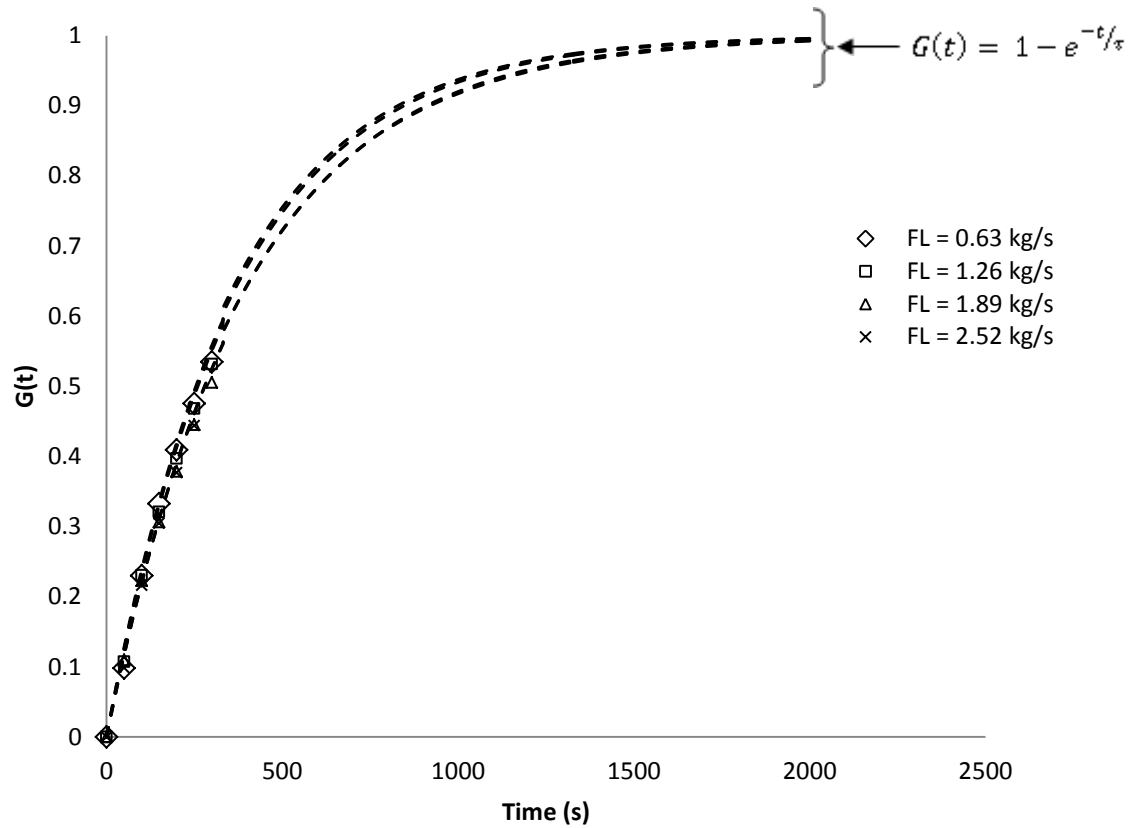


Figure 2.11: Cumulative fraction of moisture freed from agglomerates ($G(t)$) versus time for four different liquid flow rates (0.6, 1.2, 1.9, 2.5 kg/s) (GLR = 2%)

Figure 2.12 shows how τ varies with liquid flow rate.

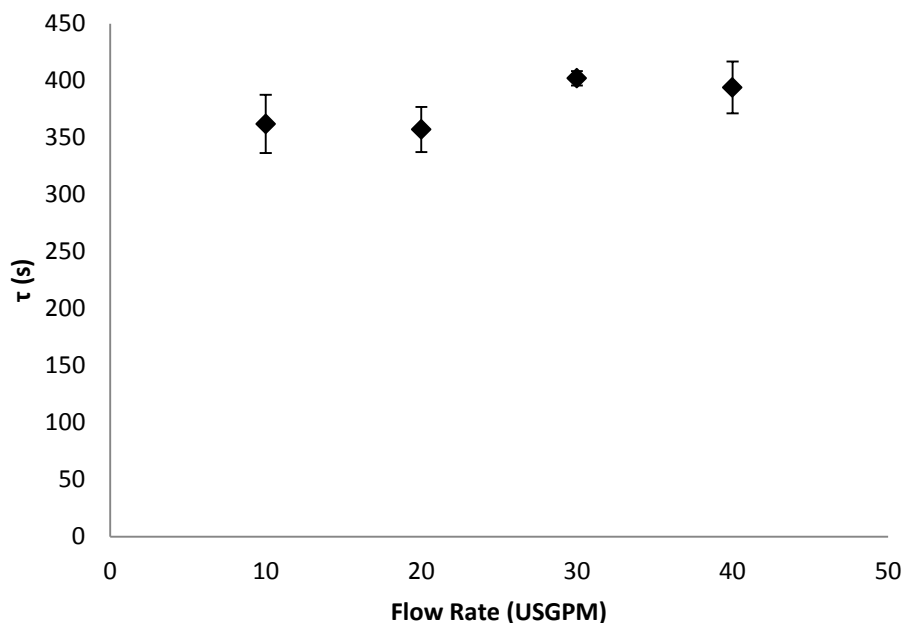


Figure 2.12: Effect of liquid mass flow rate on moisture release rate time constant (2% GLR)

The results indicate that increasing the liquid mass flow rate at a constant GLR did not significantly impact the rate at which liquid is released from agglomerates. Increasing the liquid flow rate at a constant GLR increased the pressure inside the nozzle. A higher pressure inside the nozzle corresponds to greater atomization energy and smaller drop sizes. This should lead to better liquid distribution among the fluidized solids. However, a greater pressure also introduced more liquid into the fluidized bed per unit time, and therefore increased the liquid to solid ratio within the spray cavity. The increased liquid-to-solid ratio helped to stabilize agglomerates. A balance of opposing effects may explain why the liquid was not released from agglomerates at a different rate as the liquid flow rate was varied.

2.4.3 Evolution of Free Moisture throughout the Fluidized Bed

The preceding results were obtained using conductance measurements from each electrode to determine average bed free moisture content throughout the fluidized bed at each time after liquid injection completed. It was previously shown (ZirGachian et al. 2013) that the measured electrical conductance at each electrode location within the fluidized bed is proportional to the free moisture content in the same region (Equation 2.3). Plots of conductance versus time may then be used to illustrate the distribution of free moisture throughout the bed. ZirGachian et al. (2013) created contours of the defluidized bed at one time after liquid injection, and was able to show how free moisture distribution changed with GLR. With the current technique, it is possible to illustrate the free moisture distribution inside the fluidized bed at any time after liquid injection. Figures 2.13 and 2.14 show the free moisture distribution in the fluidized bed with a liquid flow rate of 1.35 kg/s and a GLR of 2%. Similar profiles may be produced for any nozzle or any operating condition.

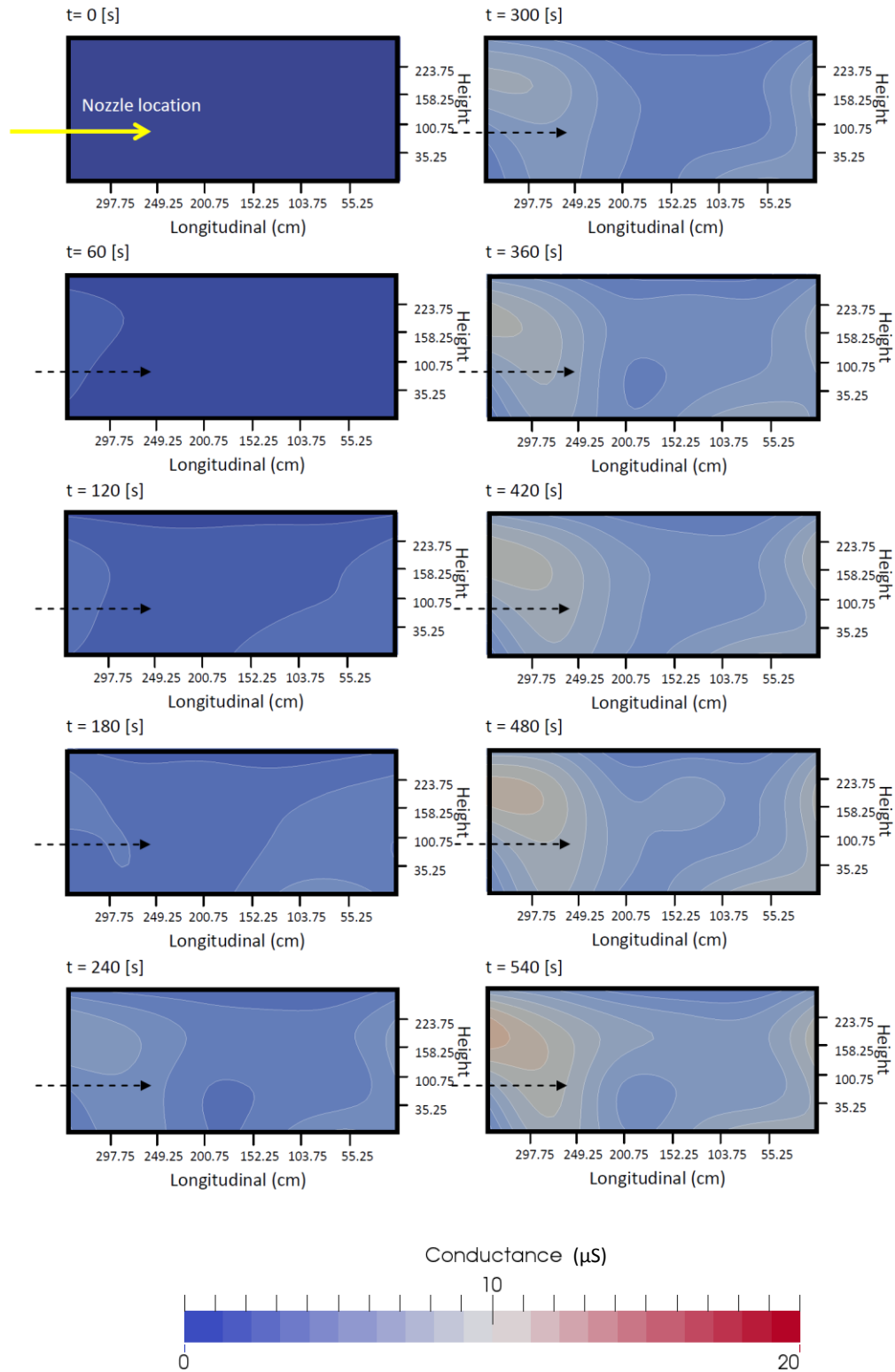


Figure 2.13: Evolution of free moisture in fluidized bed after liquid injection is complete. Liquid flow rate = 1.35 kg/s. GLR = 2%. First 9 minutes

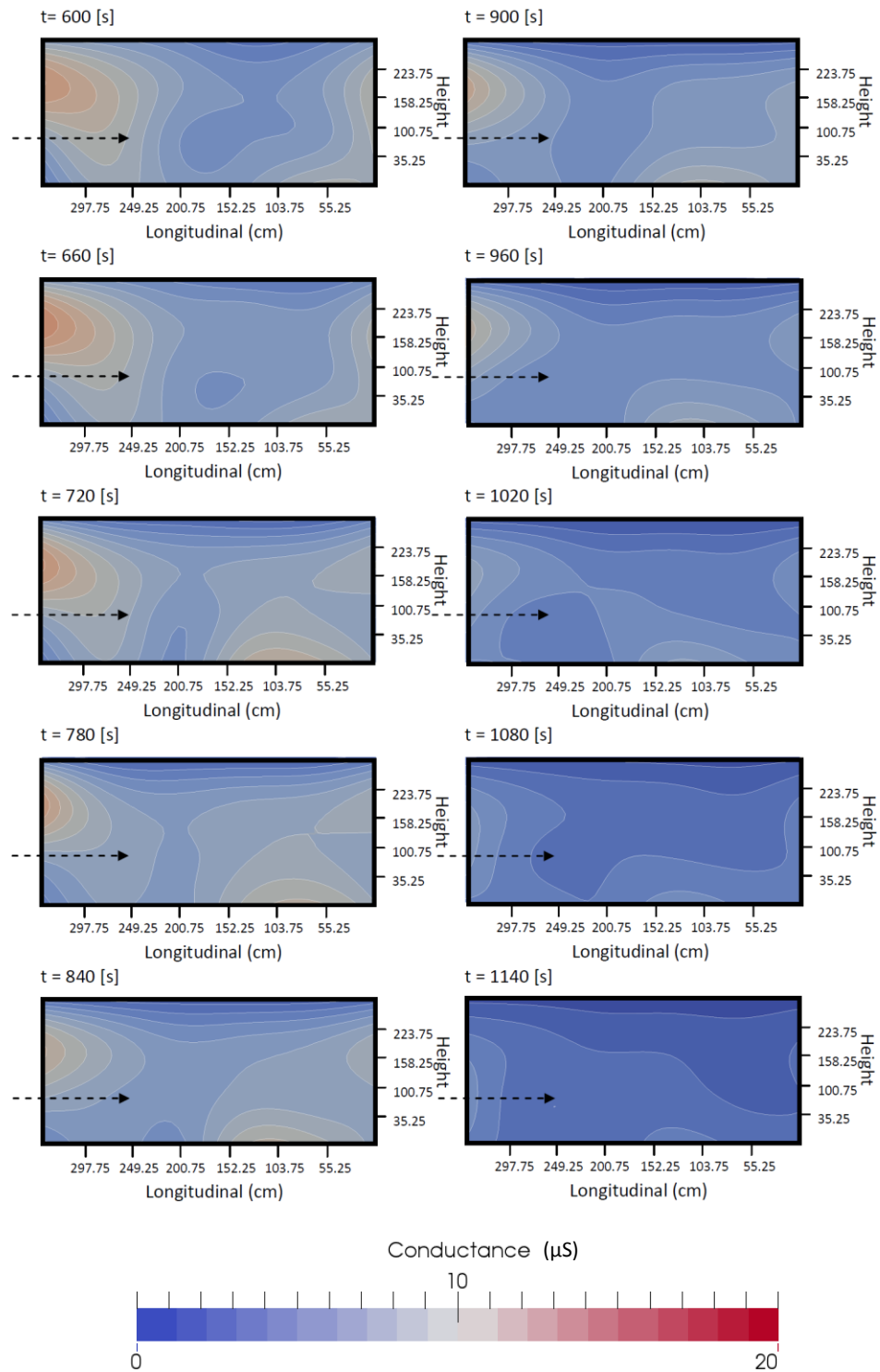


Figure 2.14: Evolution of free moisture in fluidized bed after liquid injection is complete. Liquid flow rate = 1.35 kg/s. GLR = 2%. Time step = 1 min.

From Figures 2.13 and 2.14, it is observed that initially all moisture injected into the fluidized bed became trapped in agglomerates; therefore there is no electrical conductance across the bed.

Free moisture appears in higher concentration around the sides of the fluidized bed, and lower in the middle region. Wetted particles are carried to the top of the bed, and ejected towards the sides, where there is a higher density of solids. The solids in the dense region along the sides of the fluidized bed descend towards the distributor plate, where they are once again very quickly entrained in the wake of gas bubbles and carried back towards the top of the bed. Thus, a solids circulation pattern develops in the fluidized bed. Because the wet solids move very quickly within the bubble wakes in the central region, their concentration in the central region is small.

2.5 Conclusions

It has been demonstrated that measuring the electrical conductance of an active fluidized bed can be used as a method to measure the rate of moisture released from agglomerates. The method was used to study the effect of varying the atomization gas flow rate and the liquid mass flow rate of a spray inside a fluidized bed produced by a commercial scale fluid coker nozzle. An increase of atomization gas flow rate lead to smaller droplet sizes and better liquid distribution in the fluidized bed. A better distribution of liquid reduced the mass of liquid trapped in agglomerates and the rate at which liquid was subsequently released from these agglomerates in the fluidized bed. On the other hand, increasing the liquid mass flow rate did not significantly change the rate at which moisture was released from agglomerates.

The conductance measurements obtained from 24 non-intrusive electrodes installed on one wall of the bed can be used to produce free moisture profiles of the fluidized bed at any time after liquid injection. These profiles may be used to visualize the circulation pattern in the fluidized bed, as well as compare the free moisture distribution created by different nozzle geometries or operating conditions.

2.6 References

- Ariyapadi, S., Holdsworth, D.W., Norley, C.J.D., Berruti, F., Briens, C. (2003) “Digital X-ray Imaging Technique to Study the Horizontal Injection of Gas-Liquid Jets into Fluidized Beds”, *International Journal of Chemical Reactor Engineering*, vol. 1 Article A56.
- Ariyapadi, S., Berruti, F., Briens, C., McMillan, J., Zhou, D. (2004) “Horizontal Penetration of Gas-Liquid Sprays in Gas-Solid Fluidized Beds”, *International Journal of Chemical Reactor Engineering*, vol. 2 Article A22.
- Base, T.E., Chan, E.W., Kennett, R.D., Emberley, D.A. (1999) *U.S. Patent 6,003,789*. Washington, D.C.: U.S. Patent and Trademark Office.
- Bruhns, S., Werther, J. (2005) “An Investigation of the Mechanism of Liquid Injection into Fluidized Beds”, *Particle Technology and Fluidization*, vol. 51, no. 3, pp. 766-775.
- Farkhondehkavaki, M. (2012) “Developing Novel Methods to Characterize Liquid Dispersion in a Fluidized Bed”, *PhD Thesis*, University of Western Ontario, London.
- Geldart, D. (1973) “Types of gas fluidization”, *Powder Technology*, vol.7
- Gray, M.R. (2002) “Fundamentals of bitumen coking process: a critical review”, *Canadian Journal of Chemical Engineering*, vol. 80, no. 3, pp. 393-401.
- Jenkins III, J.M., Jones, R.L., Jones, T.M., Beret, S. (1986) *U.S. Patent 4,588,790*. Washington, D.C.: U.S. Patent and Trademark Office.
- Knapper, B.A., Gray, M.R., Chan, W., Mikula, R. (2003) “Measurement of Efficiency of Distribution of Liquid Feed in a Gas-Solid Fluidized Bed Reactor”, *International Journal of Chemical Reactor Engineering*, vol. 1, Article A35.

- Leach, A., Portoghese, F., Briens, C., Berruti, F. (2008) “A new and rapid method for the evaluation of the liquid-solid contact resulting from liquid injection into a fluidized bed”, *Powder Technology*, vol. 184, no. 1, pp. 44-51.
- Mohagheghi M., Hamidi, M., Berruti, F., Briens, C., McMillan, J. (2013) “Study of the effect of local hydrodynamics on liquid distribution in a gas–solid fluidized bed using a capacitance method”, *Fuel*, vol. 107, pp. 236-245.
- Mohagheghi M., Hamidi, M., Berruti, F., Briens, C., McMillan, J. (2014) “The effects of liquid properties and bed hydrodynamics on the distribution of liquid on solid fluidized particles in a cold-model fluidized bed”, *Powder Technology*, vol. 256, pp 5-12.
- Niccum, P.K. (1985) *European Patent 0 220 349 A1*, European Patent Office, Germany.
- Pfeiffer, R.W., Borey, D.S., Jahnig, C.E. (1959) *U.S. Patent No. 2,881,130*. Washington, D.C.: U.S. Patent and Trademark Office.
- Portoghese, F., House, P.k., Berruti, F., Briens, C. (2008) “Electric conductance method to study the contact of injected liquid with fluidized particles”, *AIChE Journal*, vol. 54, no. 7, pp. 1770-181.
- Rahman, M.A., Balzan, M., Heidrick, T., Fleck, B.A. (2012) “Effects of the gas phase molecular weight and bubble size on effervescent atomization”, *International Journal of Multiphase Flow*, vol. 38, no. 1, pp. 35-52.
- Weber, S., Briens, C., Berruti, F., Chan, E., Gray, M. (2008) “Effect of agglomerate properties on agglomerate stability in fluidized beds”, *Chemical Engineering Science*, vol. 63, no. 17, pp. 4245-4256.
- ZirGachian, M.A., Soleimani, M., Briens, C., Berruta, F. (2013) “Electric conductance method for the assessment of liquid–gas injection into a large gas–solid fluidized bed”, *Measurement*, vol. 46, no. 2, 893-903.

Chapter 3

3 Effect of Nozzle Erosion on Jet Interaction in a Fluidized Bed

Nicholas Prociw¹, Cedric Briens¹, Franco Berruti¹

¹Institute for Chemicals and Fuels from Alternative Resources (ICFAR)
Engineering, University of Western Ontario
London, On, Canada N6A 5B9

3.1 Introduction:

Increasing energy demand and decreasing supply of non-renewable energy reserves have increased the need to develop non-conventional energy sources. The oil sands of Alberta contain a vast supply of heavy oil (bitumen) that was at one time too expensive to extract and process due to its high molecular weight and contaminant content. Increased demand and technological advances have made processing bitumen a viable option for replacing conventional fuel sources.

Bitumen is extracted from oil sands and sent to an upgrading facility before it is transported to conventional crude oil refineries (Speight, 2001). The upgrading process reduces the vacuum distillation residual content of the oil and removes sulfur, heavy metals, and other undesirable impurities. One of the key processes used at upgrading facilities to reduce the molecular weight of the oil (and increase the fraction of distillable components) is Fluid CokingTM.

Fluid Coking is a process in which bitumen is injected into a bed of hot fluidized coke particles. Heat is supplied by the coke particles and is transferred to the bitumen, thereby raising its temperature. Endothermic thermal cracking reactions then occur, reducing the molecular weight of the bitumen. The products of the reaction are volatile organic components that can be separated using atmospheric and vacuum distillation units found in conventional refineries (Pfeiffer et al. 1959).

Bitumen is supplied to the Fluid Coker reactor through a series of spray nozzles located at various locations around the circumference and height of the reactor. At room temperature, bitumen has a very high viscosity, making flow very difficult. To enable

better flow characteristics, bitumen is heated to about 350 °C to reduce its viscosity. During injection, bitumen is mixed with steam to help atomize the liquid into small droplets, which helps to distribute the bitumen more evenly in the fluidized coke particles (Base et al. 1999).

Fluid cokers use special atomization nozzles. When compared to commonly used gas-atomization nozzles, they use a relatively low flow rate of atomization steam. They are also designed without complex internals, which allows them to be steam washed or mechanically rodded when fouled by coke deposits. Fluid coker nozzles incorporate a succession of converging and diverging sections. A bubbly two phase flow is created in the premixing chamber, which is located upstream of the first converging section of the nozzle. The two phase flow accelerates through the converging sections, and decelerates through the diverging section. As the velocity of the two phase flow changes, shear forces between the gas and liquid stretch the liquid into elongated ligaments. At the nozzle exit, the flow becomes choked, and the resulting large pressure drop and possible shockwave structures shatter the liquid ligaments into small droplets. These disperse in the interior of the Fluid Coker, where they contact the fluidized coke particles and react.

The process through which bitumen distributes itself among the fluidized coke particles is reviewed by Gray (2002). Ideally, the size of the droplets produced by the spray nozzles are of a similar size to the coke particles to increase the probability of collision, and the layer of bitumen coating each coke particle is the same. An experiment carried out by Knapper et al. (2003) indicated that the distribution of liquid formed by the spray nozzles was not as effective as expected as much of the coke did not make contact with the injected bitumen.

Poor liquid distribution in the Fluid Coker leads to the formation of liquid/solid agglomerates. Agglomerates trap liquid, and reduce the rate of heat transfer from the surface of the coke particles to the reacting bitumen (Pirooz, 2010). Since agglomerates trap liquid, they remain wetted for a period of time after they are formed. Wet agglomerates that flow through the stripper sheds near the bottom of the reactor release vapors that contribute to the fouling of the stripper, which can lead to premature coker shutdown (Sanchez, 2013). To increase heat transfer through wet agglomerates and

mitigate stripper fouling, the coker temperature is raised, which leads to overcracking of the product vapors, reducing the yield of valuable condensable vapors. Reducing stable agglomerates would, therefore, be greatly beneficial to the Fluid Coking process.

Agglomerates can remain intact, despite the shearing forces exerted on the agglomerates by fluidizing gas and solid particles. A previous study has developed a measure of the rate of liquid released from agglomerates in a large scale fluidized bed using a standard commercial scale nozzle (Prociw et al. 2014). This method can be used to compare the performance of different spray nozzles and their effect on agglomerate reduction.

The Fluid Coker spray nozzles are subject to extreme heat and pressure, and the bitumen flowing through them contains small concentrations of fine, abrasive clay particles. As a result, the geometry of the inside of the nozzle changes with time. Past experiments have indicated that the geometry of the spray nozzle can strongly impact the distribution of liquid in a fluidized bed (House et al. 2008), (Portoghese et al. 2010). In these experiments, the altered nozzle geometry was modified in a systematic manner in an attempt to improve the spray nozzle performance. When internal geometry modifications are produced by harsh reactor conditions, they are not produced in a predictable manner, and as such can produce an unknown and deleterious effect on agglomerate formation and spray distribution.

The objectives of the present investigation are the following

1. To develop a method to characterize the extent of erosion in a Fluid Coker spray nozzle based on the pressure drop across the nozzle or increased nozzle volume,
2. Determine how the modified internal geometry of an eroded Fluid Coker spray nozzle impacts the lifespan of agglomerates in a fluidized bed

One of three outcomes of this investigation was expected:

1. The liquid trapped in the agglomerates produced by the eroded nozzles is released at a faster rate compared to a standard TEB nozzle, indicating the

internal geometry alteration was beneficial to Fluid Coker performance. Further investigation would be required to determine what aspect of the modified nozzle geometry boosts spray performance.

2. There is no appreciable difference between the rates of liquid released from agglomerates produced by spray nozzles subject to erosion. This would indicate that the nozzles do not need to be immediately replaced when their geometry changes.
3. The liquid trapped in the agglomerates is released at a slower rate when the standard TEB nozzle is subject to erosion. This would indicate a need to monitor the spray nozzles in order to identify when they should be replaced with new, undamaged nozzles.

3.2 Apparatus

3.2.1 Fluidized Bed

A schematic of the fluidized bed used for these experiments is shown in Figure 3.1.

The cross sectional dimensions of the vessel (Figure 3.2) were 0.2 m x 1.2 m x 3.5 m, and the height was 6.1 m. The cross sectional area of the bed was chosen to represent the jet penetration zone of one Fluid Coker nozzle. The expansion angle of the bed was chosen based on a previous jet expansion study (Ariyapadi et al. 2003), and the length of the bed was chosen based on a previous jet penetration study (Ariyapadi et al. 2004).

Silica sand ($\rho = 2650 \text{ kg/m}^3$, Sauter mean diameter = 150 μm , Type B powder according to Geldart (1973)) was chosen to model coke in a cold model Fluid Coker. The injected liquid was deionized water (20 °C, $\rho = 998.5 \text{ kg/m}^3$) and the atomization gas was compressed nitrogen. Water at room temperature was used as it has a similar viscosity to bitumen at upstream nozzle conditions (about 350°C). Silica sand and water also have similar wettability characteristics to that of bitumen and coke, and this has been used in previous experiments (ZirGachian et al. (2013)). Steam flow through the nozzle was simulated using nitrogen, as a past experiment has shown that the molecular weight of the atomization gas has a negligible impact on spray droplet size (Rahman et al. 2012).

The static height of solids inside the bed was 1.6 m, giving a total mass of approximately 6200 kg. The height of the bed was monitored using a manometer with pressure taps located at heights of 0.1, 0.89, 1.5, 2.11, and 3.93 m above the gas distributor.

The bed was fluidized at 0.15 m/s and air was supplied from a compressor capable of a maximum output pressure of about 100 psig. A bank of sonic nozzles controlled the mass flow rate of fluidization air, and air pressure was regulated using Wilkerson R40-OC-000 regulators with a pressure transducer (model # PT-1PTG0100D5F5) rated for 100 psig.

3.2.2 Spray Nozzle Apparatus

The nozzle used to spray the gas-atomized liquid was a full scale Fluid Coker nozzle of approximately 25 mm O.D., and has a similar geometry to the nozzle patented by Base et al. (1999) (Figure 3.3). The nozzle was installed on the narrow side of the bed,

approximately 0.9 m above the distributor plate, and penetrated a distance of about 0.7 m into the bed. The nozzle penetration distance was chosen based on an estimation of the spray penetration using a correlation developed by Ariyapadi et al. (2004), and was chosen such that the jet would not reach the opposite side or walls of the vessel.

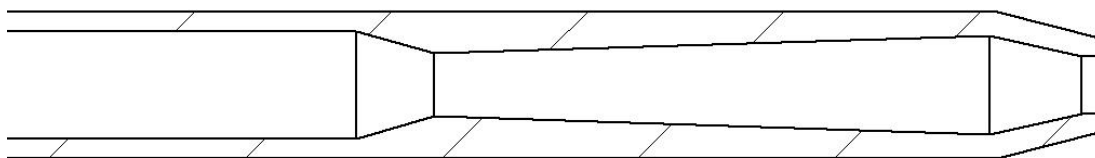


Figure 3.3: Standard TEB nozzle (Base et al. 1999)

A premix chamber was installed upstream of the spray nozzle to mix atomization gas and water. The premixer used (Figure 3.4) contains two branch pipes that connect to the nozzle entrance at an angle of 30° below the horizontal axis of the nozzle.

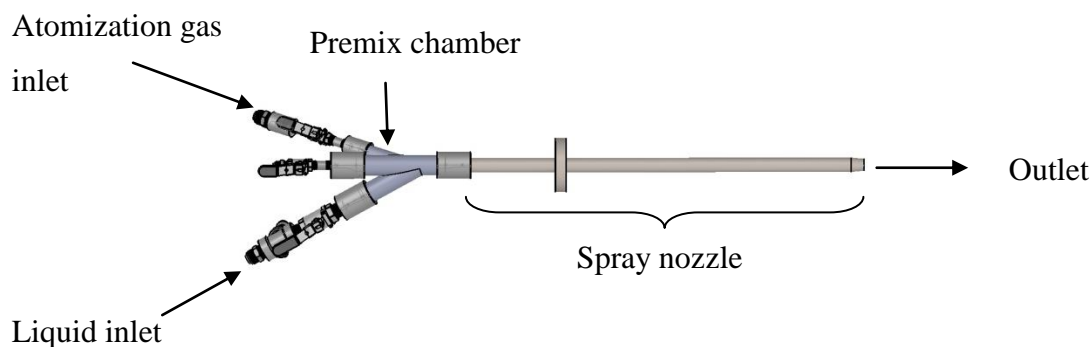


Figure 3.4: Premix chamber and nozzle assembly

To achieve flow rates similar to those used in industrial Fluid Coker reactors, a bank of high pressure cylinders (4500 psig) were connected to a blow tank filled with 15.3 L of water. When the liquid inlet valve was opened on the premix assembly, pressure exerted by nitrogen in the blow tank was used to push a float, forcing water

through the ensuing piping and premix chamber to the spray nozzle. The flow rate of nitrogen to the blow tank was controlled using a Pro Star PRS 4095331 gas pressure regulator, and the pressure was monitored using a pressure transducer (Omega PX181B-500 psig).

Atomization gas was supplied using an identical nitrogen cylinder bank and pressure regulator. In order to achieve the desired mass flow rate of atomization gas, a sonic nozzle was installed inside the gas port of the premix chamber. The size of the sonic nozzle was chosen to ensure the upstream pressure was at least double the downstream pressure during water injection. This ensured the mass flow rate of atomization gas did not fluctuate during liquid injection.

A pressure transducer (Omega PX181B-500 psig) was installed at the mixing point of the fluids in order to measure the pressure drop upstream of the nozzle.

In order to ensure the temperature of the bed was kept constant for the start of each liquid injection, 3 J-type thermocouples were inserted into the bed, and another was located in the secondary cyclone inlet. The temperature of the bed was controlled using an electric air heater connected to the fluidization gas inlet line.

3.2.3 Conductance Measurement Apparatus

Fluidized bed conductivity was measured using twenty-four metallic electrodes (25.4 x 25.4 cm), which were installed on one wall of the bed. Sheets of 19 mm thick high density polyethylene were placed between the wall of the bed and the electrodes in order to provide isolation from the metal wall of the vessel, which was electrically grounded. A power supply and signal generator were used to send a 6.5 V sinusoidal signal through a measurement resistor to the measurement electrodes (Figure 3.5). Current flowed from the 24 electrodes, through the fluidized bed, to the opposite grounded vessel wall. The voltage drop across the measurement resistor was recorded at a rate of 1000 Hz after spray completion, and was used to determine the instantaneous electrical conductance through the bed using the following voltage divider relationship:

$$C = \left\{ R_m \left(\frac{V_1}{V_2} - 1 \right) \right\}^{-1} \quad (3.1)$$

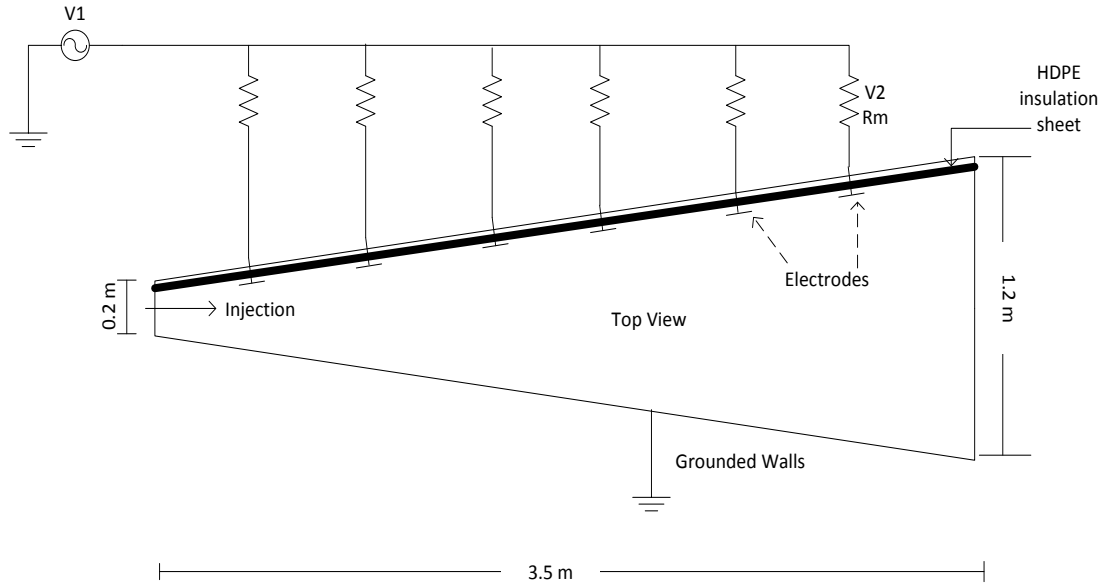


Figure 3.5: Schematic Diagram of Conductive Electrodes

3.2.4 Spray Nozzles

The performances of five spray nozzles were compared. Four of the five nozzles had an altered internal geometry due to erosion, and the fifth was a standard TEB spray nozzle. Figure 3.6 shows the appearance of the tips of the spray nozzles. A small notch had been formed at the tip of the eroded nozzles, enlarging the area of the exit orifice. A similar notch was formed on the first convergent section (Figure 3.6, bottom left), rotated approximately 120 degrees from the notch at the exit orifice. In one case, the erosion was so extreme that a perforation was formed through the side wall of the nozzle, upstream of the exit orifice (Figure 3.6, bottom right).

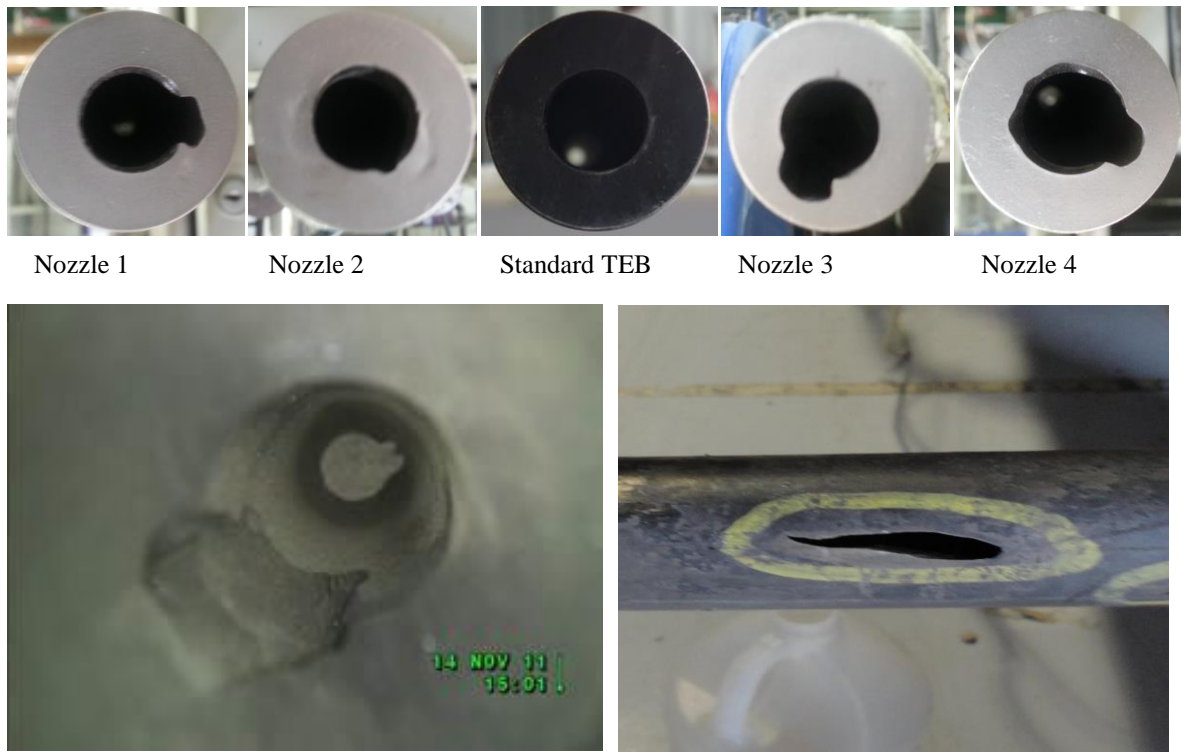


Figure 3.6: Top: Eroded nozzle and standard nozzle (middle) tips. Bottom left: Erosion located at the first throat of the TEB nozzle. Bottom right: hole formed through the wall of nozzle 3.

The cause of the erosion is not known, but one possibility may be a result of the impact of entrained solids against the inner wall of the nozzle. The bitumen may have contained traces of sand or clay particles that were not completely removed during an earlier filtering process. These sand particles were carried with the bitumen through the nozzle at a high velocity, and may have impacted the surface of the first throat of the nozzle (Figure 3.6 bottom left). The solids may have bounced off the throat and impacted the wall in another location (Figure 3.7).

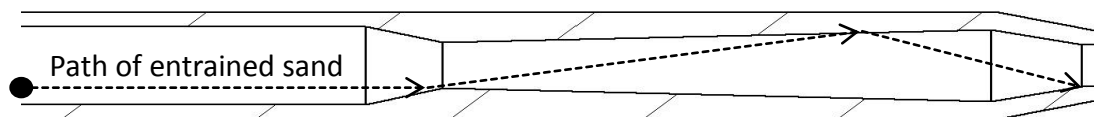


Figure 3.7: Possible trajectory of entrained solid particle within two phase flow through a Fluid Coker spray nozzle (based on visual inspection of nozzle interior)

It was also observed that the conduit connecting the nozzle to the premix chamber was slightly bent for each eroded nozzle (Figure 3.8). This bend may have produced a centrifugal force and/or a secondary flow pattern, separating the solid particles from the two phase flow, and dragging them along the wall of the nozzle. When the solid particles reached the first throat, they were deflected, and impacted another portion of the nozzle wall further downstream. The particles continued to collide with the inner wall of the nozzle until they reach the exit.

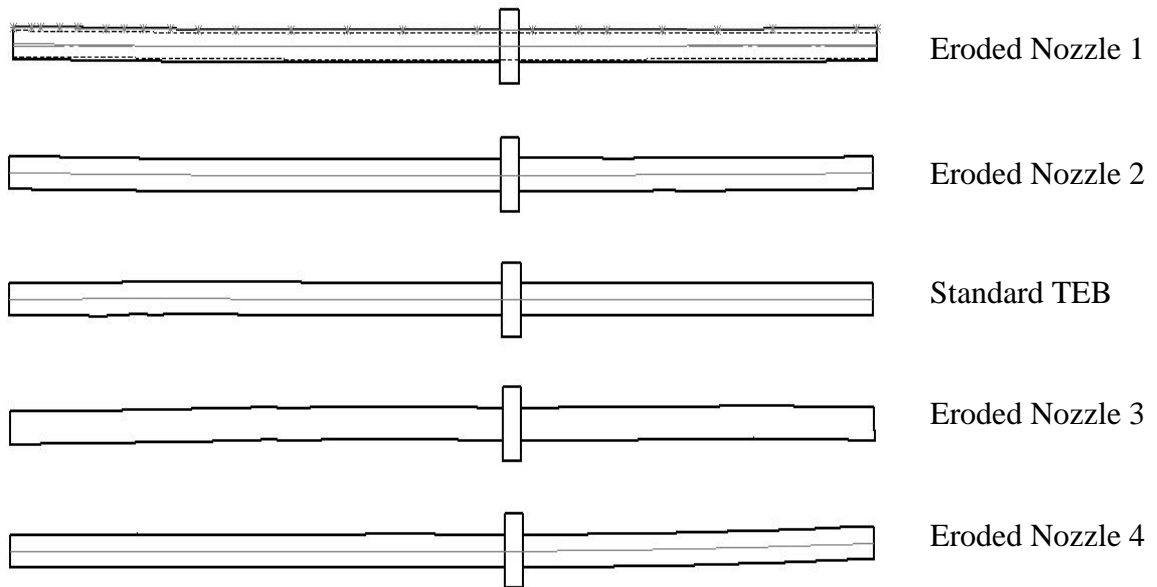


Figure 3.8: Side view of each nozzle showing curved profile. The non-eroded TEB nozzle is shown in the middle for comparison.

3.3 Procedure

Nozzle performance was evaluated by comparing the rate of moisture released from agglomerates. A higher rate of moisture released from agglomerates corresponded to a better performing nozzle. The following steps were carried out to investigate how erosion affected nozzle performance in a fluidized bed.

1. *Quantify characteristics of the eroded nozzles that deviate from the standard TEB nozzle.* The quantifiable characteristics of the nozzles measured were:
 - a. The change in internal volume
 - b. The atomization power input of the nozzle
 - c. The angle of the jet produced in the open air.
 - d. The change in nozzle throat area
2. *Measure the effect of the atomization gas to liquid ratio (GLR) on nozzle performance in a fluidized bed.* The ratio of the mass flow rate of atomization gas

to the mass flow rate of atomized liquid, or GLR, is known to have a significant impact on nozzle performance, and an increased GLR is known to distribute liquid more effectively (Portoghese et al. 2008) as well as produce agglomerates that release moisture at a higher rate (Prociw et al. 2014). It is currently not known how erosion affects the TEB nozzle performance at different GLRs. These experiments were performed at a low flow rate of 1.5 kg/s (23 USGPM) in order to achieve sprays with a GLR of 0.5%, 3.5%, and 5.6 wt%. The standard TEB nozzle performance at each GLR was compared to the eroded nozzle with the highest extent of erosion, as determined in step 2.

3. *Measure the effect of erosion on nozzle performance with the upstream liquid pressure held constant.* Constant liquid pressure was used as a condition to simulate how the nozzles perform when they are operated in the Fluid Coker. All nozzles in the Fluid Coker are connected to a common header, so that the liquid pressure upstream of each nozzle is the same, regardless of the flow rate through it (i.e. regardless of the extent of erosion). Sprays are produced with a liquid pressure corresponding to a liquid flow rate of 3 kg/s (47 USGPM) in uneroded nozzles to approximate the liquid flow rate through commercial scale Fluid Coker spray nozzles. The atomization gas flow rate was maintained at a constant value corresponding to a GLR of 2 wt% for the standard liquid flow rate since, in commercial cokers, the gas flow rate is maintained constant with a restriction orifice operating under sonic conditions.
4. *Measure the effect of erosion on nozzle performance with the liquid flow rate held constant.* This step was taken in order to eliminate the effect of liquid flow rate on the results, and to provide a fair comparison of each nozzle when operated at the desired flow rate. Once again, sprays are produced at a liquid flow rate of 3 kg/s (47 USGPM) and GLR = 2 wt% to approximate the operating conditions used for commercial scale Fluid Coker spray nozzles.

3.3.1 Nozzle Characteristics

3.3.1.1 Change in Nozzle Volume due to Erosion

Each nozzle was filled with water, and the mass of water was measured to evaluate the volume of each nozzle.

3.3.1.2 Atomization Power Input

The pressure drop produced by each nozzle multiplied by the volumetric flow rate of fluid travelling through the nozzle was calculated in order to estimate the rate of energy transferred to the liquid for atomization.

3.3.1.3 Open Air Spray Angle Measurement

To measure the spray angles produced by each nozzle, sprays from each nozzle were produced in an open air environment. Images of the spray were produced and the length of the nozzle was included in each image as a reference length. This reference was used to measure the width of the spray at a distance of one nozzle length from each nozzle's exit orifice.

Previously, Dawe et al. (2009) showed that the expansion angle of a jet produced in an open air environment is larger than the expansion angle produced in a fluidized bed. However, it was expected that characteristics of the spray due to erosion under atmospheric conditions would be similar to spray characteristics found in the fluidized bed.

3.3.1.4 Extent of Nozzle Throat Erosion

A simplified model was developed to estimate from upstream pressure measurements the increase in area of the nozzle throat due to erosion. The increase in nozzle throat area was used to characterize the extent of erosion for each nozzle tested.

Previous experiments using TEB nozzles (Ariyapadi et al. 2004) have been used to develop a model to predict the pressure at the tip of the nozzle using the measured upstream nozzle pressure (downstream of the premix chamber). It has been shown that:

$$\frac{P_{up}}{P_{throat}} = k \quad (3.2)$$

where k is a constant that ranges in value between 2.2-2.4 (Ariyapadi et al. 2004).

The area of the throat of a nozzle can be estimated with compressible gas relations using the density of the fluid, the speed of sound, and the mass flow rate through the restriction. The speed of sound in a two phase gas-liquid mixture can be estimated using the following correlation (Bar-Meir, 2013):

$$u_{sound} = u_{gas} \left(\frac{\rho_g}{y} \right)^{0.5} \quad (3.3)$$

Where the speed of sound in a pure gas is given by:

$$u_{gas} = \left(\frac{\gamma RT}{M_g} \right)^{0.5} \quad (3.4)$$

And:

$$y = \varepsilon_g [\rho_L (1 - \varepsilon_g) + \rho_g \varepsilon_g] \quad (3.5)$$

$$\varepsilon_g = \frac{F_g / \rho_g}{F_g / \rho_g + F_L / \rho_L} \quad (3.6)$$

For this simplified model, the following assumptions were made:

1. There is no radial velocity gradient within the nozzle
2. The slip velocity between gas bubbles and liquid is negligible
3. The density of the gas can be calculated using the ideal gas equation of state

$$\rho_g = \frac{P_{throat} M_g}{RT} \quad (3.7)$$

Using equations (3.2)-(3.7) and the preceding assumptions, the area of the throat of a nozzle may be estimated using equation (3.8):

$$A_{throat} = \frac{F_g}{\rho_g \varepsilon_g u_{sound}} \quad (3.8)$$

The following iterative procedure was used to calculate k for the standard TEB nozzle used in this experiment:

1. Assume k , measure P_{up} , and calculate P_{throat} from eq. (3.2)
2. Calculate ρ_g from eq. (3.7)
3. Calculate the void fraction from eq. (3.6)
4. Using the void fraction of gas, the mass flow rates and densities of the gas and liquid, as well as the speed of sound in a pure gas, the speed of sound in the two phase mixture was calculated using eq. (3.3).
5. The area of the TEB nozzle throat can then be calculated using eq. (3.8)
6. The calculated nozzle throat area is compared to the measured standard TEB nozzle throat area. The difference is minimized by repeating steps 1-5.

Once the difference between the calculated and measured throat areas had been minimized, the corresponding k value was used in conjunction with steps 1-5 to calculate the throat area of each eroded nozzle.

Using this procedure, a value of 2.39 was determined for k by using the uneroded TEB nozzle data. This value was in good agreement with previously determined k values for TEB nozzles found by Aryiapadi et al. (2004).

3.3.2 Measuring the Rate of Liquid Released from Agglomerates to Assess Nozzle Performance in a Fluidized Bed

3.3.2.1 Gas-Atomized Liquid Spray Procedure

Using a previously developed electrode conductance calibration technique, the following procedure was used to calculate the fraction of injected water released from agglomerates using a commercial scale Fluid Coker nozzle:

1. Pressure regulators located at the atomization gas cylinders and liquid pressure cylinders were used to set the desired flow rate and GLR.
2. Pressure regulators on the fluidization gas line were used to set the fluidization velocity at 0.15 m/s.
3. The bed freeboard was heated to a temperature of 24.5°C before each spray injection.
4. Liquid was injected into the bed at a specified flow rate, and the conductance of the bed was measured at a rate of 1000 Hz.
5. The temperature of the bed at three different locations, and the temperature of the freeboard were measured at a rate of 2.4 Hz. The temperature of the outlet air was used to calculate the humidity of the air, which in turn was used to calculate the mass flow rate of water from the bed (eq. 2.5)
6. The bed remained fluidized throughout the duration of the experiment. When the electrode conductance measurements reached the pre-injection values, data acquisition was ceased.

3.3.2.2 Free Moisture Measurement Using Conductance Model

After injection into the bed, some of the liquid was distributed throughout the fluidized solids in the form of free moisture. The free moisture content was accounted for using the conductance measurements and electrode calibration curves. A portion of the liquid formed liquid-solid agglomerates, which were heavier than individual solid particles, and were likely to sink to the bottom of the fluidized bed. Agglomerates do not register conductance readings, as they do not provide a path for current to travel from the electrodes to the grounded wall of the bed (ZirGachian et al. 2013).

The total amount of water in the bed at any time was determined by subtracting the amount evaporated from the total mass of water injected as given by eq. (3.9):

$$f_e = \dot{v}_a \cdot A_{bed}(\mathcal{H}^* - \mathcal{H}_{in}) \quad (3.9)$$

Free moisture can be produced through the destruction of agglomerates, and is consumed through the evaporation of water from the fluidized bed (Mohagheghi et al. 2013). Thus the rate of change of free moisture in the fluidized bed is:

$$\frac{d(M_s \bar{x})}{dt} = \left[\frac{d(M_s \bar{x})}{dt} \right]_{agg} - f_e \quad (3.10)$$

The term on the left hand side of eq. (3.10) can be measured using the conductance measurements and the calibration curves for each electrode (developed in a previous experiment by Prociw et al. (2014)). The second term on the right hand side of equation (3.10) represents the rate of water exiting the fluidized bed due to evaporation, and can be determined using eq. (3.9). Rearranging eq. (3.10) for the unknown term gives:

$$\left[\frac{d(M_s \bar{x})}{dt} \right]_{agg} = \frac{d(M_s \bar{x})}{dt} + f_e \quad (3.11)$$

The cumulative mass of water released from agglomerates since the end of liquid injection can be calculated by integrating eq. (3.11)

$$(M_s \bar{x})_{\text{agg}} = \int_0^t \left[\frac{d(M_s \bar{x})}{dt} + f_e \right] dt \quad (3.12)$$

The fraction of water released from agglomerates (i.e. the fraction of injected liquid in the form of free moisture, $G(t)$) may be calculated using the following expression:

$$G(t) = \frac{(M_s \bar{x})_{\text{agg}}}{M_L} = \frac{M_s}{M_L} \left[\int_0^t \left[\frac{d\bar{x}}{dt} + \frac{f_e}{M_s} \right] dt \right] \quad (3.13)$$

where M_L and M_s are the mass of liquid injected and solids present in the fluidized bed, respectively, \bar{x} is the average free moisture content of the bed as determined using the conductance electrode measurements, and f_e is the flow rate of evaporated water leaving the bed. The function $G(t)$ ranges from 0 at the start of the experiment (where all moisture injected is initially trapped in agglomerates) to 1 at the end of the experiments (where the fraction of water not trapped in agglomerates equals 1 or 100%). The faster $G(t)$ approaches 1, the faster agglomerates were broken and release their moisture into the surrounding fluidized solids.

For each nozzle and operating condition tested, $G(t)$ was plotted as a function of time. A curve was fit through the experimental data of the form:

$$G(t) = 1 - e^{-t/\tau} \quad (3.14)$$

where τ represents the amount of time necessary for 62.5% of the moisture trapped in agglomerates to be released in the fluidized bed as free moisture. Values of τ are evaluated for each experiment to compare the performance of nozzles inside the fluidized bed.

3.4 Results

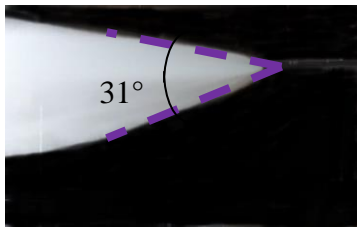
3.4.1 Eroded Nozzle Characteristics

3.4.1.1 Open Air Spray Visualization

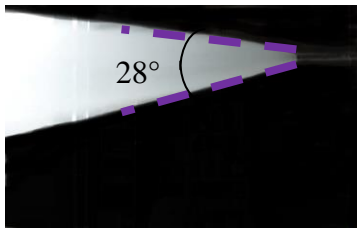
The sprays produced by each eroded nozzle are shown in Figure 3.9. Each eroded nozzle was installed such that the groove formed at the nozzle tip was facing downwards in the open air spray tests, and upwards in the fluidized bed. Placing the groove upward in the fluidized bed ensured the spray did not interact with the walls of the vessel or the distributor plate at the bottom of the vessel.

The free jet spray angle for each eroded nozzle appears to be significantly larger than the spray angle of the standard TEB nozzle, indicating better radial dispersion of the liquid. Visual inspections of the sprays produced by each eroded nozzle indicate that the sprays are not symmetric. A substantial portion of the liquid flows through the notch created through erosion, and flows out the nozzle exit at a higher angle from the longitudinal axis of the nozzle compared to the rest of the spray. The grooved tip of each eroded spray nozzle (Figure 3.6) appears to help redirect a portion of the liquid in the radial direction.

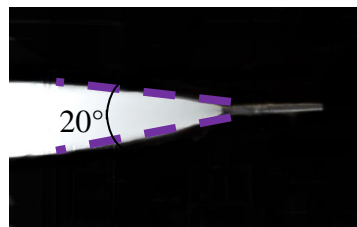
Although it was expected that the jet expansion angle inside a fluidized bed will be smaller compared to the jet expansion angle produced in open air experiments, it was further expected that an increase in jet expansion angle in open air experiments would correspond to an increase in the jet expansion angle inside a fluidized bed.



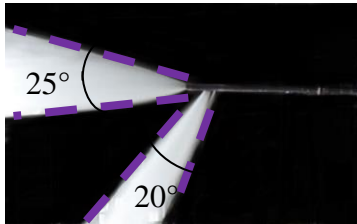
Eroded Nozzle 1



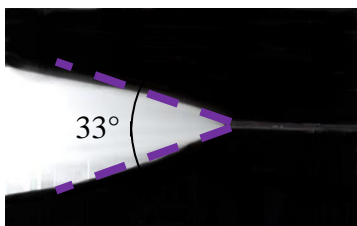
Eroded Nozzle 2



Standard TEB



Eroded Nozzle 3



Eroded Nozzle 4

Figure 3.9: Images of free jets produced by each nozzle.

3.4.1.2 Nozzle Throat Area, Volume, and Open Air Spray Angle

Each calculated nozzle throat area and volume was divided by the TEB nozzle throat area and volume to produce a normalized data set. The spray angles reported are the vertical jet expansion angle in the open air spray tests. These expansion angles include the effect of the groove located at the tip of each eroded nozzle.

Table 3.1: Calculated nozzle throat areas based on upstream pressure drop measurement. * The angle produced by both jets was added together for Nozzle 3.

Nozzle	Normalized Throat Area	Normalized Volume	Open Air Spray Angle (°)
Standard TEB	1	1	21
Eroded Nozzle 1	1.14	1.39	31
Eroded Nozzle 2	1.11	1.11	28
Eroded Nozzle 3	1.68	1.79	45*
Eroded Nozzle 4	1.24	1.07	33

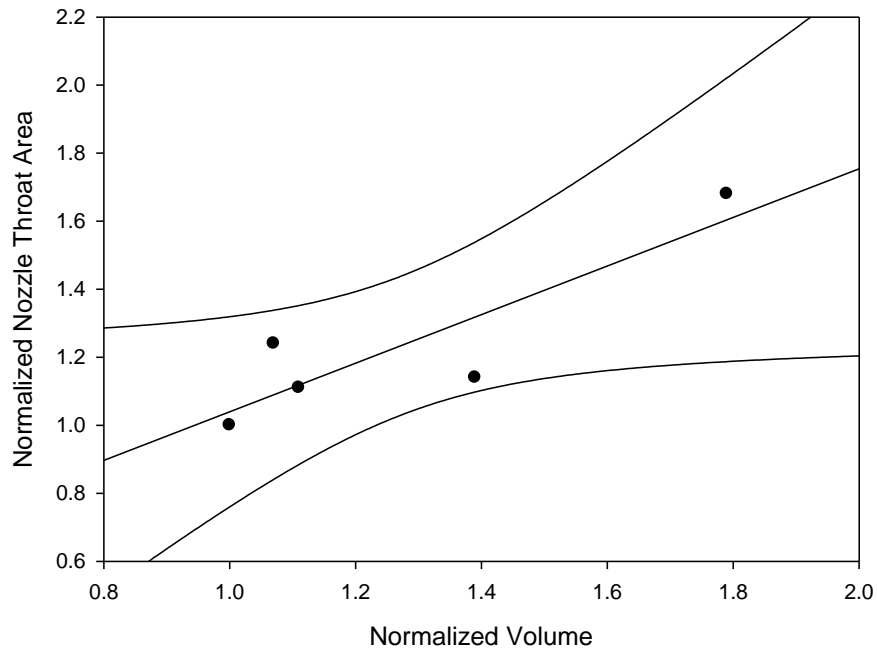


Figure 3.10: Normalized throat area as a function of nozzle volume (95% confidence interval shown)

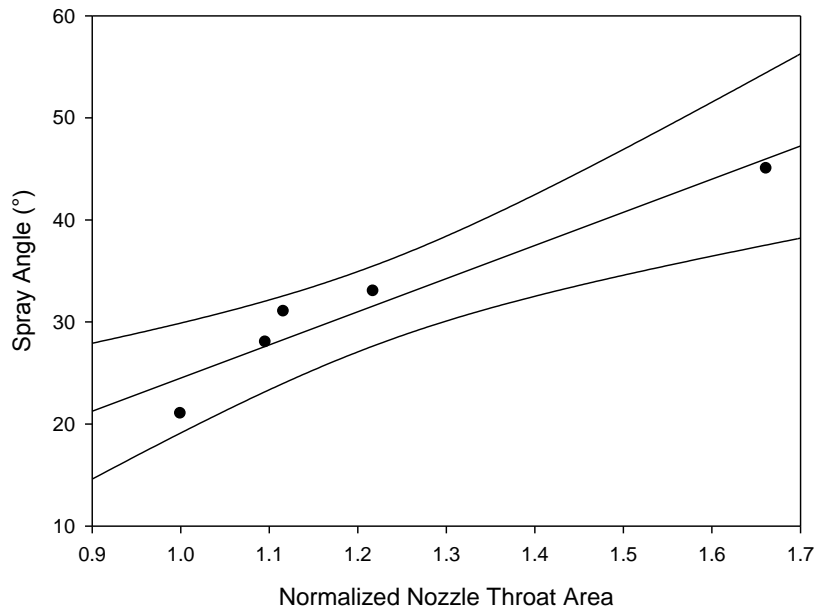


Figure 3.11: Open air spray angle as a function of normalized nozzle throat area (95% confidence interval shown)

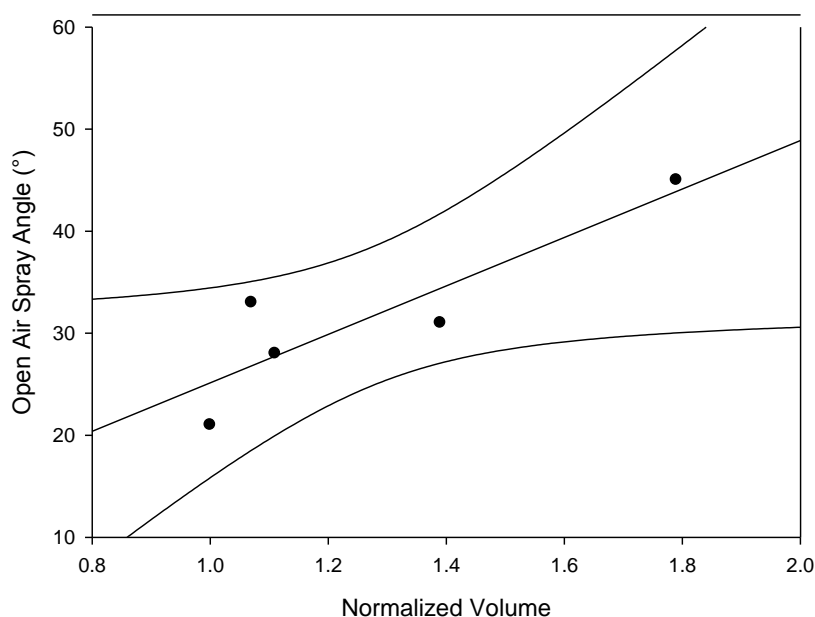


Figure 3.12: Open air spray angle as a function of normalized volume (95% confidence interval shown)

Figures 3.10-3.12 indicates that there is a relationship between each variable investigated in Table 3.1, and that there is a strong correlation between the throat area of the nozzle and the open air spray angle. Increased erosion corresponds to a greater nozzle volume, and greater throat diameter, which appear to lead to a greater open air spray angle (Figure 3.11 and 3.12). Because of the stronger correlation between nozzle throat area and jet expansion angle, the calculated throat area was chosen to characterize the extent of nozzle erosion for subsequent nozzle performance analysis.

3.4.2 Effect of GLR on Standard TEB Nozzle and Eroded TEB Nozzle

Liquid injections were carried out inside the fluidized bed with the standard TEB nozzle, and one eroded TEB nozzle (Eroded Nozzle 3, Figure 3.6, and Figure 3.9). Eroded nozzle 3 produced a main jet and a secondary jet (Figure 3.9). Figure 3.13 illustrates the cumulative fraction of the injected water that has been released from agglomerates as a function of time for a standard TEB nozzle. A similar plot is produced

for the eroded nozzle. Curves are fitted to the experimental data in order to obtain the agglomerate moisture release constant τ .

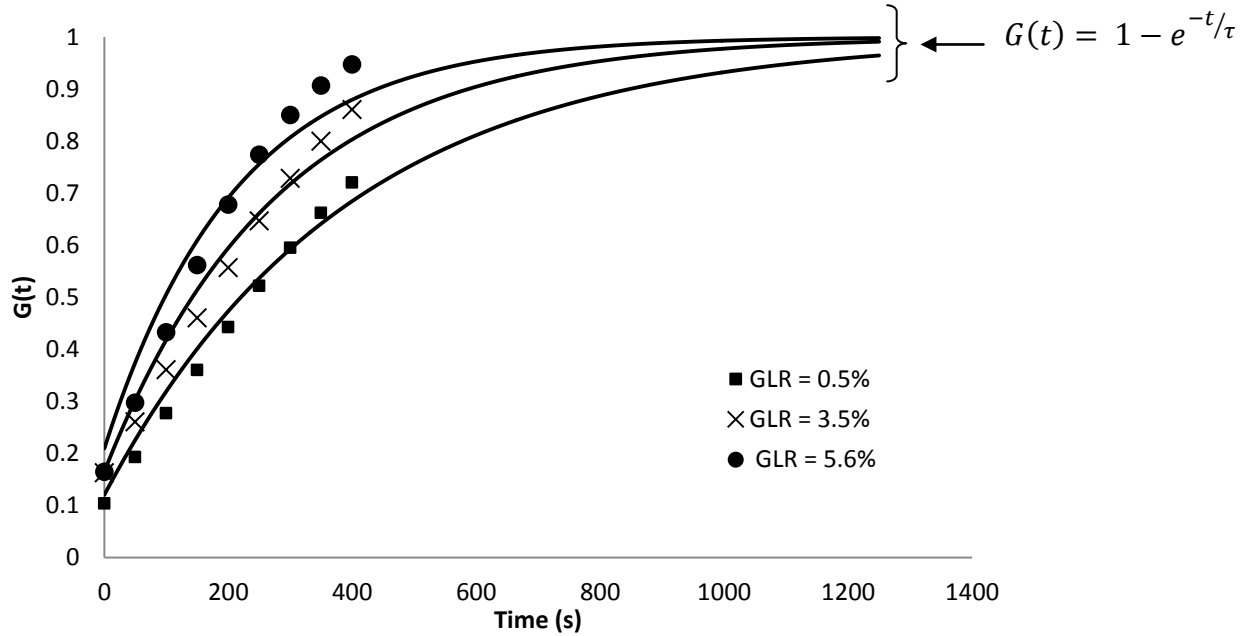


Figure 3.13: Fraction of injected liquid released from agglomerates vs. time after spray completion

Increasing the GLR increased the rate of moisture released from agglomerates. This trend was expected, since the increased atomization gas flow rate produces a higher pressure drop at the tip of the nozzle. The higher pressure drop corresponds to a higher rate of energy input for atomization (defined in section 3.3.1.2), leading to smaller droplet size, and greater jet expansion inside the fluidized bed (Figure 3.14).

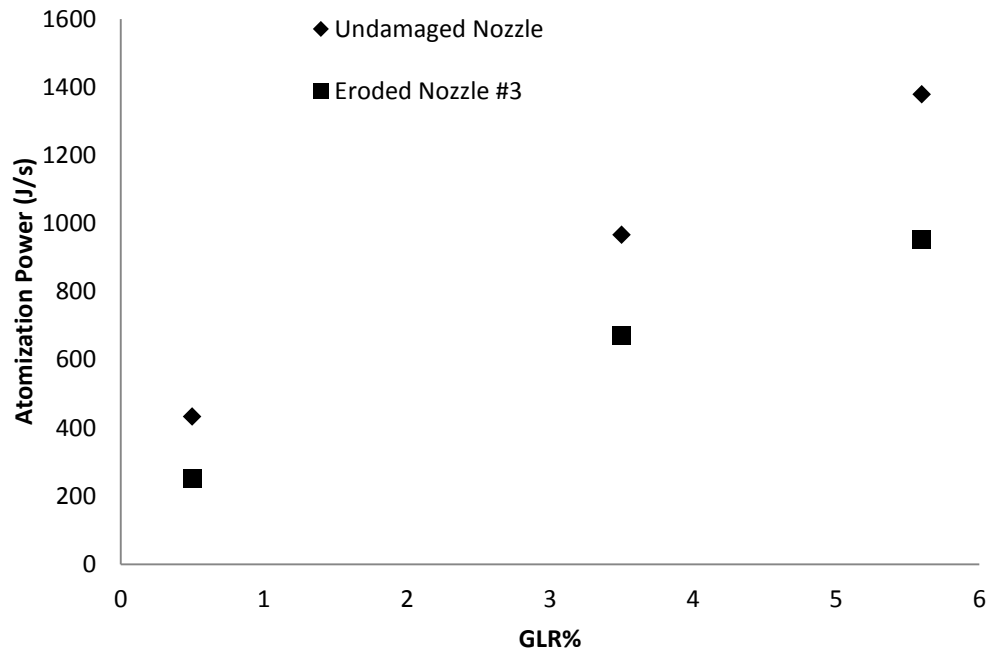


Figure 3.14: Atomization power as a function of GLR for each nozzle

The same GLR and liquid flow rate were applied to Eroded Nozzle 3. The moisture release rate time constant is plotted as a function of GLR for both the standard TEB nozzle and the eroded TEB nozzle.

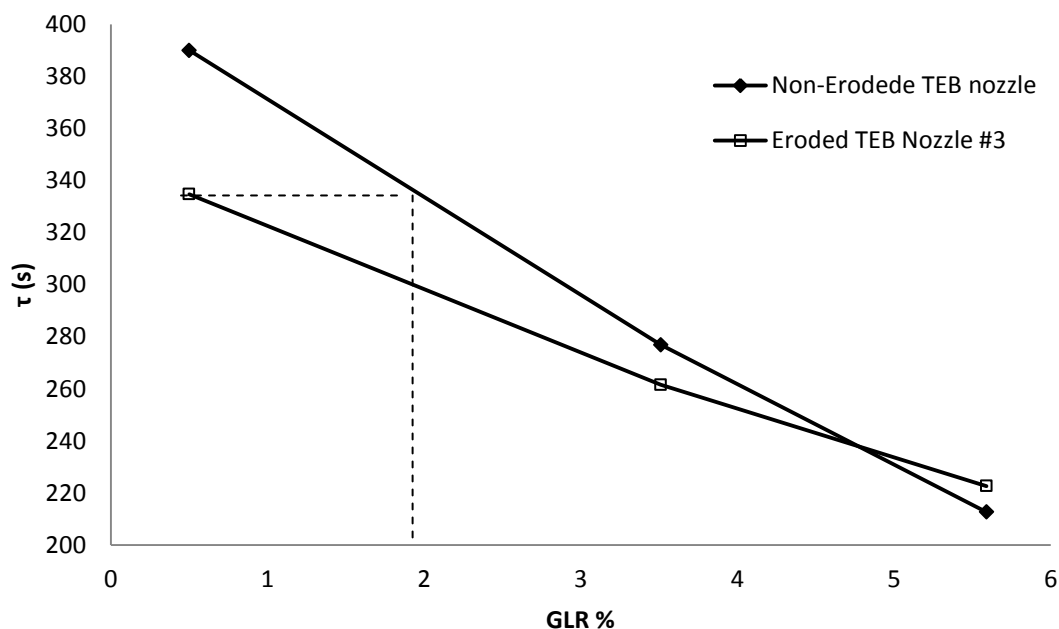


Figure 3.15: Agglomerate moisture release rate time constant vs. GLR for non-eroded TEB nozzle, and Eroded Nozzle 3 (1.5 kg/s).

Figure 3.15 shows similar trends for both eroded and non-eroded nozzles. As GLR is increased, τ is decreased. This is attributed to better atomization due to higher injection pressure in each nozzle. A surprising observation was the margin of superior performance of the eroded nozzle over the standard TEB nozzle at low GLR. This could not be explained by atomization power, since the eroded nozzle exhibited lower atomization power at those GLRs, as indicated in Figure 3.14. Although the pressure in the eroded nozzle was substantially lower than in the standard TEB nozzle, moisture released from agglomerates at a higher rate when using the eroded nozzle.

It is apparent that another mechanism must play a role in affecting the rate at which liquid was released from agglomerates. Images of the open air sprays (Figure 3.9) indicate that with the secondary jet, Eroded Nozzle 3 directs a significant portion of the injected liquid to a region of the bed that is not reached using the standard TEB nozzle. The liquid volume in the main horizontal jet is smaller with the eroded nozzle, which appears to be beneficial in producing weaker agglomerates. The secondary jet also

appears to be well atomized and allows the liquid to reach an otherwise dry portion of the bed, far away from the main horizontal spray. The wide initial distribution of liquid inside the fluidized bed may account for the formation of less stable agglomerates, despite the lower pressure inside the spray nozzle.

A higher distribution of liquid inside the fluidized bed also corresponds to a higher jet-bed interfacial area. The larger area covered by the spray may aid in entraining more solids into the spray, further reducing the concentration of liquid in the jet region of the fluidized bed.

3.4.3 The Effect of Nozzle Erosion on Jet-Bed Interaction at High Liquid Flow Rate

In addition to the standard TEB nozzle, and Eroded Nozzle 3, three additional eroded nozzles were used to inject liquid inside a fluidized bed.

Figures 3.16 – 3.18 plot the effect of effective nozzle throat area on the agglomerate moisture release time constant τ . The atomization gas flow rate used for each constant upstream liquid pressure condition was held constant, and was equal to the gas flow rate required to produce a spray with 2% GLR using the standard TEB nozzle. Considering that the area of the eroded nozzle exit orifice was larger compared to the standard TEB nozzle, the resulting liquid flow rate through the eroded nozzles was higher than the standard TEB nozzle, and the corresponding GLR was lower. Despite the decrease in GLR for the eroded nozzles, the rate of moisture release from the agglomerates produced by these nozzles was significantly higher than the rate measured using the standard TEB nozzle. Therefore, another important effect, besides GLR, must be responsible for the observed trend.

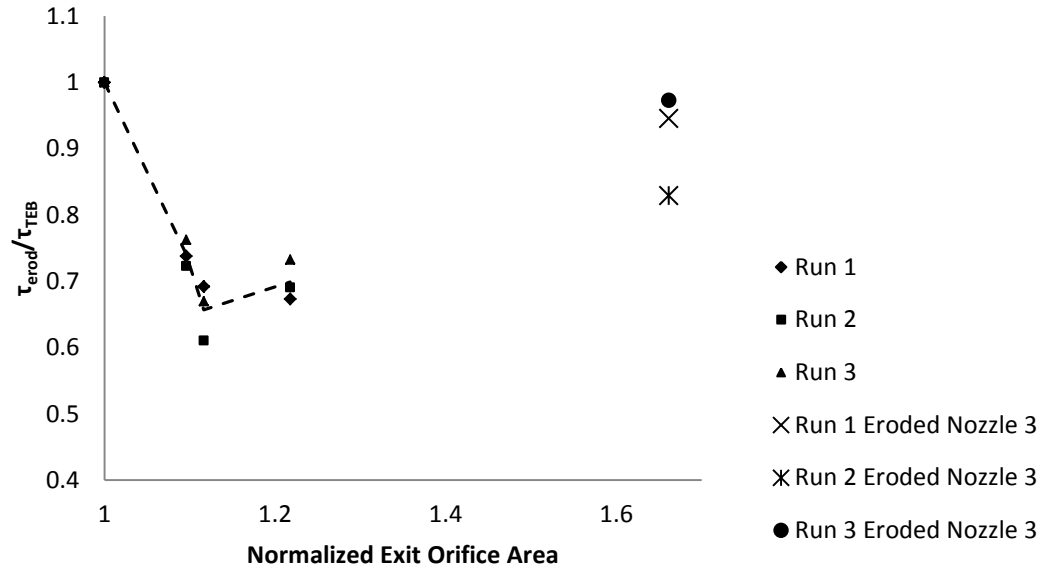


Figure 3.16: Agglomerate moisture release rate time constant versus normalized nozzle exit orifice area. Constant upstream liquid pressure (2600 kPa (gauge)). Replicates for each nozzle are shown.

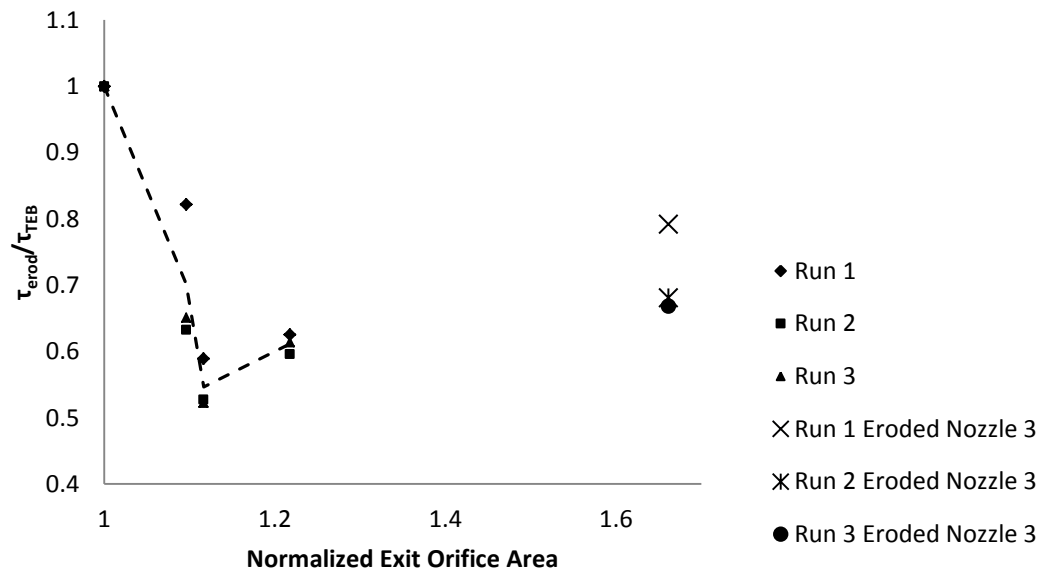


Figure 3.17: Agglomerate moisture release rate time constant versus normalized nozzle exit orifice area. Constant liquid flow rate (3 kg/s, GLR = 2%). Replicates for each nozzle are shown.

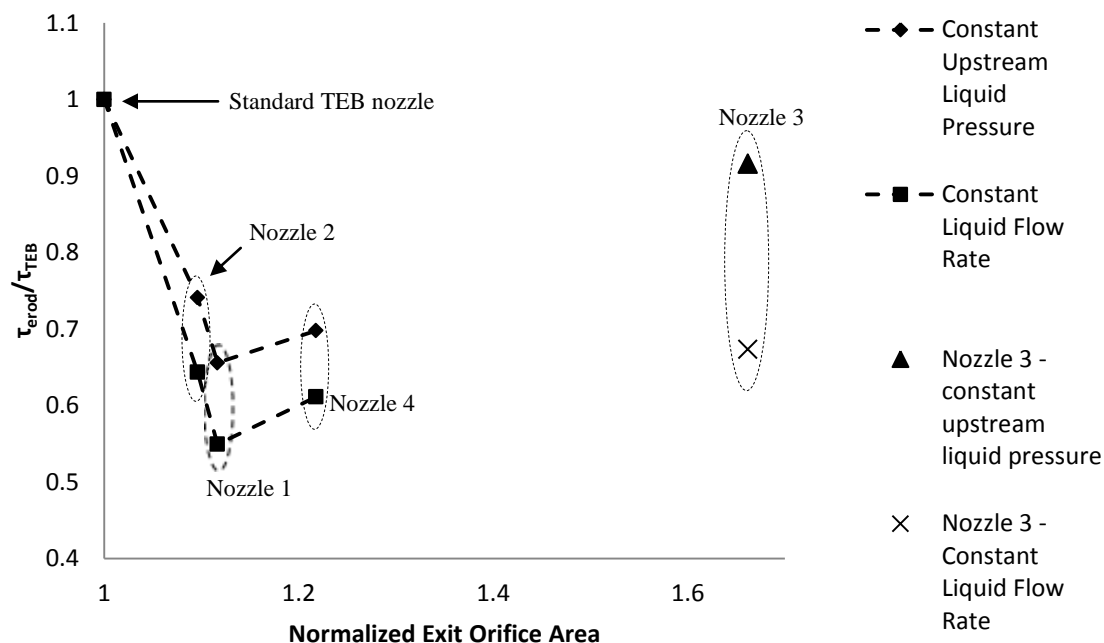


Figure 3.18: Comparison of the effect of nozzle erosion on the agglomerate moisture release rate time constant for constant upstream liquid pressure case and constant liquid flow rate case.

Images of the open air sprays (Figure 3.9) indicate that the spray angle produced by the eroded nozzles is larger than the spray angle produced by the standard TEB nozzle, despite the lower GLR. This is likely due to the altered geometry of the TEB nozzle tip due to erosion. Figure 3.6 shows images of each of the nozzle tips used in this investigation. Each of the eroded nozzles have a section of the nozzle tip removed, making the exit orifice area larger. Visual analysis of the open air spray jets indicate that the sprays are not radially symmetric, and that the increased spray angle is due to a fraction of the atomized liquid flowing through the eroded portion of the nozzle tip. This suggests that in addition to the GLR, the direction through which the liquid is expelled from the nozzle also plays an important role in affecting the rate of liquid released from agglomerates produced by the sprays.

When liquid is atomized into the fluidized bed, it forms a jet cavity consisting mostly of gas through which liquid droplets and entrained solid particles move from the nozzle tip region to the cavity tip region. Digital x-ray imaging experiments carried out

by Ariyapadi et al. (2003) indicated that agglomerates tend to form at the end of the tip of the jet cavity, close to its maximum penetration length inside the fluidized bed. Although some solids are entrained into the jet cavity and may contact with the liquid droplets within the cavity, most of the liquid is sprayed on the dense fluidized bed solids at the cavity tip. The increased spray angle caused by the eroded nozzle geometry may distribute the liquid over a wider area at the cavity tip, resulting in agglomerates with lower liquid concentration that are thus weaker and break up more easily.

In addition to constant upstream liquid pressure, sprays were produced inside the fluidized bed for each nozzle at a constant liquid flow rate (3 kg/s). In order to achieve a constant liquid flow rate, the liquid pressure for each nozzle had to be lowered to match the liquid flow rate produced by the standard TEB nozzle. Figure 3.17 shows the effect of eroded nozzle throat area on the time constant τ at a constant liquid flow rate.

The value of τ was further decreased for each eroded nozzle as the liquid pressure was reduced to achieve the same liquid flow rate in each nozzle. As a result of reducing the liquid pressure, the liquid flow rate dropped compared to the constant upstream liquid pressure case (Figure 3.18), but the atomization gas flow rate remained the same in all cases. The drop in liquid flow rate resulted in an increased GLR for each eroded nozzle. This increased GLR corresponds to a higher degree of atomization within the nozzle (more atomization energy per unit mass of liquid), and therefore produced a spray with a greater entrainment rate of solids, and better a distribution of liquid droplets on fluidized solids.

3.5 Conclusions

It has been shown that increasing the atomization gas flow rate produces wet agglomerates that release their liquid content faster. This trend is observed for both a standard TEB nozzle, and an eroded TEB nozzle.

Nozzle erosion increases the liquid flow rate through the spray nozzle when it is operated at a constant liquid upstream pressure and constant mass flow rate of atomization gas. Erosion also changes the geometry of the tip of the spray nozzle, resulting in the distribution of liquid over a larger area of fluidized solids at the tip of the

spray jet cavity. This reduces the liquid concentration within the wet agglomerates that are formed near the tip of the jet cavity, resulting in weaker agglomerates that release moisture at a higher rate.

3.6 References

- Ariyapadi, S., Holdsworth, D.W., Norley, C.J.D., Berruti, F., Briens, C. (2003) “Digital X-ray Imaging Technique to Study the Horizontal Injection of Gas-Liquid Jets into Fluidized Beds”, *International Journal of Chemical Reactor Engineering*, vol. 1 Article A56.
- Ariyapadi, S., Berruti, F., Briens, C., McMillan, J., Zhou, D. (2004) “Horizontal Penetration of Gas-Liquid Sprays in Gas-Solid Fluidized Beds”, *International Journal of Chemical Reactor Engineering*, vol. 2 Article A22.
- Bar Meir, G. (2013) “Fundamentals of Compressible Fluid Mechanics”, Free Software Foundation Inc., Boston.
- Base, T.E., Chan, E.W., Kennett, R.D., Emberley, D.A. (1999) *U.S. Patent 6,003,789*. Washington, D.C.: U.S. Patent and Trademark Office.
- Berruti, F., Dawe, M., Briens, C. (2009) “Study of gas-liquid jet boundaries in a gas-solid fluidized bed”, *Powder Technology*, vol. 192, no. 1, pp 250-259.
- Davuluri, R.P., Bielenberg, J.R., Sutton, C.R., Raich, B.A. (2011) *U.S. 2011/0114468*. Washington, D.C.: U.S. Patent and Trademark Office.
- Geldart, D. (1973) “Types of gas fluidization”, *Powder Technology*, vol.7
- Gray, M.R. (2002) “Fundamentals of bitumen coking process: a critical review”, *Canadian Journal of Chemical Engineering*, vol. 80, no. 3, pp. 393-401.
- Gray M., Le, T., McCaffrey, W. Berruti, F., Soundarajan, S., Chan, E., Huq, I. Thorne, C., (2001) “Coupling of mass transfer and reaction in coking of thin films of an

- Athabasca Vacuum Residue”, *Industrial & Engineering Chemistry Research*, vol. 40, no. 15, pp. 3317-3324.
- House, P.K., Briens, C.L., Berruti, F., Chan, E. (2009) “Effect of spray nozzle design on liquid–solid contact in fluidized beds”, *Powder Technology*, vol. 186, no. 1, pp. 89-98.
- Knapper, B.A., Gray, M.R., Chan, W., Mikula, R. (2003) “Measurement of Efficiency of Distribution of Liquid Feed in a Gas-Solid Fluidized Bed Reactor”, *International Journal of Chemical Reactor Engineering*, vol. 1, Article A35.
- Pfeiffer, R.W., Borey, D.S., Jahnig, C.E. (1959) *U.S. Patent No. 2,881,130*. Washington, D.C.: U.S. Patent and Trademark Office.
- Pirooz, D., Pougatch, K., Salcudean, M., Grecov, D. (2010) “Agglomeration of Biturmen-Coated Coke Particles in Fluid Cokers”, *International Journal of Chemical Reactor Engineering*, vol. 8, Article A122.
- Portoghese, F., Ferrante, L., Berruti, F., Briens, C., Chan, E. (2010) “Effect of the injection-nozzle geometry on the interaction between a gas–liquid jet and a gas–solid fluidized bed”, *Chemical Engineering and Processing Process Intensification*, Vol. 49, no. 6, pp. 605-615.
- Portoghese, F., Ferrante, L., Berruti, F., Briens, C., Chan, E. (2008) “Effect of injection nozzle operating parameters on the interaction between a gas-liquid jet and a gas-solid fluidized bed”, *Powder Technology*, Vol. 184, no. 1, pp. 1-10.
- Prociw, N. (2014) “Effect of Nozzle Geometry on Jet-Bed Interaction. Experiments with Commercial Scale Nozzles and Eroded Nozzles”, *Masters Thesis*, The University of Western Ontario, London.
- Rahman, M.A., Balzan, M., Heidrick, T., Fleck, B.A. (2012) “Effects of the gas phase molecular weight and bubble size on effervescent atomization”, *International Journal of Multiphase Flow*, vol. 38, no. 1, pp. 35-52.

Sanchez, F. (2013) “Hydrodynamics in Recirculating Fluidized Bed Mimicking the Stripper Section of a Fluid Coker”, *PhD Dissertation*, The University of Western Ontario, London.

Speight, J., Baki Ozum (2001) “Petroleum Refining Processes”, Marcel Dekker Inc. New York.

Chapter 4

4 Effect of Spray Nozzle Attachment Geometry on Rate of Liquid Released from Agglomerates Produced by Gas-Atomized Liquid Injection into a Fluidized Bed

Nicholas Prociw¹, Cedric Briens¹, Franco Berruti¹

¹Institute for Chemicals and Fuels from Alternative Resources (ICFAR)
Engineering, University of Western Ontario
London, On, Canada N6A 5B9

4.1 Introduction

Liquid injection into a fluidized bed is employed in several chemical processes in order to maximize contact between liquid reactants and solid particles. The solid particles may be catalysts, such as those found in Fluid Catalytic Cracking, or simply heat carriers, as found in Fluid Coking TM. Fluid Coking uses steam atomized liquid injection nozzles to distribute bitumen droplets into a bed of hot coke particles. When the bitumen droplets contact the coke particles, they form wet agglomerates that restrict heat transfer from the bed to the reacting bitumen, slowing down the bitumen cracking reactions. The results are reduced reactor operability and a lower yield of valuable liquid product (see Chapter 1).

Base et al. (1999) patented one of the typical spray nozzles used to distribute liquid reactants in a Fluid Coker (Figure 4.5). Upstream of the spray nozzle, steam and bitumen are mixed at a high pressure to create a two phase bubbly flow. The gas-liquid mixture flows through a converging/diverging nozzle, which accelerates the flow, and aids in the breakup of liquid into small droplets. At the tip of the nozzle, the two phase compressible flow becomes choked, and a large pressure drop is created, leading to rapid gas expansion. The expanding gas bubbles exert a force on the liquid exiting the nozzle, shattering it into small droplets, and directing these small droplets in a radial direction away from the central axis of the spray nozzle. The purpose of the spray nozzle is to produce small bitumen droplets, and distribute these droplets as evenly as possible among the fluidized coke particles inside the reactor.

Knapper et al. (2003) investigated the quality of liquid distribution inside a pilot scale Fluid Coker using a scaled down version of the nozzle developed by Base et al. A copper naphthenate tracer was injected with the bitumen into the bed of coke particles. Samples of coke were withdrawn from the reactor and analyzed for copper content. Results of this tracer technique indicated that the distribution of bitumen among the coke particles was poor, and that a more effective nozzle was required to enhance the liquid-solid contact efficiency.

In an attempt to improve spray nozzle performance, Zhou et al. (2004) investigated the effect of adding a hollow cylindrical tube (draft tube or Enhanced Solids Entrainment device) downstream of the spray (Figure 4.1)

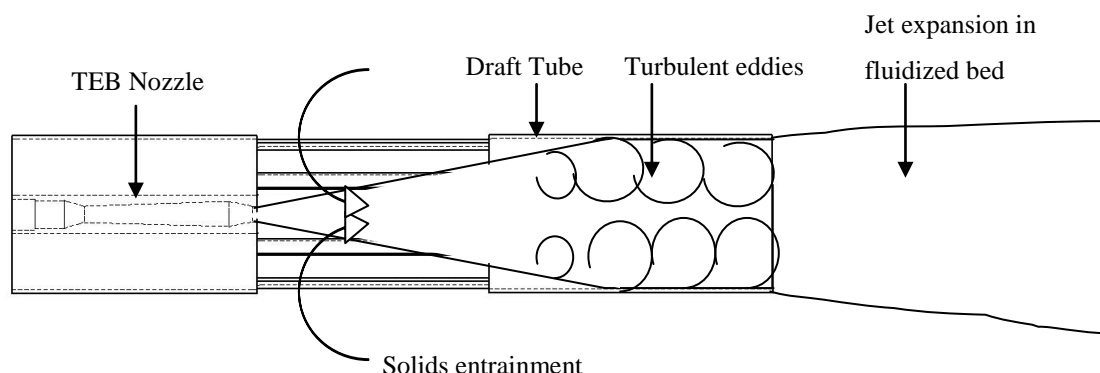


Figure 4.1: Turbulent eddy formation inside draft tube (Zhou et al. 2004)

As the spray entered the draft tube, it entrained solids from the surrounding environment due to the low pressure in the surrounding jet region. When the jet made contact with the wall of the draft tube, a large velocity gradient was formed between the wall of the draft tube and center of the jet, creating large turbulent eddies. These eddies enhanced the mixing efficiency between the liquid spray droplets and the entrained solid particles, and distributed the droplets more evenly over the whole cross-section of the spray jet cavity. Results of this test were confirmed by House et al. (2004) and McMillan et al. (2005). One of the disadvantages with this proposed idea is the formation of coke on the surface of the draft tube. This may lead to fouling, thereby requiring frequent maintenance.

House et al. (2009) investigated the effect of adding gas to the jet periphery using both a sonic shroud and an annular shroud (Figure 4.2). Both shrouds surrounded the tip of the nozzle. High velocity gas was directed parallel to the direction of the liquid droplets in an attempt to entrain more solids into the spray, redirect liquid droplets away from the center of the spray, and enhance the expansion of the gas-liquid jet inside the fluidized bed. Both shrouds decreased the distribution of the liquid concentration in the resulting agglomerates when compared to a stand-alone Fluid Coker spray nozzle. The decreased agglomerate liquid concentration indicated that more liquid was distributed throughout the fluidized bed, and less liquid became trapped inside agglomerates. Therefore the implementation of gas shrouds was found to benefit liquid distribution among the fluidized solids.

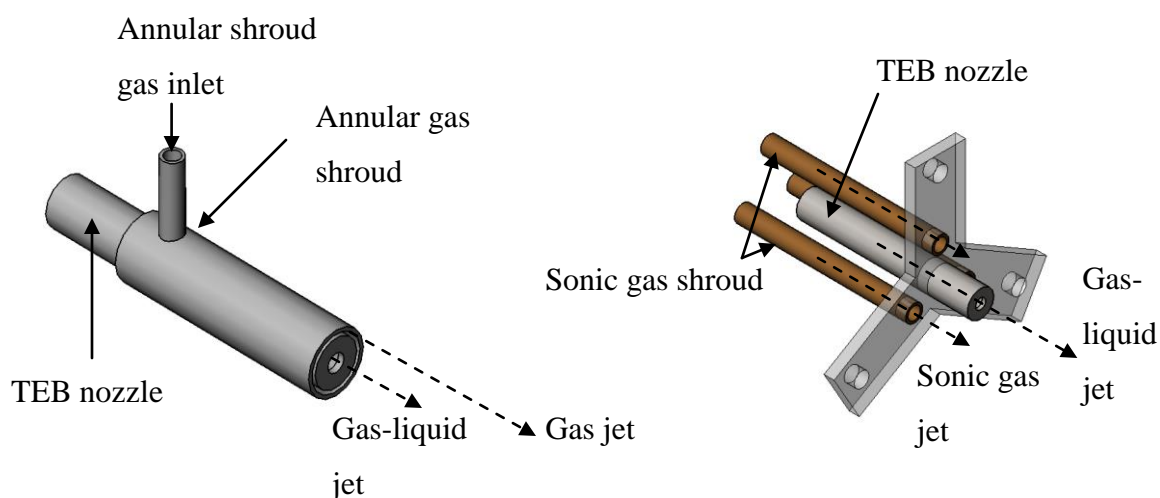


Figure 4.2: Annular shroud (left) and sonic shroud (right) investigated by House et al. (2008)

Several nozzle geometries have been proposed to enhance the liquid solid contact efficiency inside a fluidized bed. One such geometry involved adding a conical diverging section to the end of the standard Fluid Coker spray nozzle (Portoghese et al. 2010) (Figure 4.3).

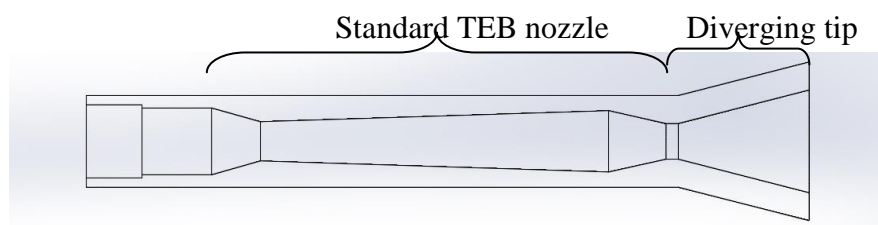


Figure 4.3: TEB nozzle with diverging nozzle tip investigated by Portoghese et al. (2010)

This diverging section reduced the pressure drop between the nozzle exit and the ambient pressure inside the fluidized bed, and accelerated the two phase flow to supersonic speed. The increased speed of the jet resulted in a lower pressure surrounding the jet cavity, which promoted solids entrainment into the jet, increasing liquid-solid contact efficiency. House et al. (2008) also studied the effect of diverging nozzle attachment, and found that the attachment helped produce agglomerates with a lower distribution of liquid concentration compared to agglomerates formed by the standard Fluid Coker nozzle developed by Base et al. (1999). The lower liquid concentration corresponded to less liquid trapped inside agglomerates, and the formation of weaker agglomerates.

The successes of the diverging nozzle tip lead to the development of two more nozzle tip attachments. The first is a cloverleaf attachment (Figure 4.7). This attachment is added to the end of a standard Fluid Coker spray nozzle. It acts as a diffuser, similar to the nozzle studied by Portoghese et al. (2010), and it consists of four divergent, quasi-conical flow passages located symmetrically around the longitudinal axis of the nozzle. The shape of the diverging tip is believed to increase the interfacial area between the jet and the fluidized bed, which enhances the entrainment of solids into the jet cavity, and improves the liquid-solid contact area (Chan et al. 2012).

Another proposed extension to the diverging nozzle attachment involved keeping the same conical shape, but to changing the diffuser expansion angle (Figure 4.8). Pougatch et al. (2012) investigated the effect of this nozzle attachment on the jet-bed interaction using a numerical model. Results indicate that decreasing the natural

expansion angle of the jet has a stabilizing effect on the spray downstream of the nozzle exit. Due to the decreased expansion angle however, the surface area of the jet-bed interface was reduced when the nozzle attachment angle was reduced, thereby reducing the jet-bed interfacial area. Increasing the diverging nozzle attachment angle allowed the spray to spread out wider, increasing the jet-bed interface, and therefore entrain more solids. The authors found that if the expansion angle of the diverging nozzle attachment was increased beyond a critical angle, fluctuations started to occur in the spray downstream of the nozzle exit. These fluctuations destabilized the spray, causing particles to be periodically drawn into and expelled out of the jet cavity. Due to the conflicting effects of increased jet-bed surface area and increased spray stability as the conical nozzle attachment angle increased, an optimal nozzle expansion angle was found.

It was previously determined that increasing the spray jet expansion angle inside the fluidized bed lead to the formation of weaker agglomerates that released trapped liquid at a faster rate compared to the standard TEB nozzle (Chapter 3). It was hypothesized that this could be due to a larger jet-bed surface area, which increased the entrainment of solids into the jet cavity. A higher solids concentration in the jet cavity should increase the probability of contact between liquid droplets and solid particles, and therefore enhance liquid-solid contact efficiency. The geometry of the cloverleaf nozzles produce a similar effect, and are thus expected to lead to the formation of less stable agglomerates.

It was also hypothesized in Chapter 3 that an increased jet expansion angle increased the area of liquid distribution at the tip of the jet cavity in the fluidized bed. It was previously determined by Ariyapadi et al. (2003) that agglomerates tend to form at the tip of the jet cavity. Therefore distributing the liquid over a larger area at the spray cavity tip should reduce the concentration of liquid in this region, leading to agglomerates with a lower liquid content. Agglomerates with a lower liquid content would be expected to break apart more easily and release trapped liquid at a faster rate. The geometry of the variable-angle conical nozzle tip attachments produces a similar effect. It is expected that an increase in the expansion angle of these nozzle attachments should lead to the formation of weaker agglomerates that release moisture at a faster rate due to a lower concentration of liquid at the jet cavity tip.

The first objective of the current investigation is to test the effect of three different cloverleaf nozzle attachments on the rate at which moisture is released from agglomerates in a large scale fluidized bed. The different cloverleaf attachments produce a different spray shape when compared to a standard Fluid Coker nozzle. The faster moisture is released from agglomerates, the more effective the spray nozzle attachment.

The second objective of the current investigation is to determine how the angle of a diverging conical nozzle attachment affects the rate at which moisture is released from agglomerates. It is known that small diverging angles will enhance spray stability and extend the length of the spray inside the fluidized bed, however, larger jet angles lead to a larger jet-bed interface, which Chapter 3 suggests would be beneficial.

The third objective of the current investigation is to compare the performance of the cloverleaf and conical nozzle attachments to the performance of the eroded nozzle geometries investigated in Chapter 3.

4.2 Apparatus

4.2.1 Fluidized Bed

A schematic of the fluidized bed used for these experiments is shown in Figure 4.4.

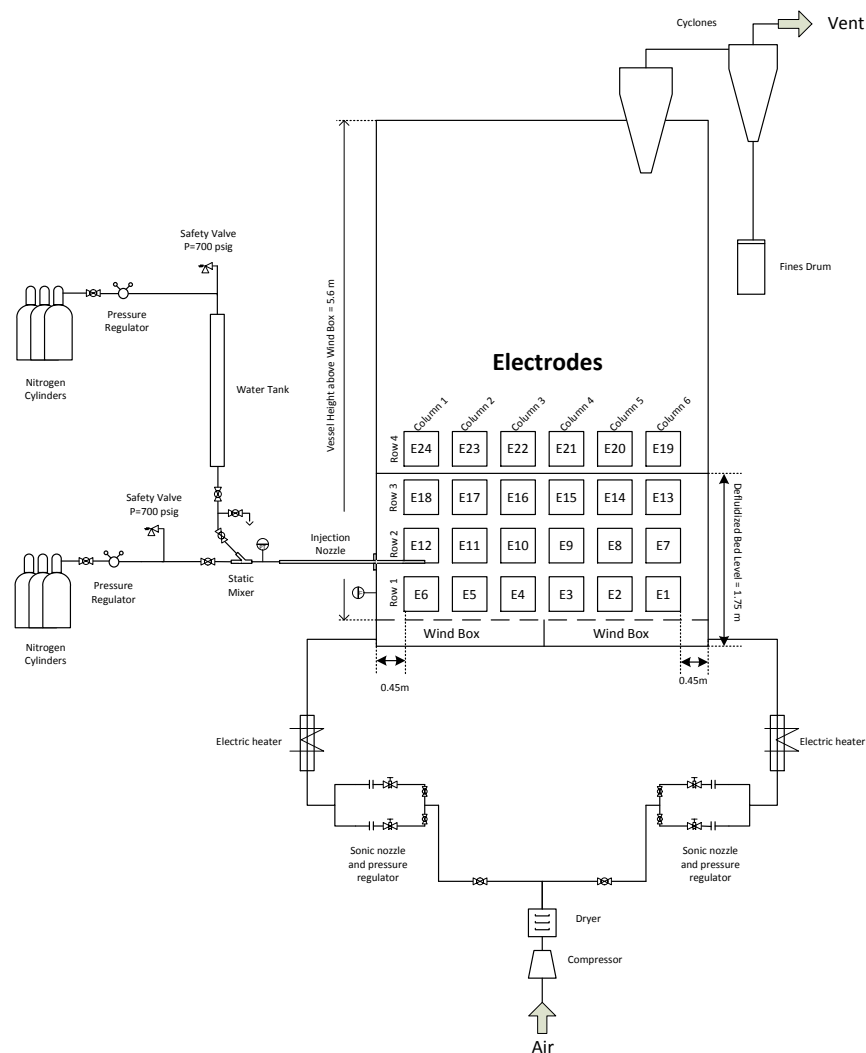


Figure 4.4: Simplified Process Flow Diagram of Experimental Apparatus

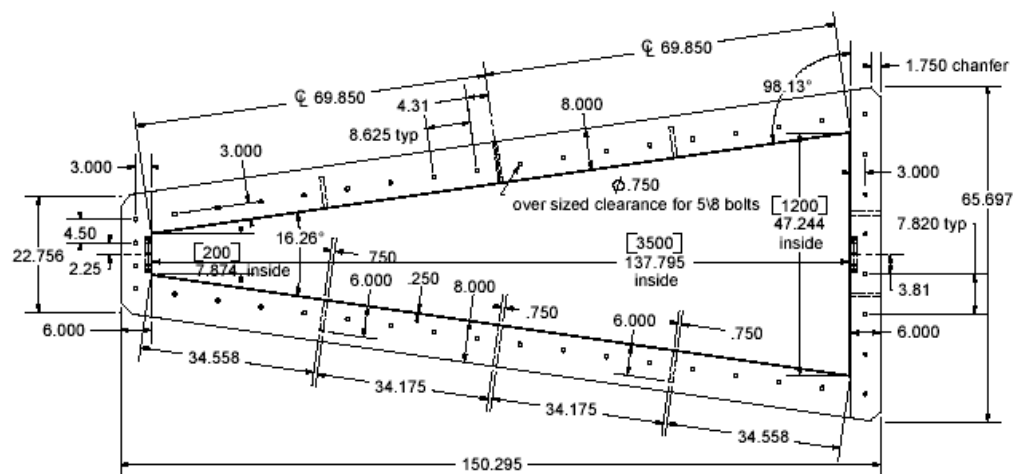


Figure 4.5: Top view of fluidized bed vessel (dimensions in inches)

The cross sectional dimensions of the vessel (Figure 4.5) were 0.2 m x 1.2 m x 3.5 m, and the height was 6.1 m. The cross sectional area of the bed was chosen to represent the jet penetration zone of one Fluid Coker nozzle. The expansion angle of the bed was chosen based on a previous jet expansion study (Ariyapadi et al. 2003), and the length of the bed was chosen based on a previous jet penetration study (Ariyapadi et al. 2004).

Silica sand ($\rho = 2650 \text{ kg/m}^3$, Sauter mean diameter = $150 \text{ }\mu\text{m}$, Type B powder according to Geldart (1973)) was chosen to model coke in a cold model Fluid Coker. The injected liquid was deionized water ($20 \text{ }^\circ\text{C}$, $\rho_L = 998.5 \text{ kg/m}^3$) and the atomization gas was compressed nitrogen. Water at room temperature was used as it has a similar viscosity to bitumen at upstream nozzle conditions (about 350°C). Silica sand and water also have similar wettability characteristics to that of bitumen and coke, and this has been used in previous experiments. Steam flow through the nozzle was simulated using nitrogen, as a past experiment has shown that the molecular weight of the atomization gas has a negligible impact on spray droplet size (Rahman et al. 2012).

The static height of solids inside the bed was 1.6 m, giving a total mass of approximately 6200 kg. The height of the bed was monitored using a manometer with pressure taps located at heights of 0.1, 0.89, 1.5, 2.11, and 3.93 m above the gas distributor.

The bed was fluidized at 0.15 m/s and air was supplied from a compressor capable of a maximum output pressure of about 100 psig. A bank of sonic nozzles controlled the mass flow rate of fluidization air, and air pressure was regulated using Wilkerson R40-OC-000 regulators with a pressure transducer (model # PT-1PTG0100D5F5) rated for 100 psig.

The temperature of the bed was kept constant for the start of each liquid injection. The temperature was measured using 3 J-type thermocouples were connected to the wall of the bed, and another connected to the secondary cyclone inlet. The temperature of the bed was controlled using an electric air heater, which was connected to the fluidization gas inlet line.

4.2.2 Spray Nozzles

Each nozzle used to spray the gas-atomized liquid was a full scale Fluid Coker nozzle, and has a similar geometry to the standard TEB nozzle patented by Base et al. (1999) (Figure 4.6). The nozzle was installed on the narrow side of the bed, approximately 0.9 m above the distributor plate, and penetrated a distance of about 0.7 m into the bed. The nozzle penetration distance was chosen based on an estimation of the spray penetration using a correlation developed by Ariyapadi et al. (2004), and was chosen such that the jet would not reach the opposite side of the fluidized bed vessel.

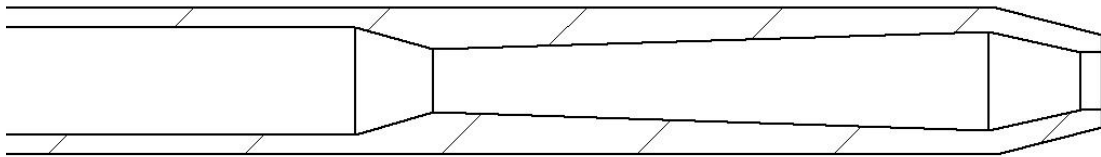


Figure 4.6: Standard TEB nozzle used to distribute liquid in the Fluid Coking process

Three cloverleaf attachments were added to the tip of the TEB nozzle and are shown in Figure 4.7. The first cloverleaf attachment has four diverging, quasi-conical lobes connected to the throat of a standard Fluid Coker spray nozzle. The second cloverleaf attachment is similar in geometry to the first, except each of the four lobes have a larger diameter than the first cloverleaf attachment. The larger lobes are intended to represent an eroded version of the first cloverleaf attachment. The lobes on the third attachment are further increased in diameter, such that they form a square shape at the tip of the nozzle.

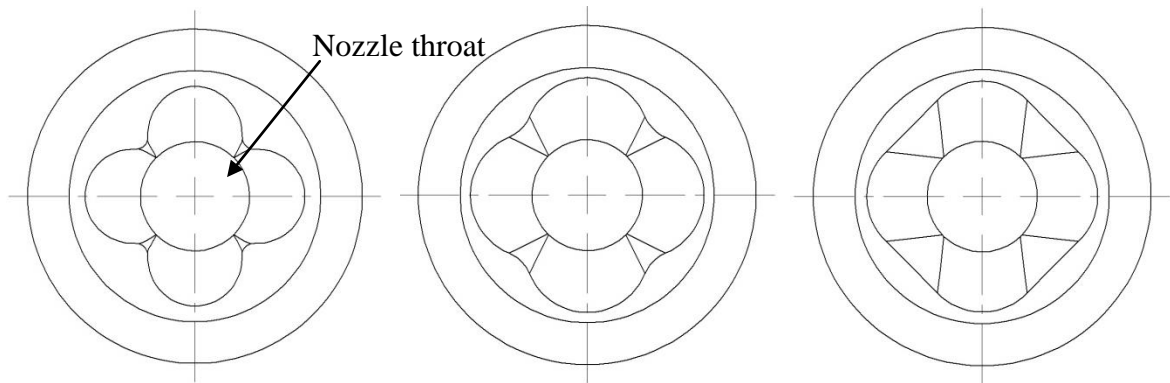


Figure 4.7: Geometry of cloverleaf nozzle attachments. Left: Standard cloverleaf. Middle: Eroded Cloverleaf. Right: Square cloverleaf.

Five diverging conical nozzle attachments were also used to produce a spray inside the fluidized bed (Figure 4.8). The diverging nozzle tip angles tested were 5°, 10°, 20°, 30°, 40°. Each nozzle attachment was compared to the performance of a standard Fluid Coker nozzle.

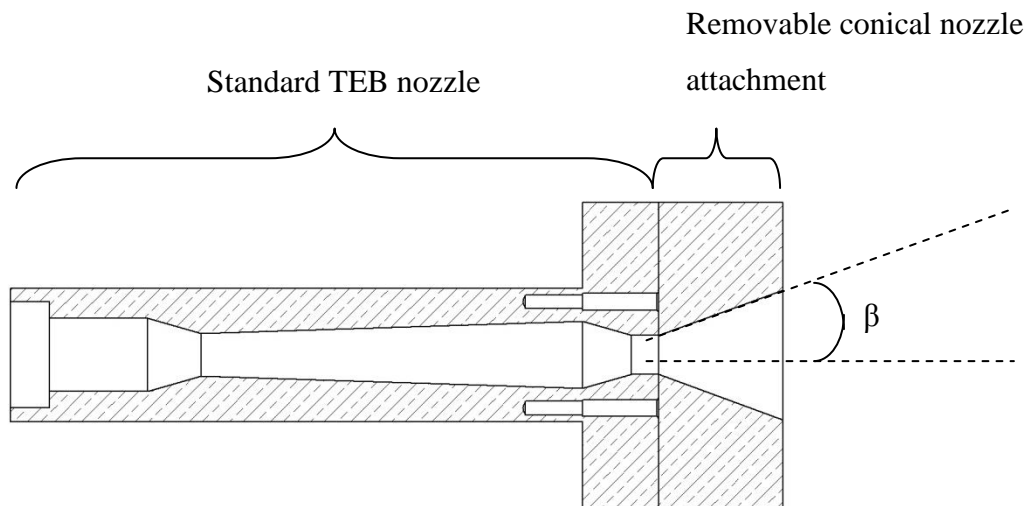


Figure 4.8: Side view of diverging conical nozzle attachment ($\beta = 5^\circ, 10^\circ, 20^\circ, 30^\circ, 40^\circ$)

A premix chamber was installed upstream of the spray nozzle to mix atomization gas and water. The premixer used (Figure 4.9) contains two branch pipes that connect to the nozzle entrance at an angle of 30° below the horizontal axis of the nozzle.

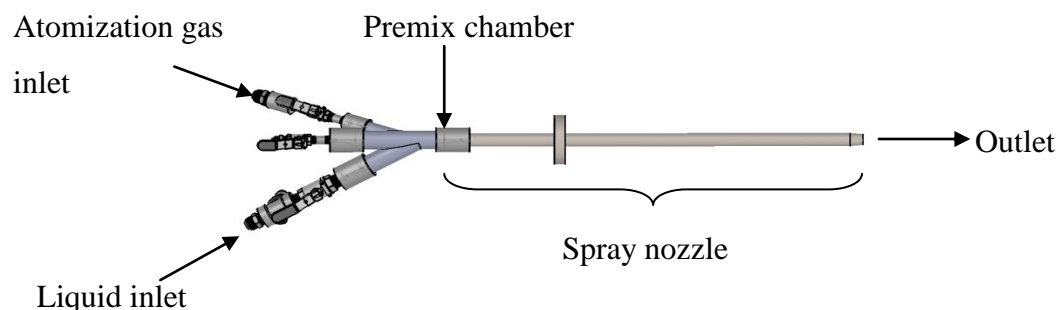


Figure 4.9: Premix chamber and nozzle assembly

In order to achieve flow rates similar to those used in industrial Fluid Coker reactors, a bank of high pressure cylinders (4500 psig) were connected to a blow tank filled with 15.3 kg of water. When the liquid inlet valve was opened on the premix assembly, pressure exerted by nitrogen in the blow tank was used to push a float, forcing water through the ensuing piping and premix chamber to the spray nozzle. The flow rate of nitrogen to the blow tank was controlled using a Pro Star PRS 4095331 gas pressure regulator, and the pressure was monitored using a pressure transducer (Omega PX181B-500 psig).

Atomization gas was supplied using an identical nitrogen cylinder bank and pressure regulator. In order to achieve the desired mass flow rate of atomization gas, a sonic nozzle was installed inside the gas port of the premix chamber. The size of the sonic nozzle was chosen to ensure the upstream pressure was at least double the downstream pressure during water injection. This ensured the mass flow rate of atomization gas did not fluctuate during liquid injection.

A pressure transducer (Omega PX181B-500 psig) was installed at the mixing point of the fluids in order to measure the pressure drop upstream of the nozzle.

4.2.3 Conductivity Measurement Apparatus

Fluidized bed conductivity was measured using twenty-four metallic electrodes (25.4 x 25.4 cm), which were installed on one wall of the bed. Sheets of 19 mm thick high density polyethylene were placed between the wall of the bed and the electrodes in order to provide isolation from the metal wall of the vessel, which was electrically grounded. A power supply and signal generator were used to send a 6.5 V sinusoidal signal through a measurement resistor to the measurement electrodes (Figure 4.10). Current flowed from the 24 electrodes, through the fluidized bed, to the opposite grounded vessel wall. The voltage drop across the measurement resistor was recorded at a rate of 1000 Hz after spray completion, and was used to determine the instantaneous electrical conductance through the bed using the following voltage divider relationship:

$$C = \left\{ R_m \left(\frac{V_{a1}}{V_2} - 1 \right) \right\}^{-1} \quad (4.1)$$

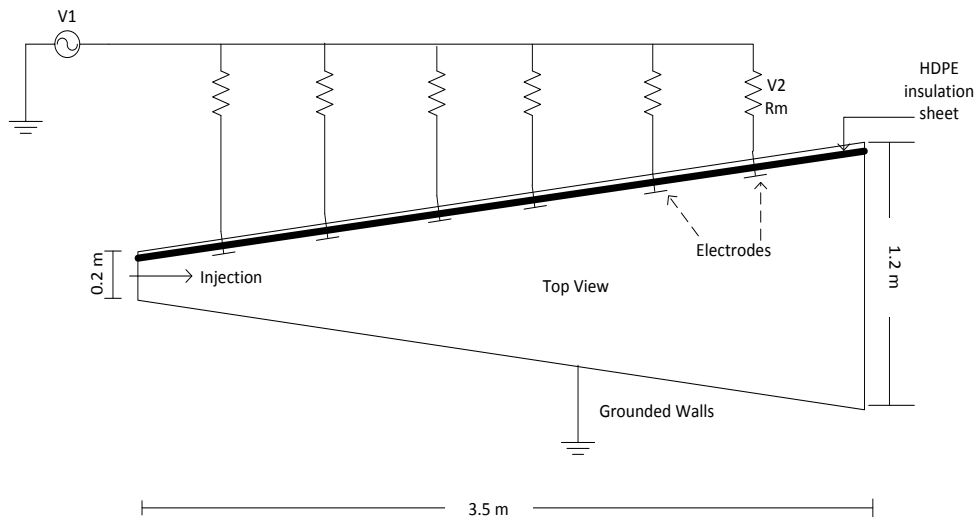


Figure 4.10: Schematic Diagram of Conductive Electrodes

4.3 Procedure

As was done in Chapters 2 and 3, electrical conductance measurements were used to determine the free moisture content in the fluidized bed at any time after liquid injection was complete. Free moisture is defined as

$$\%free\ moisture = \frac{\text{mass of water measured by conductance electrodes}}{\text{mass of water remaining in the fluidized bed}} \cdot 100\% \quad (4.2)$$

Calibration curves were used to relate the electrical conductance measurements to the bed free moisture content. Chapter 2, section 2.3.1 reviews the electrode calibration procedure.

The following procedure was used to calculate the cumulative fraction of injected water released from agglomerates using a commercial scale fluid coker nozzle:

1. Pressure regulators located at the atomization gas cylinders and liquid pressure cylinders were used to set the liquid flow rate to 3 kg/s and the gas-to-liquid mass flow rate ratio (GLR) to 2%.
2. Pressure regulators on the fluidization gas line were used to set the fluidization velocity at 0.15 m/s.
3. The bed freeboard was heated to a temperature of 24.5°C before each spray injection.
4. Liquid was injected into the bed at a specified flow rate, and the conductance of the bed was measured at a rate of 1000 Hz.
5. The temperature of the bed at three different locations, and the temperature of the freeboard were measured at a rate of 2.4 Hz. The temperature of the outlet air was used to calculate the humidity of the air, which in turn was used to calculate the mass flow rate of water from the bed (eq. 2.5)
6. The bed remained fluidized throughout the duration of the experiment. When the electrode conductance measurements reached the pre-injection values, data acquisition was ceased.

After injection into the bed, some of the liquid was distributed throughout the fluidized solids in the form of free moisture. A portion of the liquid formed liquid-solid agglomerates, which were heavier than individual solid particles, and likely sank to the bottom of the fluidized bed. Agglomerates did not register conductance readings, as they do not provide a path for current to travel from the electrodes to the grounded wall of the bed (ZirGachian et. al., 2013).

The total mass of water in the bed at any time was determined by subtracting the amount evaporated from the total mass of water injected. The free moisture of the bed was determined by matching the measured conductance reading to a free moisture value using the calibration curves for each electrode. The following mass balance was then used to calculate the cumulative mass of water freed from agglomerates:

$$G(t) = \frac{M_s}{M_L} \left[\int_0^t \left[\frac{d\bar{x}}{dt} + \frac{f_e}{M_s} \right] dt \right] \quad (4.3)$$

where M_L and M_s are the mass of liquid injected and solids present in the fluidized bed, respectively, \bar{x} is the average free moisture content of the bed as determined using the conductance electrode measurements, and f_e is the flow rate of evaporated water leaving the bed (as defined in Chapter 2).

Equation 4.3 may also be read as follows:

$$\left\{ \begin{array}{l} \text{Fraction of injected} \\ \text{liquid freed from} \\ \text{agglomerates} \\ \text{since the end} \\ \text{of the spray} \end{array} \right\} = \left\{ \begin{array}{l} \text{free moisture} \\ \text{in the bed at time } t \\ \text{injected liquid} \end{array} \right\} + \left\{ \begin{array}{l} \text{liquid evaporated} \\ \text{from the} \\ \text{bed since the} \\ \text{end of the spray} \\ \text{injected liquid} \end{array} \right\} \quad (4.4)$$

The function $G(t)$ ranges from 0 at the start of the experiment (where all moisture injected is initially trapped in agglomerates) to 1 at the end of the experiments (where the fraction of water not trapped in agglomerates equals 1 or 100%). The faster $G(t)$ approached 1, the faster the agglomerates released their moisture into the surrounding fluidized solids. Values of $G(t)$ were determined and compared for each nozzle tested.

A curve in the form of equation 4.5 was fitted through each set of data points obtained from each nozzle.

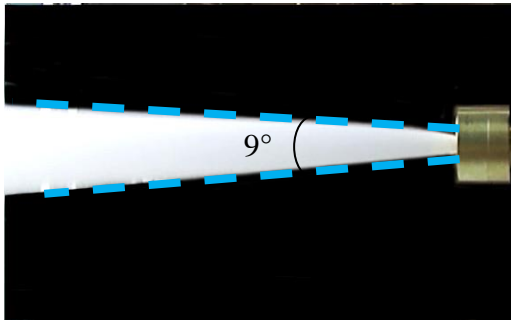
$$G(t) = 1 - e^{-t/\tau} \quad (4.5)$$

where τ represents the amount of time necessary for 62.5% of the moisture trapped in agglomerates to be released in the fluidized bed as free moisture. Values of τ were evaluated for each experiment to compare the performance of nozzles inside the fluidized bed.

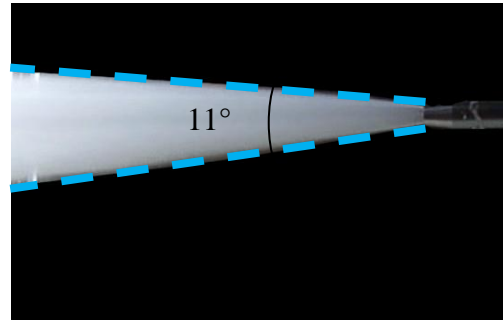
4.4 Results and Discussion

4.4.1 Open Air sprays

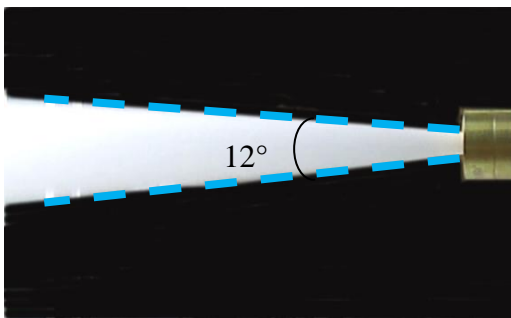
Open air sprays of each cloverleaf nozzle attachment and conical nozzle attachment are shown in Figure 4.11.



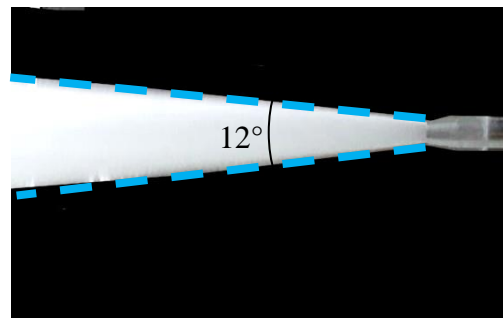
5° nozzle attachment



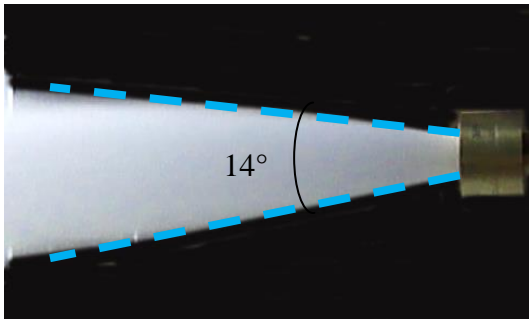
Cloverleaf #1



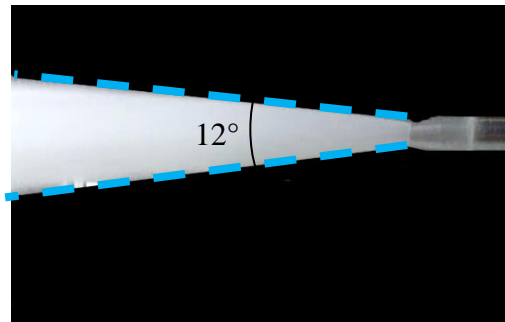
10° nozzle attachment



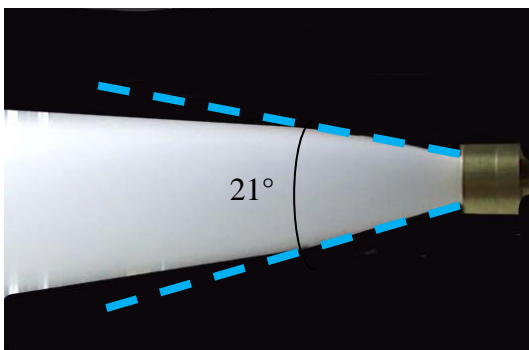
Cloverleaf #2



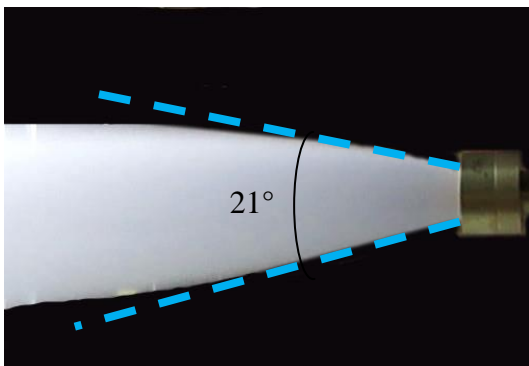
20° nozzle attachment



Cloverleaf #3



30° nozzle attachment



40° nozzle attachment

Figure 4.11: Open air sprays produced with conical nozzle attachment (left). Open air sprays produced with cloverleaf nozzle attachment (Right)

It is apparent that there is no difference between the open air spray angles produced using the 30° and 40° diverging tips. This provides evidence to support the fact

that a diverging nozzle tip angle greater than 20° allows the jet to expand to its natural expansion angle. Since the conical nozzle tips do not hinder the jet expansion and the nozzle are both operated under the same conditions, the agglomerates produced by these nozzles are not expected to vary significantly. The open air spray angle of each spray is plotted as a function of nozzle attachment expansion angle in Figure 4.12.

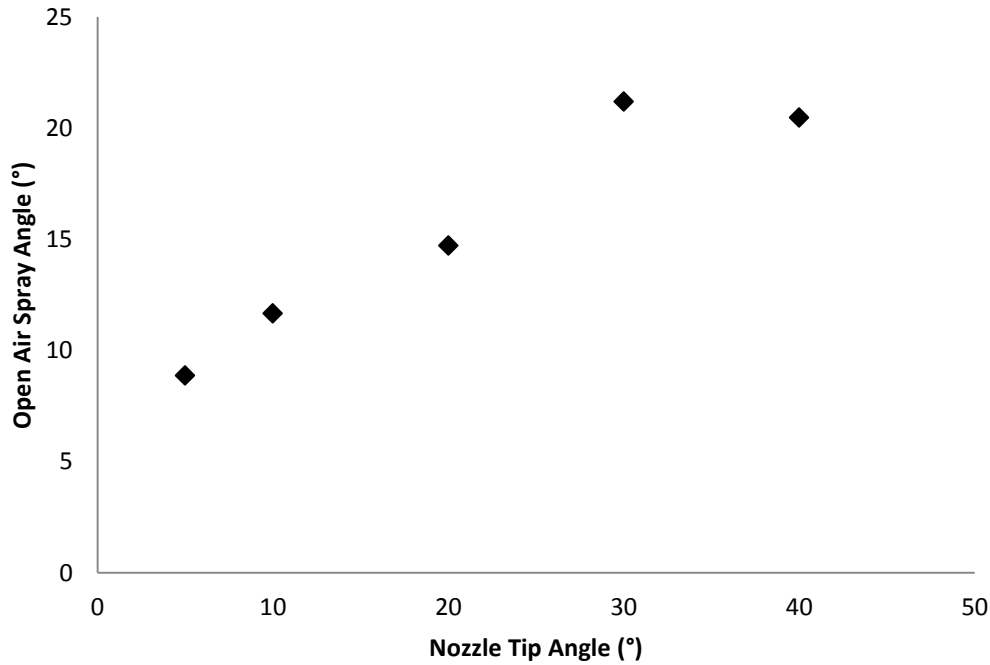


Figure 4.12: Open air spray angles produced by conical nozzle tip attachments

Based on results obtained in Chapter 3, it is also expected that the conical nozzle attachments with an expansion angle of 30° and 40° should perform best when sprayed inside the fluidized bed, as these nozzle attachments produce sprays with the greatest jet expansion angle should. A greater jet expansion angle should lead to greater liquid distribution at the jet cavity tip in the fluidized bed, resulting in agglomerates that contain lower liquid content, and therefore release liquid at a faster rate.

Although the jet expansion inside the fluidized bed is expected to be smaller than the jet expansion of a spray open to atmospheric conditions, it was still expected that a greater open air jet expansion will lead to a greater jet expansion inside the fluidized bed (Berruti et al, 2009).

The open air expansion angle produced by each cloverleaf nozzle attachment can also be observed in Figure 4.11. The jet expansion angle of each cloverleaf nozzle tip is plotted in Figure 4.13, and is compared to the open air jet expansion produced by the standard TEB nozzle.

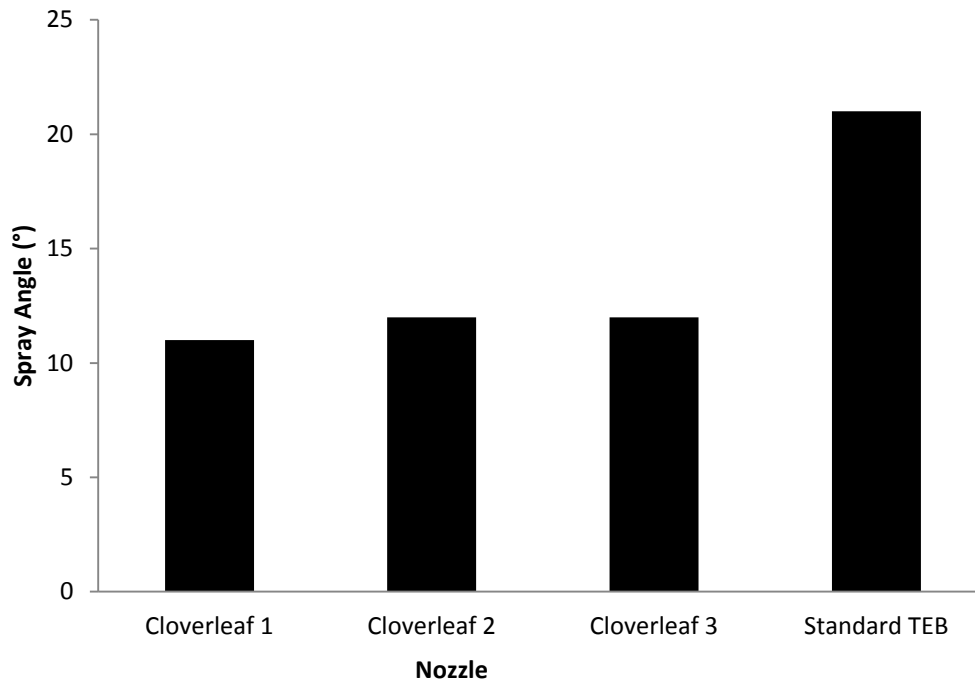


Figure 4.13: Open air spray angles produced by each cloverleaf nozzle tested.

The cloverleaf nozzle attachments produce an open air jet expansion that is smaller than that produced by the standard TEB nozzle. Based on expansion angle alone, the cloverleaf nozzles would not be expected to perform as well as a standard TEB nozzle in a fluidized bed. However, the geometry of the nozzle tip impacts the jet-bed interaction in two additional ways. The cross-sectional geometry of the cloverleaf attachment produced a spray with a higher perimeter to surface area ratio. This was expected to entrain more solids into the jet cavity, thereby increasing the concentration of solids within the jet cavity, and enhancing liquid solid contact. As well, the conical nozzle attachment also acts as a diffuser, similar to the geometry investigated by Portoghese et al. (2010) (Figure 4.3). The effect of this diffuser was found to increase the velocity of the jet at the tip of the nozzle, leading to an increased entrainment rate of solids. Thus, the

cloverleaf nozzles were expected to entrain more solids compared to the standard TEB nozzle, which should increase the concentration of solids and decrease the liquid-to-solids ratio within the jet cavity. The resulting agglomerates should contain a lower concentration of liquid, and should break apart at a faster rate compared to the standard TEB nozzle.

4.4.2 Cloverleaf Nozzle Attachment Performance in the Fluidized Bed

It was expected that the increased surface area of spray produced by the cloverleaf nozzle attachments would entrain more solids into the spray, and spray the liquid droplets over a wider area of dense phase fluidized solids. A higher perimeter to area ratio of the nozzle attachment would lead to higher solids entrainment. Thus the cloverleaf nozzle attachment 1 was expected to show the best performance, followed by cloverleaf 2, and finally cloverleaf 3. All three nozzle attachments were expected to enhance the entrainment of solids compared to the standard TEB nozzle.

Figure 4.14 illustrates the effect of the cloverleaf nozzle attachment on the rate of moisture released from agglomerates compared to the standard TEB nozzle.

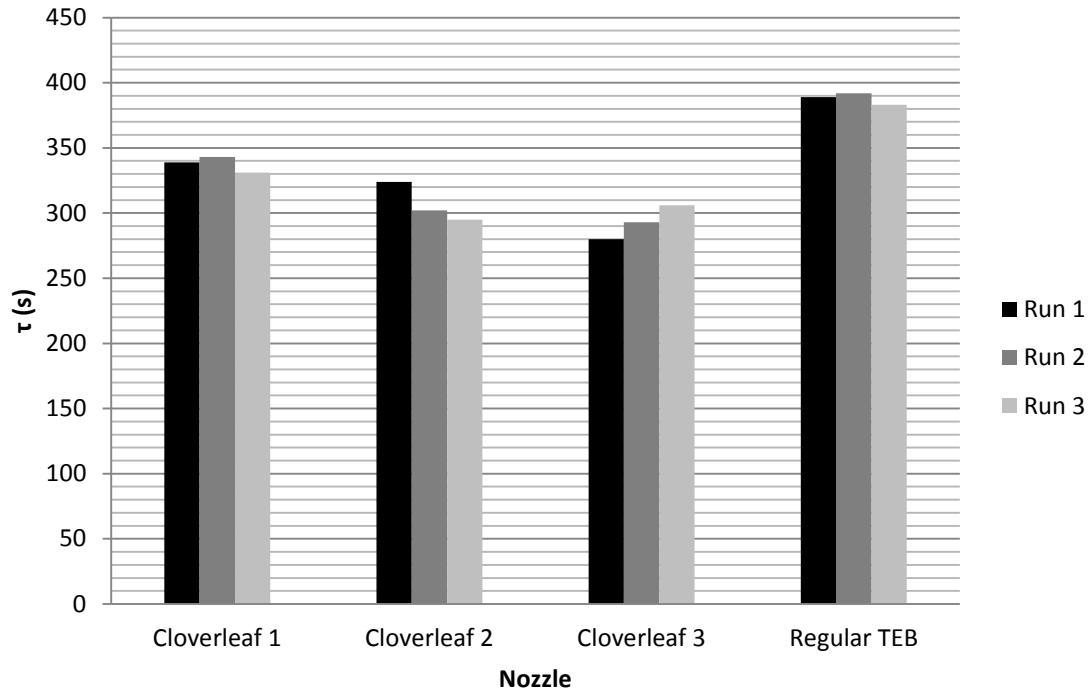


Figure 4.14: Agglomerate moisture released rate time constant for each cloverleaf nozzle tested. Results are compared to standard TEB nozzle. Liquid flow rate = 3 kg/s. GLR = 2% for each case.

The mean τ values for each nozzle were compared with a t-test using a 95% confidence interval. Results show that all three cloverleaf geometries perform better than the standard TEB nozzle.

Open air spray images suggest that the spray produced by the cloverleaf tips is more stable compared to the standard TEB nozzle. Spray stability may be important as it ensures solids are entrained, and not expelled from the jet cavity. This phenomenon has been observed in previous experiments (Portoghese et al. 2008).

The eroded cloverleaf (cloverleaf 2) and square shaped nozzle attachment (cloverleaf 3) produced agglomerates that released moisture at a faster rate compared to the original cloverleaf design, suggesting that a greater expansion angle is more beneficial than the increased surface area of the spray.

The open air jet expansion angle of the standard TEB nozzle was actually higher than the cloverleaf nozzles, yet the cloverleaf nozzle attachments demonstrated an improved performance. This emphasizes the importance of spray geometry and solids entrainment rate on the rate of moisture released from agglomerates.

4.4.3 Conical Nozzle Attachment Performance in the Fluidized Bed

Figure 4.15 illustrates the effect of the diverging nozzle tip angle on the rate of moisture released from agglomerates compared to the standard TEB nozzle. All experiments were performed at a liquid flow rate of 3 kg/s and a GLR of 2%. Three replicates were produced for each nozzle.

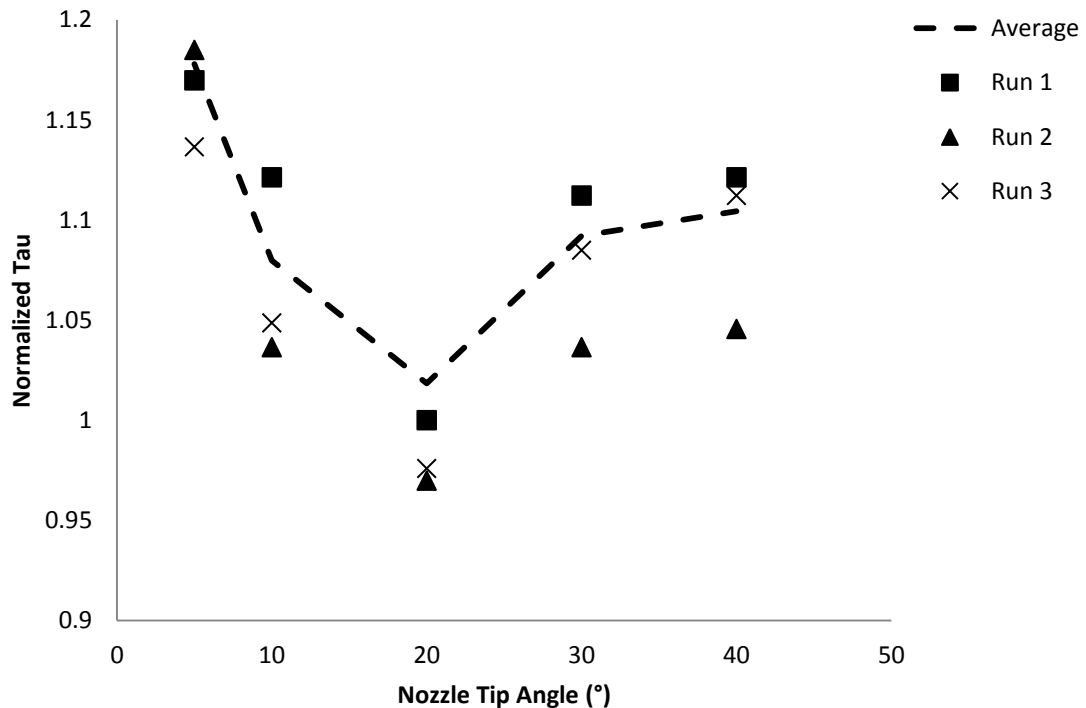


Figure 4.15: Effect of diverging nozzle tip angle on agglomerate moisture release rate time constant τ (Liquid flow rate = 3 kg/s, GLR = 2 wt%)

Results indicate that an optimal diverging nozzle tip angle is reached around 20°. Decreasing the diverging nozzle tip angle is known to stabilize the spray; however it significantly reduces the contact area between the fluidized solids and the boundary of the jet. The smaller contact area reduces the number of solids that become wetted by the spray, and increases the concentration of liquid at the jet cavity tip, where agglomerates tend to form (Ariyapadi et al. (2003).

Increasing the diverging section to 30° and above allows the spray to expand to its natural expansion angle, and introduces instabilities within the spray. The effect of these instabilities is not well known, but they may in fact help enhance the distribution of liquid inside the fluidized bed. However, since the larger conical nozzles allow the jet to expand to its natural expansion angle, it is possible that shielding the high velocity, low pressure region of the jet may actually block the jet from entraining solids in this region. Thus a lower entrainment rate would produce wetter solids and stabilize the resulting agglomerates.

4.4.4 Comparison of Eroded Nozzles, Cloverleaf, and Conical Nozzle Attachments

Figure 4.16 compares the relative performance of each spray nozzle tested in Chapters 3 and 4. A trend is observed between the agglomerate moisture release rate time constant and the free jet expansion angle produced by each spray.

Smaller spray angles with the same jet geometry as that produced by the TEB nozzle have lower performance in the fluidized bed compared to the Standard TEB nozzle. Allowing a spray produced by the conical nozzle tips to expand to the natural expansion angle of the TEB nozzle also appears to be detrimental to nozzle performance. This indicates that spray angle alone is not responsible for the performance of spray nozzles in the fluidized bed.

The cloverleaf nozzles produce a smaller spray angle compared to the standard TEB nozzle, yet perform slightly better. This may be attributed to the geometry of the jet produced by these nozzle attachments. Increasing the interfacial area between the spray and fluidized solids appears to be beneficial towards nozzle performance.

The eroded nozzles produced both a higher free-jet expansion angle, and irregularities in the geometry of the spray compared to the standard TEB nozzle. As a result, liquid distribution at the jet cavity tip was likely enhanced, lowering the liquid concentration of the agglomerates produced. Better liquid distribution at the jet cavity tip lead to the formation of dryer agglomerates, which released trapped liquid at a faster rate compared to the standard TEB nozzle. Further investigation into the cause of the change in jet geometry is recommended.

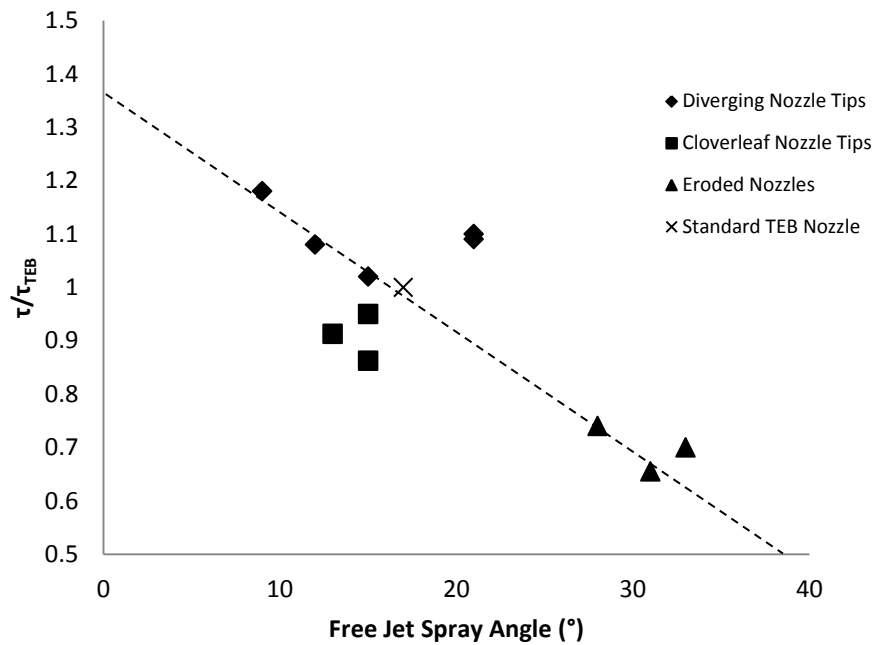


Figure 4.16: Effect of Spray Angle on Rate of Moisture Released from Agglomerates

4.5 Conclusions

The cloverleaf nozzle attachments improve the performance of the standard TEB nozzle by producing agglomerates that release liquid at a faster rate. This is believed to be due to the increased surface area of the jet-bed interface, as well as the lower pressure/higher velocity of the jet in the fluidized bed. The cloverleaf nozzles shown an improved performance, despite the smaller open air spray angles compared to the standard TEB nozzle.

The addition of a conical nozzle attachment to the end of the TEB nozzle also impacts the performance of the spray inside a fluidized bed. An optimal diverging nozzle tip angle of 20° has been identified. This nozzle tip produces an open air spray angle similar to that produced by the standard TEB nozzle. Increasing the diverging nozzle tip angle beyond 20° reduces the penetration length of the spray, and may induce instabilities downstream of the spray. Reducing the diverging nozzle tip angle stabilizes the spray, and increases its penetration depth; however, it also significantly reduces the jet-bed interface, thereby reducing the number of solid particles wetted by the spray. As a result, stronger agglomerates are produced, that take longer to release trapped liquid into free moisture.

Both spray-jet interfacial area and open air spray angle affect agglomerate formation in a fluidized bed. The increase in jet-bed interfacial area likely entrains solids at a higher rate, and the increased spray angle likely reduces the concentration of liquid at the jet cavity tip where agglomerates are most likely to form.

4.6 References:

- Ariyapadi, S., Holdsworth, D.W., Norley, C.J.D., Berruti, F., Briens, C. (2003) "Digital X-ray Imaging Technique to Study the Horizontal Injection of Gas-Liquid Jets into Fluidized Beds", *International Journal of Chemical Reactor Engineering*, vol. 1 Article A56.
- Ariyapadi, S., Berruti, F., Briens, C., McMillan, J., Zhou, D. (2004) "Horizontal Penetration of Gas-Liquid Sprays in Gas-Solid Fluidized Beds", *International Journal of Chemical Reactor Engineering*, vol. 2 Article A22.
- Base, T.E., Chan, E.W., Kennett, R.D., Emberley, D.A. (1999) *U.S. Patent 6,003,789*. Washington, D.C.: U.S. Patent and Trademark Office.
- Berruti, F., Dawe, M., Briens, C. (2009) "Study of gas-liquid jet boundaries in a gas-solid fluidized bed", *Powder Technology*, vol. 192, no. 1, pp 250-259.

- Chan, E., Knapper, B., Mueller, E., McMillan, J., Tyler, J., Kiel, D., Rathna, P.D. (2012) *United States Patent Application Publication No. US 2012/0063961 A1*. Washington, D.C.: U.S. Patent and Trademark Office.
- Geldart, D. (1973) "Types of gas fluidization", *Powder Technology*. vol.7
- Gray M., Le, T., McCaffrey, W. Berruti, F., Soundarajan, S., Chan, E., Huq, I. Thorne, C. (2001) "Coupling of mass transfer and reaction in coking of thin films of an Athabasca Vacuum Residue", *Industrial & Engineering Chemistry Research*, vol. 40, no. 15, pp. 3317-3324.
- House, P.K., Briens, C.L., Berruti, F., Chan, E. (2009) "Effect of spray nozzle design on liquid–solid contact in fluidized beds", *Powder Technology*, vol. 186, no. 1, pp. 89-98.
- House, P.K., Saberian, M., Briens, C., Berruti, F., Chan, E. (2004) "Injection of a Liquid Spray into a Fluidized Bed: Particle-Liquid Mixing and Impact on Fluid Coker Yields", *Industrial Engineering Chemistry Research*, vol. 43, pp. 5663-5669.
- Knapper, B.A., Gray, M.R., Chan, W., Mikula, R. (2003) "Measurement of Efficiency of Distribution of Liquid Feed in a Gas-Solid Fluidized Bed Reactor", *International Journal of Chemical Reactor Engineering*, vol. 1, Article A35.
- McMillan, J., Zhou, D., Ariyapadi, S., Briens, C., Berruti, F. (2005) "Characterization of the Contact between Liquid Spray Droplets and Particles in a Fluidized Bed", *Industrial & Engineering Chemistry Research*, vol. 44, no. 14, pp. 4931-4939.
- Portoghese, F., Ferrante, L., Berruti, F., Briens, C., Chan, E. (2010) "Effect of the injection-nozzle geometry on the interaction between a gas–liquid jet and a gas–solid fluidized bed", *Chemical Engineering and Processing Process Intensification*, Vol. 49, no. 6, pp. 605-615.
- Pougatch, K., Salcudean, J., McMillan, J. (2012) "Influence of conical nozzle attachments on horizontal spray dispersion in a fluidized bed", *Chemical Engineering Research and Design*, vol. 90, no. 10, pp. 1506-1516.

Rahman, M.A., Balzan, M., Heidrick, T., Fleck, B.A. (2012) "Effects of the gas phase molecular weight and bubble size on effervescent atomization", *International Journal of Multiphase Flow*, vol. 38, no. 1, pp. 35-52.

Zhou, D., Briens, C., Saberian, M., Berruti, F., Edward, W. (2004) "Enhancement of the Distribution of a Liquid Sprayed into a Fluidized Bed" *International Journal of Chemical Reactor Engineering*, vol. 2, Note S2.

Chapter 5

Conclusions and Recommendations

5

This chapter summarizes the main conclusions of this thesis, and presents some recommendations for future research

5.1 Conclusions

A method was developed to measure the rate of moisture released from agglomerates produced by a gas-atomized liquid injection into a fluidized bed. Experiments were performed with commercial scale Fluid Coker spray nozzles. The method was applied to investigate the impact of eroded nozzle geometry on agglomerate liquid release rate, as well as new nozzle geometries. The following are the main conclusions of the research:

- 1) The rate of liquid released from trapped agglomerates can be determined by measuring fluidized bed conductance after liquid is injected into the fluidized bed. Previous experiments have indicated that increasing the GLR of the gas-atomized liquid spray enhances liquid distribution inside the fluidized bed (Portoghese et al. 2008, ZirGachian et al. 2013). In this study, the GLR was varied, and results indicate that agglomerates tend to release moisture at a faster rate when the GLR is raised. Thus, increasing the GLR is beneficial towards producing agglomerates that release trapped liquid at a faster rate.
- 2) The rate of liquid released from trapped agglomerates does not vary significantly when the liquid flow rate is changed and the GLR is held constant. Increasing the liquid flow rate increases the liquid concentration at the spray cavity tip, which helps produce stable agglomerates. However, increasing the liquid flow rate also raises the pressure inside the nozzle, which allocates more energy to atomization, increases the spray penetration length, and leads to greater gas expansion at the

nozzle tip. The opposing effects may explain why there is no observable difference between the rates of liquid released from trapped agglomerates when the liquid flow rate is changed.

- 3) Nozzle erosion can greatly impact the angle of expansion of the jet produced by a Fluid Coker nozzle. The nozzles used in this study were eroded in such a way that a portion of the liquid exiting the nozzle was distributed at different locations throughout the fluidized bed when compared to the standard TEB nozzle. As a result, the agglomerates formed by the eroded nozzles released their moisture at a faster rate compared to the base case standard TEB nozzle.
- 4) Cloverleaf nozzle attachments help to stabilize the spray, and increase the jet-bed interfacial area. Both these effects may contribute to greater solids entrainment and better liquid distribution, both of which would be advantageous for liquid-solid contact. Results show that the cloverleaf nozzle tips produce agglomerates that release trapped moisture at a faster rate compared to a standard TEB nozzle.
- 5) The diverging nozzle tip attachment significantly alters the expansion of a jet produced by a standard TEB nozzle for diverging angles equal to or less than 20° . For diverging nozzle tip angles greater than 30° , the conical nozzle attachment does not impede the jet expansion, allowing the jet to expand to its natural expansion angle. It was found that an optimal diverging nozzle tip angle of 20° produces agglomerates that released trapped moisture at the fastest rate. Decreasing the diverging nozzle tip angle stabilizes the spray and increases jet penetration, but it significantly lowers the jet-bed interfacial area. As the angle is increased, jet instabilities may arise, the penetration length of the jet decreases, but the jet-bed interfacial area increases. As well, it is possible that the conical nozzle attachment acts as a shroud, separating the lowest pressure region of the spray from the fluidized bed, thereby reducing the entrainment of solids into the spray.

5.2 Recommendations

1. Due to the fluidized bed vessel trapezoidal shape, there exists the possibility that the hydrodynamics of the fluidized solids may be different in the wider portion of the bed compared to the narrow portion. This may skew results obtained from sprays that penetrate at different depths inside the bed. Sprays with a wider expansion angle may not penetrate as far into the fluidized bed as sprays with a narrow expansion angle. It has previously been shown (Ariyapadi et al. (2003)) that agglomerates form at the tip of the jet cavity. Therefore agglomerate properties may depend on the location of the jet cavity tip inside the fluidized bed. In order to understand the effect jet cavity tip location on agglomerate liquid release rate, it is recommended that a series of sprays be produced with the same nozzle geometry and operating conditions, but at different nozzle tip locations inside the fluidized bed.
2. The eroded nozzles were shown to have a wider expansion angle in open air spray tests compared to the standard TEB nozzle. It would be beneficial to observe how wide the expansion angle of the jet is inside the fluidized bed. Jet boundary measurement analysis similar to that presented by Berutti et al. (2009) could be used to measure jet expansion inside the fluidized bed. This would verify that liquid is indeed dispersed to regions of the fluidized bed that is not reached by the standard TEB nozzle, thereby enhancing liquid-solid contact.
3. Each eroded nozzle contains multiple features that distinguish them from the standard TEB nozzle. These features include erosion at the tip of the nozzle, erosion at the first throat of the nozzle (Figure 3.5), and a bend in the conduit leading up to the nozzle (Figure 3.7). As is suggested in Figure 3.6, the bent geometry of the nozzle conduit may be responsible for the erosion pattern found in the nozzle. It is recommended that the following steps be taken to determine which feature of the eroded nozzle benefits liquid distribution:

- a. Investigate the impact on agglomerate liquid release rate time constant (τ) on a standard TEB nozzle.
- b. Add a small groove to the tip of the TEB nozzle with similar dimensions as the groove found in the best performing eroded nozzle (Eroded Nozzle 1 or Eroded Nozzle 4 in Figure 3.5).
- c. Add a small groove to the nozzle used in step b at the first restriction within the nozzle, similar to that seen in Figure 3.5 (bottom left), and offset 120° from the groove at the nozzle tip. A custom made nozzle should be produced with removable sections (see Appendix A).
- d. Using one of the axial conduit profiles shown in Figure 3.7 (Eroded Nozzle 1 or Eroded Nozzle 4), place the nozzle used in step c at the end of a bent nozzle conduit. Bend profiles of each eroded nozzle have already been determined.

All parts required for this recommendation are listed in Appendix A. It may also be beneficial to use x-ray radiography to map the interior geometry of each eroded nozzle in order to gain a better understanding of how the geometry affects flow through the nozzle and the subsequent spray pattern.

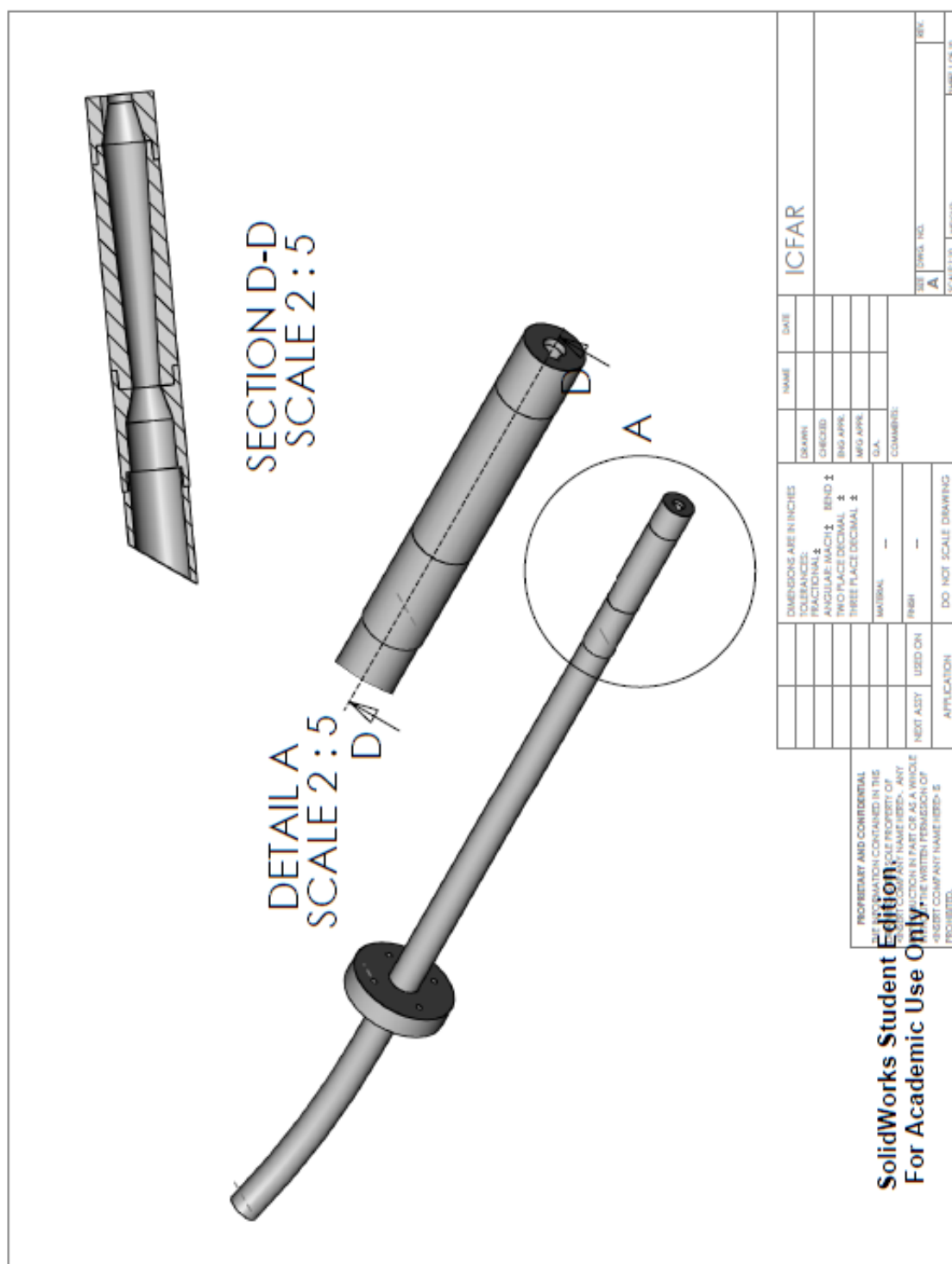
4. The fluidization air distributor in the Pie-Shape vessel leaks each time the bed is defluidized. This requires removal of solids from the windbox before the start of each run, and careful monitoring of the height of sand within the vessel. This also requires the vessel to be kept online for extended periods of time in order to prevent leakage of sand through the distributor between runs. It is recommended the distributor be upgraded in order to prevent solids leakage upon defluidization.

5.3 References

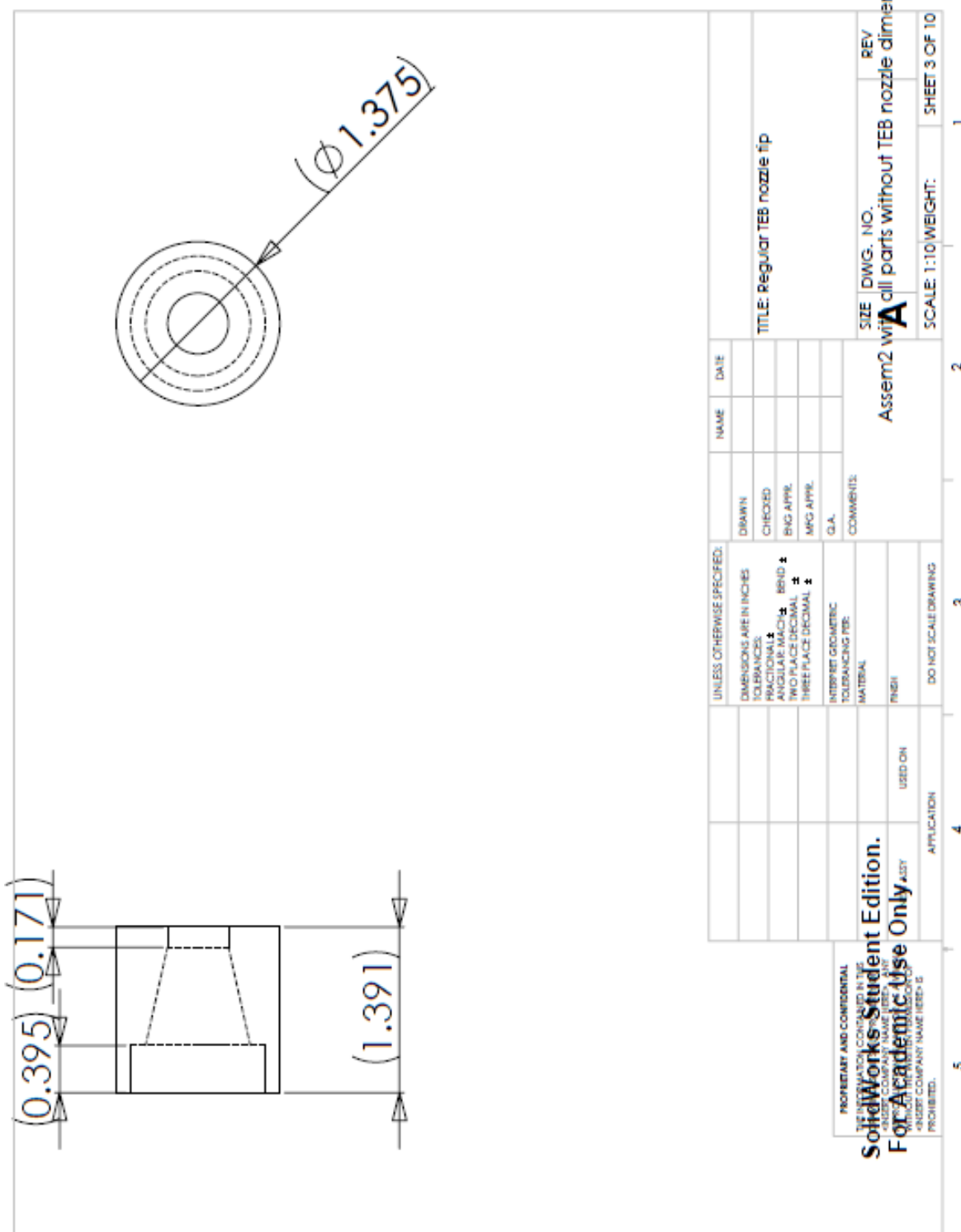
- Ariyapadi, S., Holdsworth, D.W., Norley, C.J.D., Berruti, F., Briens, C. (2003) “Digital X-ray Imaging Technique to Study the Horizontal Injection of Gas-Liquid Jets into Fluidized Beds”, *International Journal of Chemical Reactor Engineering*, vol. 1 Article A56.
- Berruti, F., Dawe, M., Briens, C. (2009) “Study of gas-liquid jet boundaries in a gas-solid fluidized bed”, *Powder Technology*, vol. 192, no. 1, pp 250-259.
- Portoghese, F., House, P.k., Berruti, F., Briens, C. (2008) “Electric conductance method to study the contact of injected liquid with fluidized particles”, *AIChE Journal*, vol. 54, no. 7, pp. 1770-181.
- ZirGachian, M.A., Soleimani, M., Briens, C., Berruta, F. (2013) “Electric conductance method for the assessment of liquid–gas injection into a large gas–solid fluidized bed”, *Measurement*, vol. 46, no. 2, 893-903.

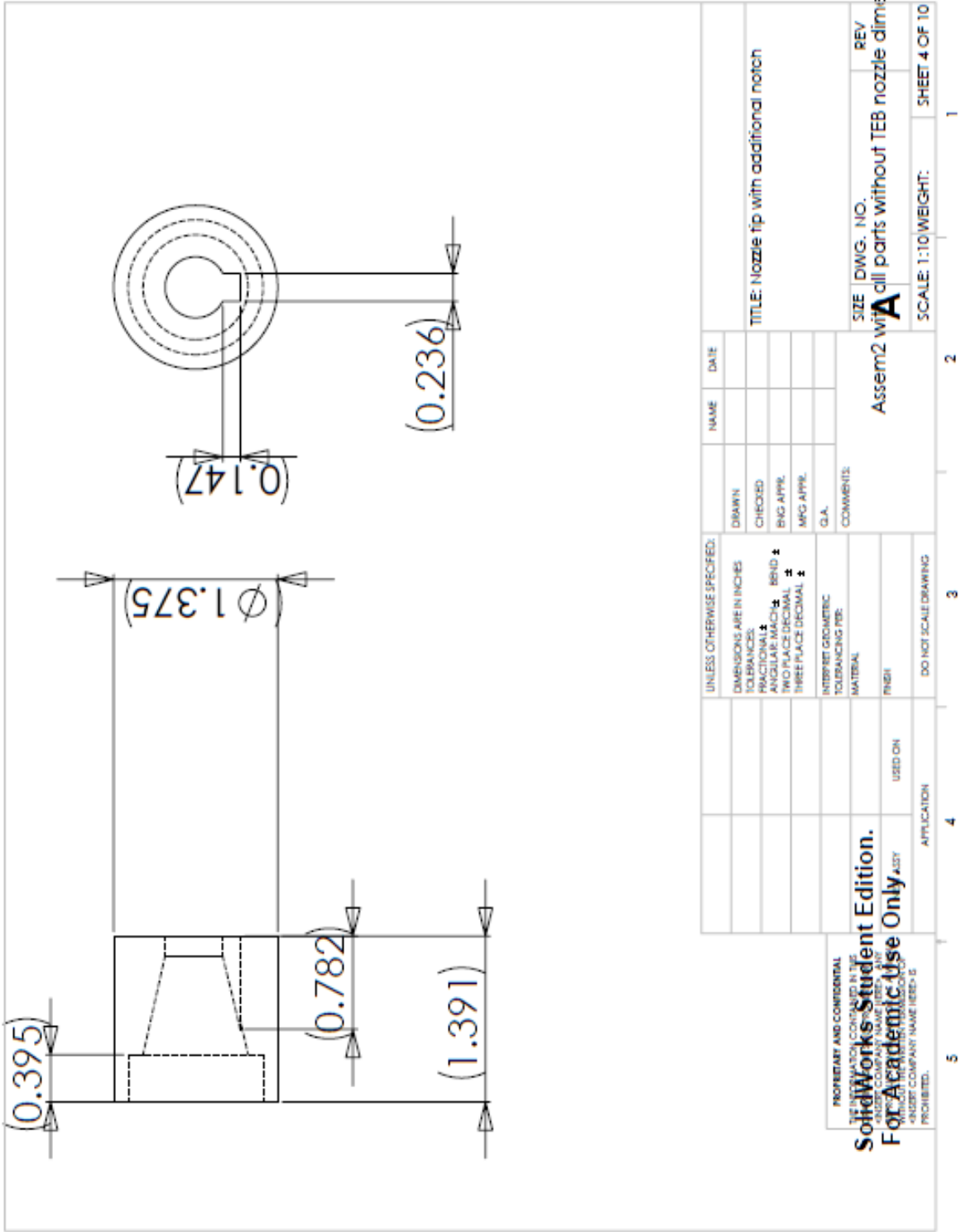
Appendix A

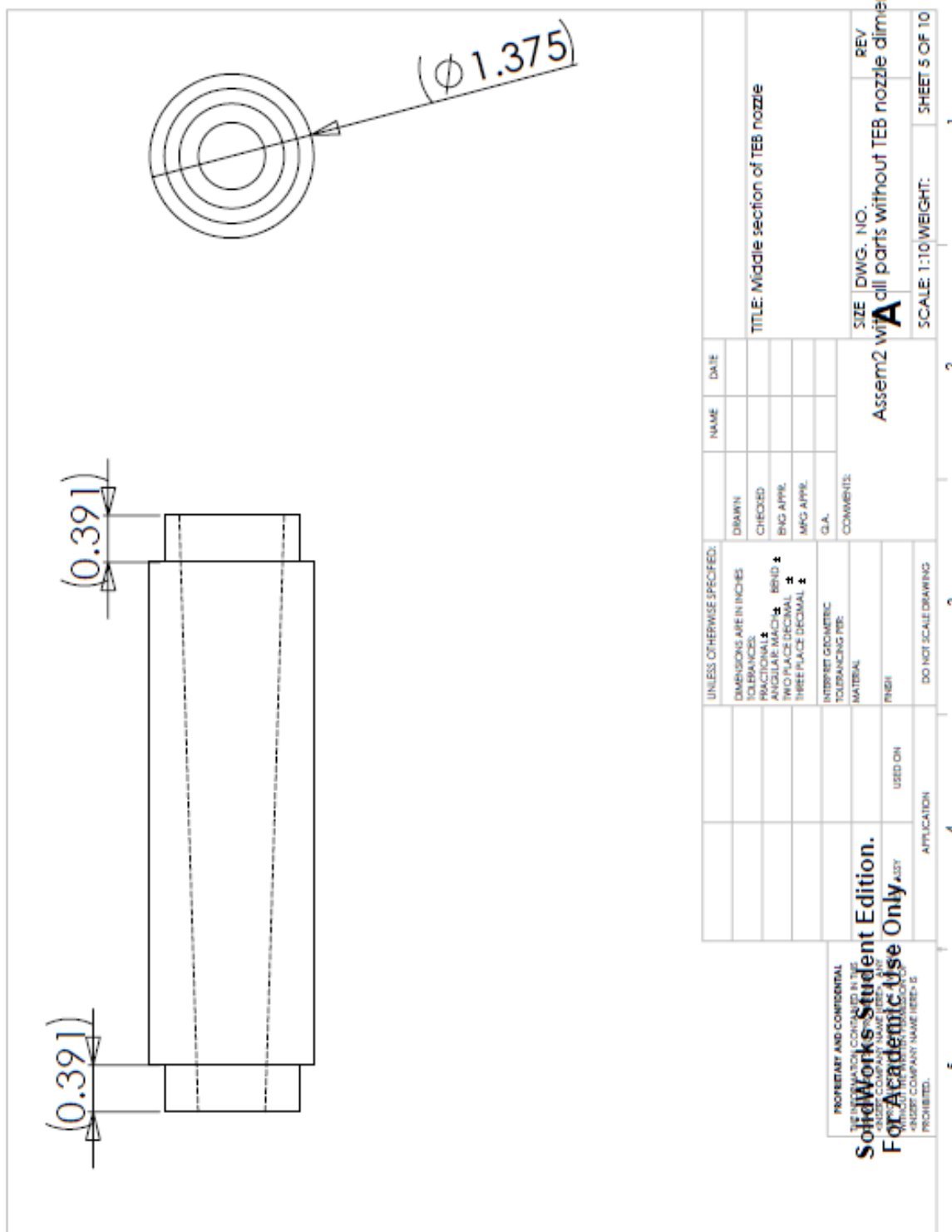
Parts Required for Custom Eroded Nozzle Investigation.

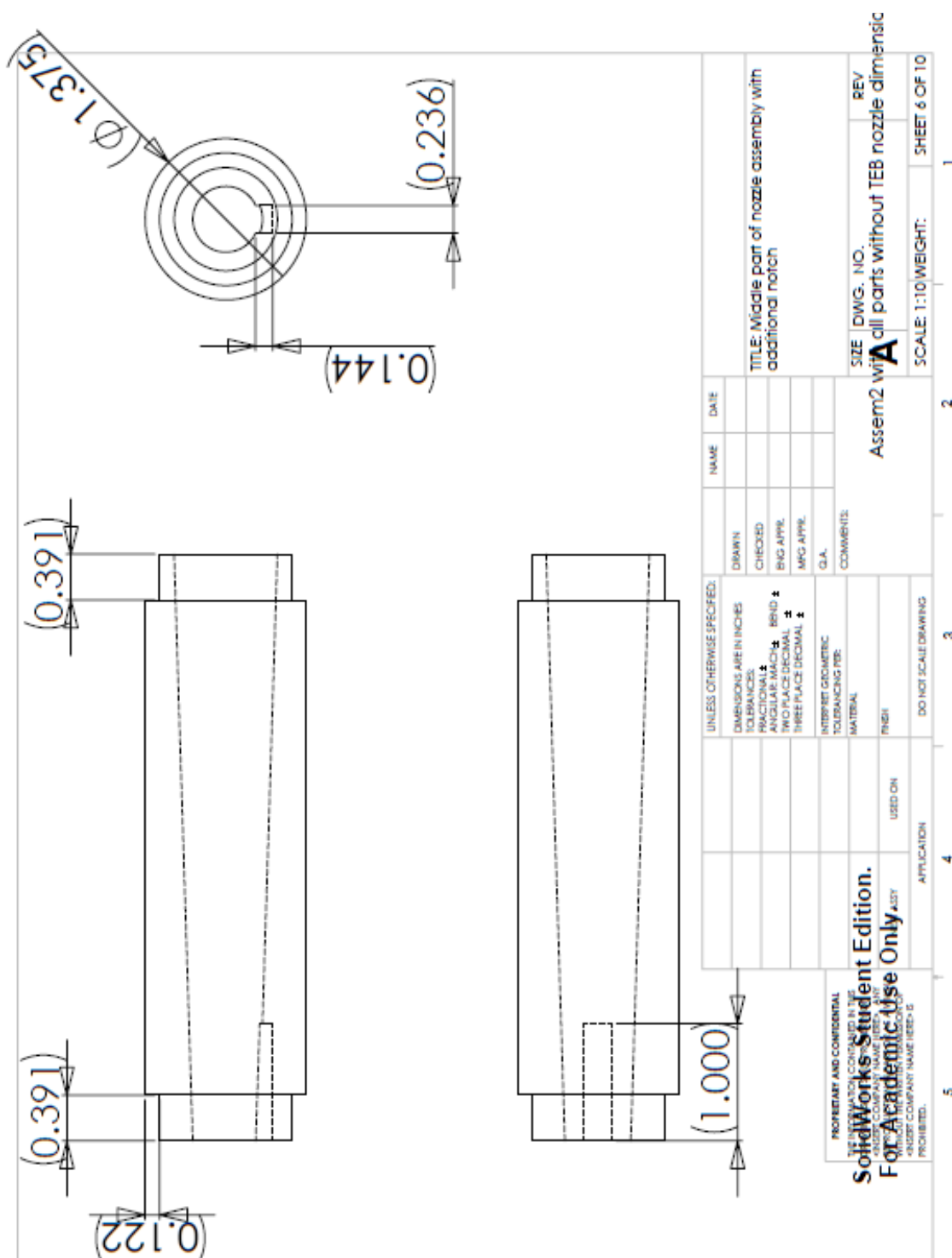


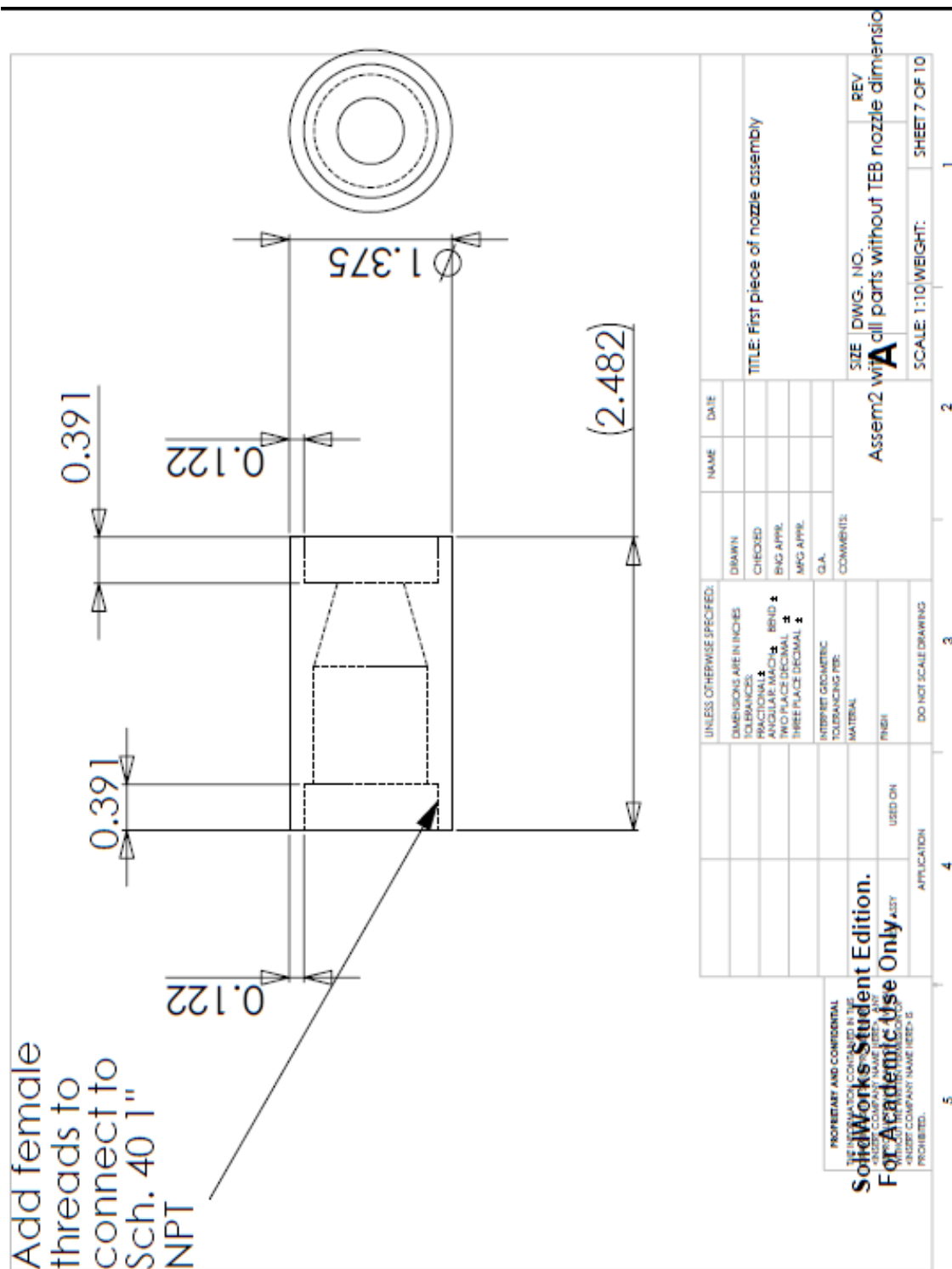
		NAME		DATE	
		DRAWN		CHECKED	
<p>UNLESS OTHERWISE SPECIFIED:</p> <p>DIMENSIONS ARE IN INCHES</p> <p>TOLERANCES:</p> <p>FRACTIONAL ±</p> <p>DECIMAL ±</p> <p>ANGULAR ±</p> <p>WELD ±</p> <p>TWO PLACE DECIMAL ±</p> <p>THREE PLACE DECIMAL ±</p> <p>WPG APPL.</p> <p>G.A.</p> <p>COMMENTS:</p>		TITLE: Front view of nozzle assembly showing alignment of nozzle bend and added nozzle grooves		SIZE DWG. NO. REV	
		MATERIAL		Assem2 with all parts	
		FINISH		SCALE: 1:10 WEIGHT: SHEET 2 OF 10	
		DO NOT SCALE DRAWING			
<p>PROPERTY AND CONFIDENTIAL</p> <p>THIS INFORMATION CONTAINED HEREIN IS THE PROPERTY OF</p> <p>1. USER COMPANY NAME HERE</p> <p>2. USER COMPANY NAME HERE</p> <p>3. USER COMPANY NAME HERE</p> <p>4. USER COMPANY NAME HERE</p> <p>5. USER COMPANY NAME HERE</p> <p>6. USER COMPANY NAME HERE</p> <p>7. USER COMPANY NAME HERE</p> <p>8. USER COMPANY NAME HERE</p> <p>9. USER COMPANY NAME HERE</p> <p>10. USER COMPANY NAME HERE</p> <p>11. USER COMPANY NAME HERE</p> <p>12. USER COMPANY NAME HERE</p> <p>13. USER COMPANY NAME HERE</p> <p>14. USER COMPANY NAME HERE</p> <p>15. USER COMPANY NAME HERE</p> <p>16. USER COMPANY NAME HERE</p> <p>17. USER COMPANY NAME HERE</p> <p>18. USER COMPANY NAME HERE</p> <p>19. USER COMPANY NAME HERE</p> <p>20. USER COMPANY NAME HERE</p> <p>21. USER COMPANY NAME HERE</p> <p>22. USER COMPANY NAME HERE</p> <p>23. USER COMPANY NAME HERE</p> <p>24. USER COMPANY NAME HERE</p> <p>25. USER COMPANY NAME HERE</p> <p>26. USER COMPANY NAME HERE</p> <p>27. USER COMPANY NAME HERE</p> <p>28. USER COMPANY NAME HERE</p> <p>29. USER COMPANY NAME HERE</p> <p>30. USER COMPANY NAME HERE</p> <p>31. USER COMPANY NAME HERE</p> <p>32. USER COMPANY NAME HERE</p> <p>33. USER COMPANY NAME HERE</p> <p>34. USER COMPANY NAME HERE</p> <p>35. USER COMPANY NAME HERE</p> <p>36. USER COMPANY NAME HERE</p> <p>37. USER COMPANY NAME HERE</p> <p>38. USER COMPANY NAME HERE</p> <p>39. USER COMPANY NAME HERE</p> <p>40. USER COMPANY NAME HERE</p> <p>41. USER COMPANY NAME HERE</p> <p>42. USER COMPANY NAME HERE</p> <p>43. USER COMPANY NAME HERE</p> <p>44. USER COMPANY NAME HERE</p> <p>45. USER COMPANY NAME HERE</p> <p>46. USER COMPANY NAME HERE</p> <p>47. USER COMPANY NAME HERE</p> <p>48. USER COMPANY NAME HERE</p> <p>49. USER COMPANY NAME HERE</p> <p>50. USER COMPANY NAME HERE</p> <p>51. USER COMPANY NAME HERE</p> <p>52. USER COMPANY NAME HERE</p> <p>53. USER COMPANY NAME HERE</p> <p>54. USER COMPANY NAME HERE</p> <p>55. USER COMPANY NAME HERE</p> <p>56. USER COMPANY NAME HERE</p> <p>57. USER COMPANY NAME HERE</p> <p>58. USER COMPANY NAME HERE</p> <p>59. USER COMPANY NAME HERE</p> <p>60. USER COMPANY NAME HERE</p> <p>61. USER COMPANY NAME HERE</p> <p>62. USER COMPANY NAME HERE</p> <p>63. USER COMPANY NAME HERE</p> <p>64. USER COMPANY NAME HERE</p> <p>65. USER COMPANY NAME HERE</p> <p>66. USER COMPANY NAME HERE</p> <p>67. USER COMPANY NAME HERE</p> <p>68. USER COMPANY NAME HERE</p> <p>69. USER COMPANY NAME HERE</p> <p>70. USER COMPANY NAME HERE</p> <p>71. USER COMPANY NAME HERE</p> <p>72. USER COMPANY NAME HERE</p> <p>73. USER COMPANY NAME HERE</p> <p>74. USER COMPANY NAME HERE</p> <p>75. USER COMPANY NAME HERE</p> <p>76. USER COMPANY NAME HERE</p> <p>77. USER COMPANY NAME HERE</p> <p>78. USER COMPANY NAME HERE</p> <p>79. USER COMPANY NAME HERE</p> <p>80. USER COMPANY NAME HERE</p> <p>81. USER COMPANY NAME HERE</p> <p>82. USER COMPANY NAME HERE</p> <p>83. USER COMPANY NAME HERE</p> <p>84. USER COMPANY NAME HERE</p> <p>85. USER COMPANY NAME HERE</p> <p>86. USER COMPANY NAME HERE</p> <p>87. USER COMPANY NAME HERE</p> <p>88. USER COMPANY NAME HERE</p> <p>89. USER COMPANY NAME HERE</p> <p>90. USER COMPANY NAME HERE</p> <p>91. USER COMPANY NAME HERE</p> <p>92. USER COMPANY NAME HERE</p> <p>93. USER COMPANY NAME HERE</p> <p>94. USER COMPANY NAME HERE</p> <p>95. USER COMPANY NAME HERE</p> <p>96. USER COMPANY NAME HERE</p> <p>97. USER COMPANY NAME HERE</p> <p>98. USER COMPANY NAME HERE</p> <p>99. USER COMPANY NAME HERE</p> <p>100. USER COMPANY NAME HERE</p>		APPLICATION		5	
USED ON		4		2	
DO NOT SCALE DRAWING		3		1	

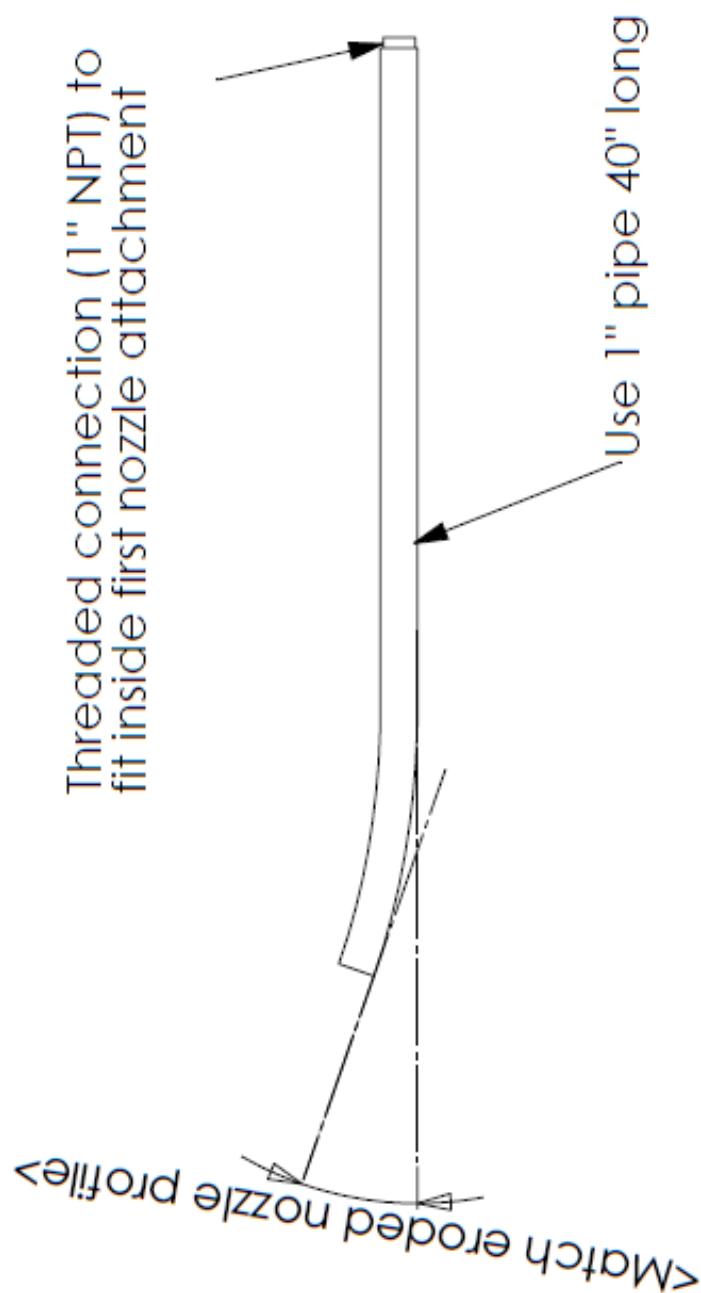












PROPRIETARY AND CONFIDENTIAL THIS DRAWING IS THE PROPERTY OF SOLIDWORKS CORPORATION. IT IS NOT TO BE REPRODUCED OR TRANSMITTED IN ANY FORM OR BY ANY MEANS, ELECTRONIC OR MECHANICAL, WITHOUT PERMISSION IN WRITING FROM SOLIDWORKS CORPORATION. *INSERT COMPANY NAME HERE* IS PROHIBITED.		UNLESS OTHERWISE SPECIFIED: DIMENSIONS ARE IN INCHES TOLERANCES: FRACTIONAL ± ANGULAR MATCH ± TWO PLACE DECIMAL ± THREE PLACE DECIMAL ±		DRAWN CHECKED ENG APPR. MFG APPR.	NAME DATE	TITLE: SIZE DWG. NO. A Nozzle conduit REV SCALE: 1:10 WEIGHT: SHEET 9 OF 10
		INTERPRET GEOMETRIC TOLERANCING PER: MATERIAL FINISH		COMMENTS: DO NOT SCALE DRAWING		
APPLICATION USED ON		USED ON		APPLICATION		1

		NAME		DATE		
		UNLESS OTHERWISE SPECIFIED: DIMENSIONS ARE IN INCHES TOLERANCES: FRACTIONAL ± ANGULAR MATCH ± HOLE POSITION ± HOLE SIZE DECIMAL ± THREE PLACE DECIMAL ±		DRAWN	CHECKED	TITLE:
<p>PROPERTY AND CONFIDENTIAL THIS INFORMATION CONTAINED IN THIS DRAWING IS THE PROPERTY OF SolidWorks Corporation. IT IS TO BE USED FOR THE PROJECT AND NOT BE REPRODUCED OR COPIED FOR ANY OTHER PROJECT WITHOUT THE WRITTEN PERMISSION OF SolidWorks Corporation. YOUR COMPANY NAME HERE IS PROHIBITED.</p>		INTERPRET GEOMETRIC TOLERANCING PER:		COMMENTS:		
		MATERIAL:				SIZE DWG. NO. Flange
APPLICATION		USED ON		FINISH		REV
DO NOT SCALE DRAWING		SCALE: 1:10 WEIGHT:		SHEET 10 OF 10		

Curriculum Vitae

Name:	Nicholas Prociw
Post-secondary Education and Degrees:	University of Waterloo Waterloo, Ontario, Canada 2006-2011 B.A.Sc. The University of Western Ontario London, Ontario, Canada 2012-2014 M.E.Sc.
Honours and Awards:	Thor E. Stephenson Memorial Scholarship 2006-2011
Related Work Experience	Facilities Engineer Co-op Imperial Oil Sept-Dec 2010 Facilities Development and Design Imperial Oil Jan-Apr. 2010 Technical Contact Imperial Oil May-Aug 2009